THE UNIVERSITY OF CAPE TOWN

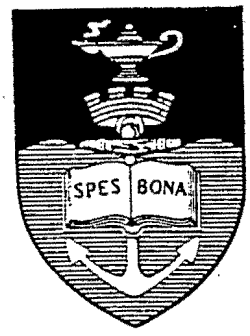

RESPONSE OF THIN CIRCULAR PLATES TO CENTRAL BLAST LOADING

by

Richard Ernest Bimha

DEPARTMENT OF MECHANICAL ENGINEERING

The University of Cape Town

Cape Town, South Africa

June, 1996

RESPONSE OF THIN CIRCULAR PLATES TO CENTRAL BLAST LOADING

by

RICHARD ERNEST BIMHA

NTDip. (Civil), The Harare Polytechnic
B.A.Sc. (Civil), The University of British Columbia

A THESIS SUBMITTED IN PARTIAL FULFILLMENT OF
THE REQUIREMENTS FOR THE DEGREE OF
MASTER OF SCIENCE IN ENGINEERING

IN

THE FACULTY OF ENGINEERING
DEPARTMENT OF MECHANICAL ENGINEERING

THE UNIVERSITY OF CAPE TOWN
CAPE TOWN, SOUTH AFRICA
JUNE, 1996

Abstract

The large ductile deformation response and rupture of thin circular metal plates subjected to central blast loading is investigated using the ABAQUS general purpose finite element code. The finite element code incorporates non-linear geometry and material effects as well as strain rate sensitivity. A material failure model is also incorporated.

The SAXI axisymmetric sheet elements are used to model the plate. The shell element uses a theory that includes shear deformation effects but degenerates to the Kirchoff classical thin shell theory for thin shell elements. An explicit time integration scheme is considered more suitable than an implicit scheme for the analysis. A uniform mesh with 1000 elements is used in modelling the experiments. The mesh size is chosen to satisfy the conditions for numerical stability in the explicit analysis scheme. Two boundary conditions are considered; a plate clamped to its supports by bolts and a plate fully built-in. The pressure loading from the explosive charge is assumed to be uniform over the loaded area and decaying exponentially to the plate boundary. The pressure pulse is assumed to be rectangular. Material parameters are obtained from uniaxial quasi-static material tensile test results.

The predicted plate responses; mid-plate permanent deflections, permanent deformation shape, strain rate dependence, strain predictions, response time and rupture are compared to experimental data and/or analytical and other numerical solutions. The predicted responses compare reasonably well with measured experimental results and/or with reported analytical and other numerical predictions.

Table of Contents

List of Tables

List of Figures

Notation

a	=	Load radius
k	=	Exponential decay constant
n	=	Strain rate sensitivity factor
p	=	Strain rate material parameter
D	=	Damage
E	=	Elastic Modulus
H	=	Plate thickness
I	=	Total impulse
L^{el}	=	Characteristic element length
Po	=	Constant pressure over load radius
$P(r)$	=	Pressure distribution profile
Q	=	Strain rate material parameter
R	=	Plate radius
$S(Tr)$	=	Transient deformation profile
Tr	=	Response time
V_b	=	Speed of detonation of explosives
V_o	=	Impulsive velocity
$V(Tr)$	=	Transient deformation rate profile
W_o	=	Deflection at the plate centre
$W(r)$	=	Deflection at radius 'r'
δ	=	Mid-plate deflection
σ_0	=	Static yield stress
$\overline{\sigma}$	=	Yield stress at non-zero plastic strain rate
$\dot{\overline{\varepsilon}}^{pl}$	=	Equivalent plastic strain rate
$\overline{\varepsilon}_p^f$	=	Plastic failure strain
$\overline{\varepsilon}_0^{pl}$	=	Offset plastic strain
$\overline{\varepsilon}_f^{pl}$	=	Plastic failure strain
$\overline{\varepsilon}_f$	=	Total strain
$\overline{\varepsilon}^{pl}$	=	Equivalent plastic strain
τ	=	Load duration
ρ	=	Material density
υ	=	Poisson's ratio
λ	=	Effective Lame's constant
μ	=	Effective Lame's constant
ξ	=	Damping ratio
ω_{max}	=	Highest element frequency
Δt	=	Stable time increment step

Acknowledgement

I am indebted to the many faculty, staff and students who generously provided their valued advice and guidance throughout the course of my study and research. In particular, the encouragement and supervision of Professor G.N. Nurick and the advice of Dr. Greg Mitchell is very much appreciated. The financial support of the University of Cape Town (through the University of Cape Town Research Scholarship) and FRD/UCT Centre for Research in Computational and Applied Mechanics (CERECAM) is gratefully acknowledged. Finally, appreciation goes to my wife, Lydia, who has been a source of encouragement and has helped with the typing of the thesis, and to my family and friends for their encouragement.

This thesis is dedicated to my wife and to my children, Kevin, Ketty and Kundai.

Chapter 1

Introduction

Events involving impulsive loading occur in a variety of circumstances. Collisions of aircraft, buses, trains and ships, impacts on pressure vessels and buildings due to accidental explosions and the destructive action of earthquakes on buildings and other civil structures are typical events involving impact. The need to understand the impact behaviour of structures and to develop rational design procedures have resulted in the study of the structural response of impulsively loaded beams, plates and shells growing over the years.

1.1 Blast Loads

A blast wave generated by detonating an explosive interacts with objects in its path by imposing impulsive or dynamic blast loads causing the objects to deform. The actual explosion pressure-time loading is a complex decaying pressure oscillation that requires, for practical reasons, simplification before applying in structural analysis. Figure 1.1 shows the smoothed pressure-time history for a typical blast wave. The peak overpressure is much larger than the peak underpressure so that the negative phase of the blast wave can be ignored [1].

Shen and Jones [2] characterised impulsive loading as a pressure pulse having a finite impulse with infinitely large magnitude and an infinitesimally short duration while The Steel Construction Institute [3] gave the following classification of blast loading: if the duration of the load is significantly less than the natural period of the structure the

structure has insufficient time to fully respond so the loading is termed 'impulsive' and if the duration is much longer than the natural period the loading is termed 'quasistatic'. Loading in the transition region between these two regimes is termed 'dynamic'. The Steel Construction Institute [3] also highlighted the important factors to be considered when idealising a blast load so that reasonable prediction of response can be achieved. Although this is a topic requiring further research, The Steel Construction Institute [3] observed that for impulsive loading, i.e., external pressure loadings of peak intensities of several Megapascals over durations typically of microseconds, preserving the exact peak load value and the exact load duration is not critical. It is however important to represent the impulse accurately. Figure 1.2 shows some of the pressure-time impulsive loading history idealisations found in the literature. Areas of uncertainty in the subject of blast loading include the derivation and idealisation of net loads on structures particularly localised blast loads [3]. In many cases an equally distributed load is assumed to act on the whole structure. In reality the interaction of the blast wave with the structure is not the same at all points, therefore, the blast load is not equally distributed. The spatial distribution of the blast load over the structure is a function of the location of the structure's elements relative to the point of initiation of the explosion [3]. Elements close to the initiation point will experience a higher intensity blast load while elements further away will experience a lower intensity blast load.

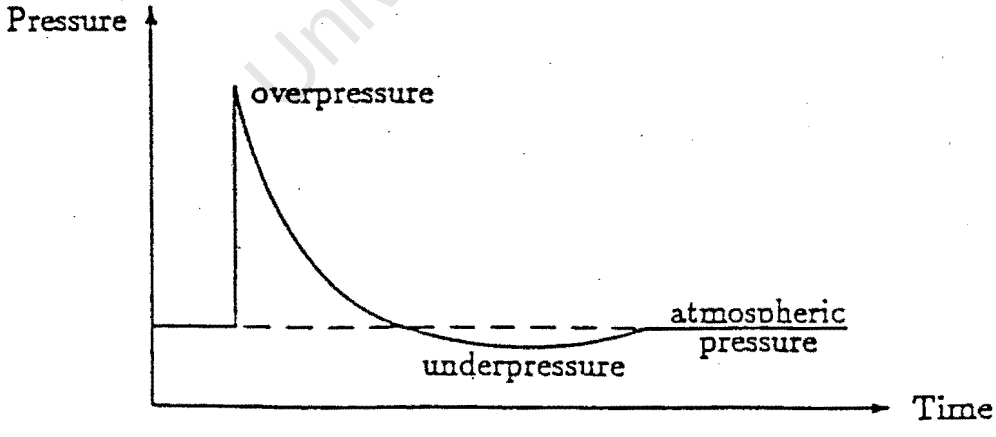

Figure 1.1: Free field blast wave pressure as a function of time [1].

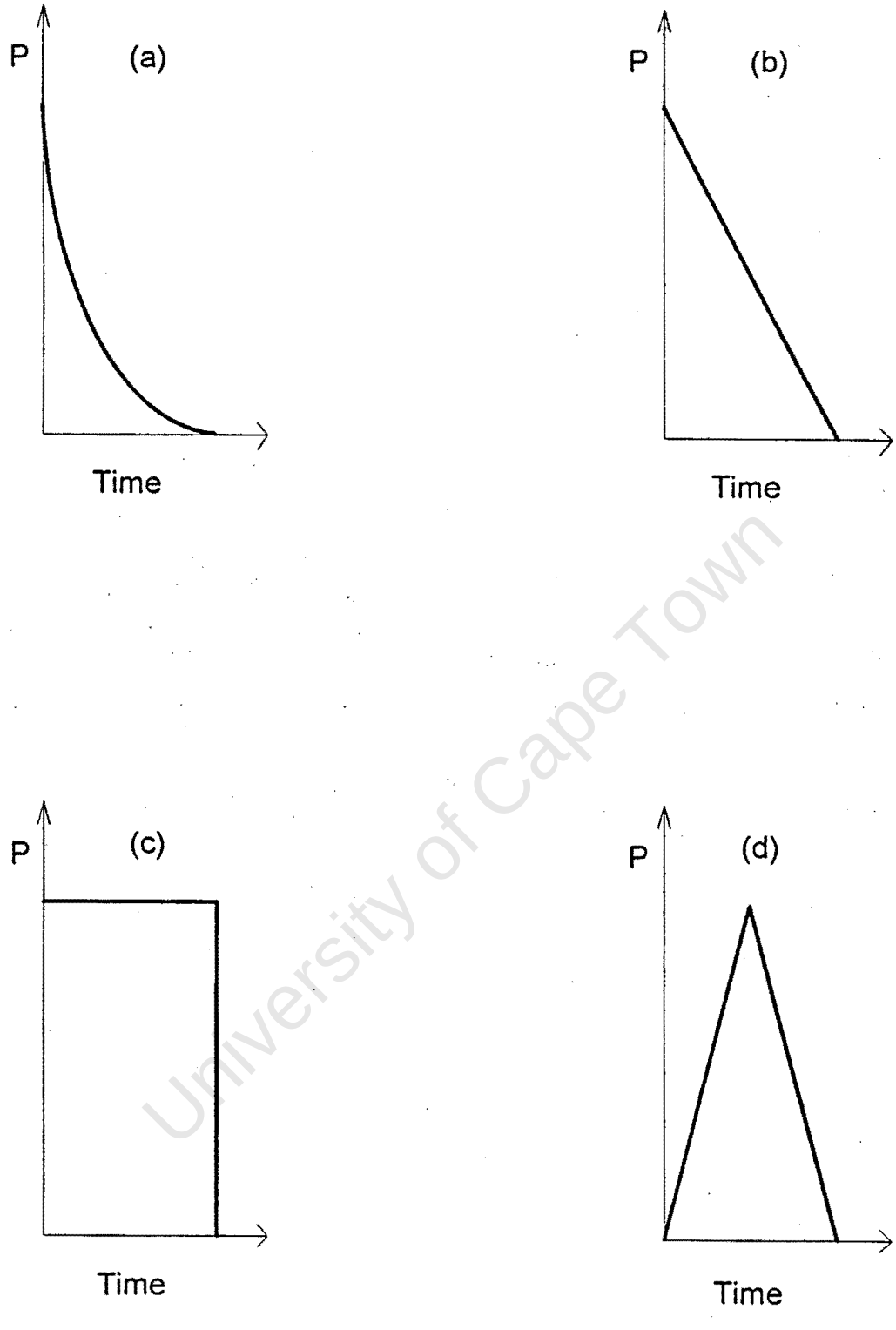

Figure 1.2: Simplified pressure-time loading histories for a typical blast wave [3].

1.2 Structural Response

The study of the structural response of structures subjected to blast loadings has been ongoing for a number of years. Extensive experimental studies have been carried out to understand the large permanent ductile deformations and rupture of beams, plates and shells. The recorded responses of these structural elements have been compared with the responses predicted by analytical and numerical methods. Exhaustive reviews of the work conducted in this field have been published by many researchers

1.2.1 Experimental Studies

Nurick and Martin [4] published a review of the experimental studies carried on the deformation and tearing of thin plates subjected to impulsive loading. Different failure modes were first reported by Menkes and Opat [5] for fully clamped metal beams loaded impulsively who identified and classified the failure modes as Mode I: large inelastic deformation of the entire beam, Mode II; tearing (tensile failure) of the beam material at the supports and Mode III; transverse shear failure of the beam material at the supports. Figure 1.3 shows the three failure modes associated with clamped metal beams. Teeling - Smith and Nurick [6] conducted and reported experiments on fully clamped circular mild steel plates subjected to a uniformly distributed impulse. The strain rate-sensitive plates exhibited Mode I (large ductile deformation), Mode II (tensile-tearing and deformation) and Mode III (transverse shear) failure modes. Threshold velocities for onset of failure Modes II and III were recorded. Nurick and Shave [7] identified three phases of Mode II as Mode II* (partial tearing), Mode IIa (complete tearing with increasing mid-point deformation) and Mode IIb (complete tearing with decreasing mid-point deformation), for clamped mild steel square plates subjected to impulsive loads. Olson, Fagnan and Nurick [8] noted that circular plates do not exhibit Mode IIa.

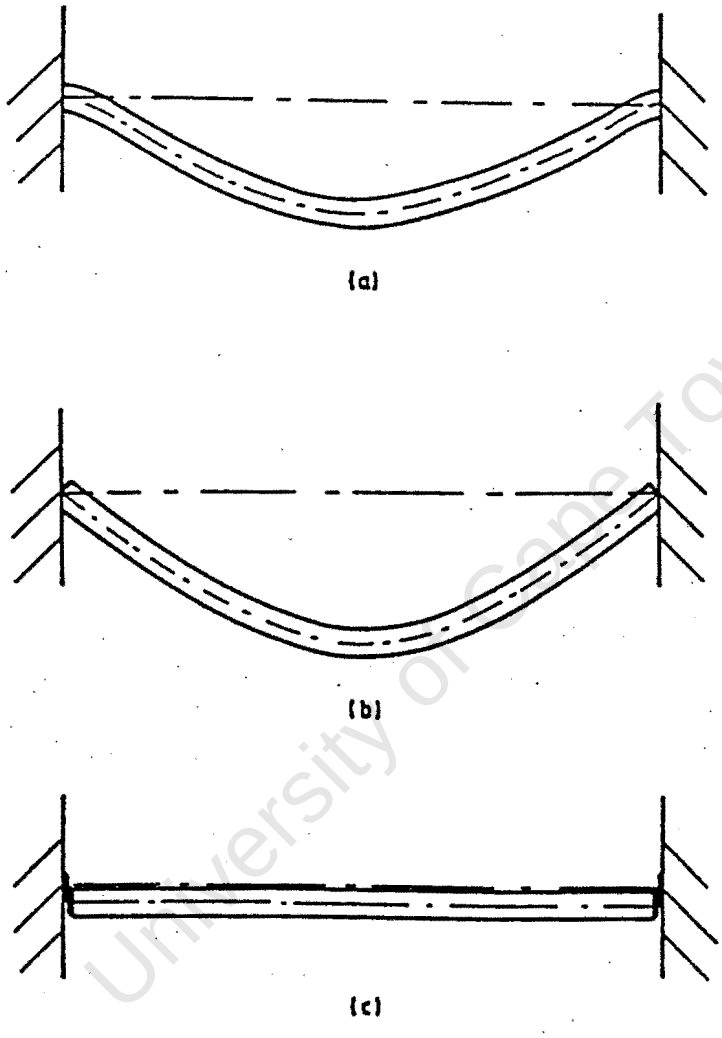

Figure 1.3: Failure modes associated with the clamped metal beams loaded impulsively [5]. (a) mode I, large permanent ductile deformation. (b) mode II, tensile tearing at supports. (c) mode III, transverse shear failure at supports.

An experimental investigation into the effects of edge boundary conditions on the failure of thin plates subjected to impulsive loading was carried out by Thomas [9]. The investigation examined the effects of edge boundary conditions by comparing the results of experiments where the plates were secured by clamping with experiments where the plates are integral with their supports. The results showed that Mode I failure is not affected by the boundary condition while the onset of Mode II failure is and that significant deformation (necking) occurs within the clamped region of the plate before plate rupture.

Radford [10] presented results of an experimental investigation into the dynamic plastic response and failure of clamped thin circular metal plates subjected to localised impulsive loads. It was observed that the plate deflection profiles had nipples at the centre of the plate, with the nipple size being proportional to the load diameter. The plate deformation increased with an increasing impulse up to a point where a cap blew out of the centre of the plate. The cap was also proportional to the load diameter. At higher impulses necking was noted around the nipples for all the load diameters. Necking was also noted at the plate boundary for the higher load diameters.

1.2.2 Theoretical Predictions

An exhaustive review of the theoretical predictions on the deformation of thin plates subjected to impulsive loading was published by Nurick and Martin [11]. The review will not be repeated herein. Instead, a small number of works will be cited.

Jones [12] proposed a rigid-plastic theoretical model that considers the influence of finite displacements. The model accounts for the influence of membrane and bending forces for Mode I and Mode II responses using a square yield criterion. The strain rate sensitivity of the material is taken into account while the influence of material strain hardening is ignored. An approximate theoretical procedure that uses conservation of energy to obtain

solutions for the maximum permanent transverse displacement and response time for a fully clamped circular plate subjected to a uniformly distributed blast loading was adopted. The approximate theoretical procedure gave reasonable agreement with the experimental results in predicting Mode I response. To predict the onset of Mode II failure, equating the maximum strain (obtained by adding the membrane strain to the bending strain) to the static uniaxial rupture strain of the material was proposed. The theoretical predictions of threshold impulses of Mode II response for beams obtained by using the maximum strain concept gave reasonable agreement with experimental results of Menkes and Opat [5]. Shen and Jones [2] also used an approximate theoretical solution that examines the dynamic plastic response and the three failure modes of fully clamped circular plates subjected to uniformly distributed transverse impulsive loads. The rigid-plastic analysis that employs an interaction yield surface which combines the bending moments, membrane forces and the transverse shear forces and includes material strain rate effects was used. Good agreement was obtained between experimental results and the theoretical predictions for Mode I failure. Correlation of theoretical predictions and experimental values of Teeling - Smith and Nurick [6] was poor for Mode II and Mode III failures. It was suggested that the poor correlation was due to inaccurate boundary condition modelling [2]. Li and Jones [13] proposed theoretical solutions for predicting Mode III failure. They investigated, with the aid of the extended Johansen yield criterion that retains the influence of the transverse shear force as well as the bending moments, the dynamic response of a uniformly blast loaded and fully clamped circular plate made from a rigid perfectly plastic strain-rate-sensitive material. No attempt was made to compare the theoretical solutions with experimental values.

It is observed that fewer studies have been reported on the response of circular plates subjected to central blast loading. Symonds and Wierzbicki [14] used the mode approximation technique to obtain the Mode I response of a clamped circular plate subjected to axially symmetric impulsive loading. The mode shapes and accelerations were determined from equations which assume simple membrane action. A rigid-perfectly plastic and strain-rate-sensitive material was assumed. It was assumed that the explosive

imparted a rectangular pressure pulse over the loaded diameter and no attempt was made to model the spread of the pressure pulse outside the loaded diameter. Final deflections and response times were found to be in good agreement with experimental values. It was however observed that the condition of complete edge fixity, as assumed in the theories, was not imposed in the tests where the plate was clamped by bolts. *At the largest impulsive loads, for higher load radius to plate radius ratios, radial slippage occurs and the deflections are underestimated.* Florence [15] also obtained theoretical solutions for a circular plate subjected to a central pressure pulse loading and with plastic yielding controlled by the Johansen yield condition. By assuming that there is movement of plastic hinges towards the centre and the boundary of the plate, predictions were made as to the load radius to plate radius ratio required for the two hinges to reach the centre and outer plate radius simultaneously. This ratio was found to be 0.56 suggesting that simultaneous tearing of the plate will occur at the plate centre and plate boundary for a load to plate radius ratio of 0.56.

Radford [10] also used the mode approximation technique to predict the deformation of and strain in thin metal plates subjected to localised impulsive loads. He proposed a theoretical displacement model for predicting the plate deformation and theoretical strains in the deformed plates. The mid-point displacements and the final plate shape compared well with experimental data. The maximum strain at failure calculated using the theoretical strain model gave good correlation to the uniaxial tensile strain and its position correlated well with the mean cap diameter.

Predictions of shear and bending response of a simply supported strain rate-sensitive and rigid-plastic plate subjected to localised blast loading have been reported by Lui and Stronge [16], however no attempt was made to correlate the predictions with experimental data.

In general, theoretical techniques are based upon assumptions and simplifications and are therefore well suited to the preliminary design of blast loaded structures. However, for a

detailed analysis of blast loaded structures, the finite element method (FEM) can provide a useful tool.

1.2.3 Finite Element Predictions

Major developments in computers and computing have resulted in the finite element method (FEM) becoming widely used in many areas of science and engineering. The analysis of non-linear problems such as the blast response of structures is one area where the use of the FEM is well suited. In fact, general purpose FEM packages that can solve these problems already exist. The development of special purpose FEM programs for use on personal computers to analyse structural impact problems has also been given great attention.

Olson, Fagnan and Nurick [8] used a special purpose program, NAAPFE, to analyse the response of a fully clamped circular plate subjected to a uniformly distributed blast load. The numerical model includes geometrical non-linearity, material non-linearity, strain rate effects and an interaction model for failure which comprises tensile and bending effects and an approximation to shearing. The numerical predictions and experiments showed good comparisons for the failure Modes I, II and III. The same authors used another special purpose FEM program, NAPSSE, to predict the response of fully clamped blast loaded square plates [17]. The finite element formulation incorporates non-linear geometry and material effects as well as strain rate sensitivity. Onset of Mode II failure was predicated by a maximum strain criterion. Mode I was predicted well for both maximum deflection and deformation shape. The Mode II failure prediction correlated reasonably well with the experimental results. Onset of Mode III was not predicted since the finite element formulation did not incorporate shear effects. NAPSSE also successively predicted the deformation (Mode I) and Tearing (Mode II) of blast-loaded stiffened square plates [18]. No attempt was made to use NAAPFE or NAPSSE for plates subjected to central blast loading.

Radford [10] attempted to use ABAQUS a general purpose finite element code to investigate the response of a clamped circular plate subjected to central blast loading. The finite element model assumed that the pressure applied by the explosive acted over the load area only, and no attempt was made to model its spread. The impulses required for numerical stability of the finite element solution were lower than those from the experiments hence no comparison between the model results and experimental data were made.

1.3 Purpose and Scope of the Present Study

The purpose of this study is to investigate the response of thin circular plates subjected to a central blast load. The investigation will be carried out using the numerical analysis of the general purpose ABAQUS/EXPLICIT finite element code [19]. The available experimental data [10] will be used to obtain an empirical load distribution function to model the spread of a central blast load. The effects of boundary conditions on the deformation and rupture of the plates will be explored. The finite element model predictions will be compared to previously reported analytical, numerical and experimental results.

Chapter 2

Finite Element Model

2.1 Finite Element Analysis Procedure

The ABAQUS program offers a finite element capability that provides non-linear dynamic analysis for a variety of solid and structural elements using an explicit time integration scheme. The explicit procedure uses the central difference operator to integrate through time by using small time increments with the use of lumped element mass matrices. The scheme is conditionally stable and the stability limit for the operator (with no damping) is given as [19]

$$\Delta t \leq \frac{2}{\omega_{\max}}, \tag{2.1}$$

where $\omega_{\max}$ is the highest element frequency.

With damping, the stable time increment limit is modified to

$$\Delta t \leq \frac{2}{\omega_{\max}}\left(\sqrt{1+\xi^2}-\xi\right), \tag{2.2}$$

where ξ is the fraction of critical damping. The fraction is greater than unity for an overdamped system and is less than unity for an underdamped system.

In ABAQUS the time incrementation scheme in the explicit procedure is automated and is

calculated using the highest element frequency to determine the stability limit. The stability limit can be rewritten (ignoring damping) in the form [19].

$$\Delta t \leq \min\left(L^{el} \sqrt{\frac{\rho}{\lambda + 2\mu}} \right), \tag{2.3}$$

where the minimum is taken over all elements in the mesh and L^{el} is a characteristic element length, ρ is the density of the material in the element, and λ and μ are the effective Lame's constants for the material in the element. This effectively means that the time increment can be no larger than the time required to propagate a stress wave across the 'critical' element. If the model contains only one material type, the stable time increment is directly proportional to the size of the smallest element in the mesh. If the mesh contains uniform size elements, the stable time increment remains constant and the number of time increments required in running a simulation will be directly proportional to the time of an event (impact duration) being simulated. For thin circular plates subjected to central blast loading, local instabilities form at the loaded edges and the stable time increment requires the use of a large number of time increments. To achieve stability the sizing of the elements in the mesh is important.

Farrow, Nurick and Mitchell [20] obtained satisfactory results using a 40 axisymmetric element mesh to model a 100mm diameter plate subjected to a uniformly distributed blast load with convergence of the solution taking place for a mesh of 4 elements. With the introduction of localised loading conditions, more elements are required to obtain numerical stability of the solution. Radford [10] used 400 axisymmetric elements to achieve numerical stability for an impulse of 1 Ns applied over a load diameter to plate diameter ratio of 0.183. To achieve numerical stability in modelling the experiments of Radford [10] 1000 axisymmetric elements were used in the present study.

2.2 Finite Element Formulation

The SAXI [19] one-dimensional axisymmetric element that deforms in the radial plane was used in the present study. The Cartesian co-ordinates in this plane are 1 (radial) and 2 (axial position). Figure 2.1 shows the SAXI axisymmetric shell element description.

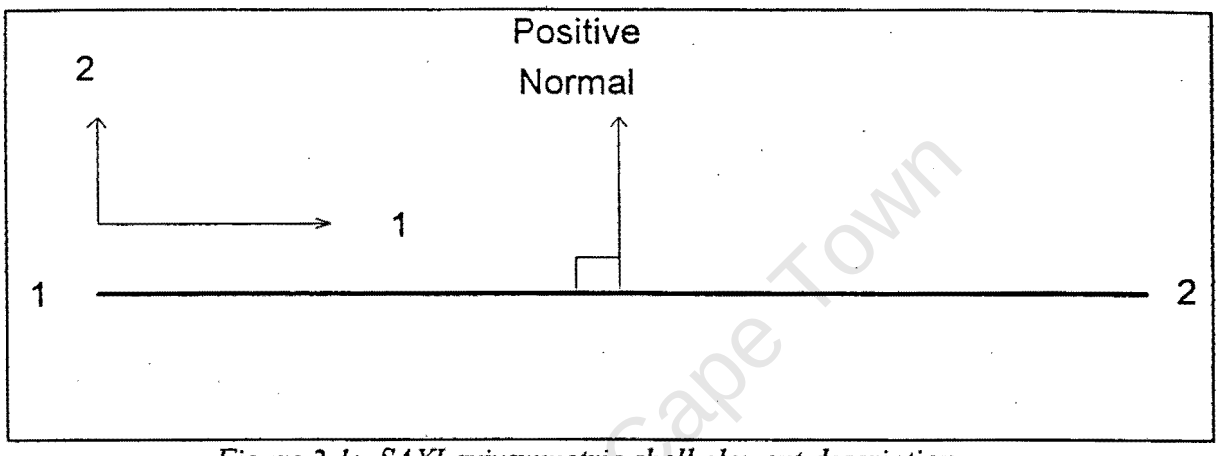

Figure 2.1: SAXI axiysmmetric shell element description.

The 2-node element (SAXI) uses one point Gaussian integration of the linear interpolation function for the distribution of loads. The SAXI axisymmetric shell element is "shear flexible", i.e., transverse shear deformation is allowed [21]. It uses thick shell theory (plane sections remain plane after deformation) as the shell thickness increases and becomes a Kirchhoff thin shell as the thickness decreases. This shell theory allows for finite strains and rotations of the shell and is intended for direct application to cases involving inelastic deformation where the stress-strain behaviour is given in terms of "true" stress and log strain, such as metal plasticity [21]. The membrane, bending and transverse shear strains are calculated at five places through the thickness at a central point per element. The change in shell thickness as a result of membrane strain (stretching) is taken into account in the theory. The through thickness stress is neglected (plane stress assumption). To prevent occurrence of spurious (hourglass) displacement patterns the theory uses the "reduced-integration penalty" method of Hughes et al. [22].

The geometry, physical properties and the loads of the circular plate subjected to central blast loading are axisymmetric making it efficient to use the axisymmetric shell elements in the model. The cost of analysis is reduced due to fewer elements being needed to model the plate, and meshes are easy to design. To achieve numerical stability of the analysis a uniform mesh with 1000 axisymmetric shell elements was used in the model. A typical axisymmetric element mesh is shown in Figure 2.2.

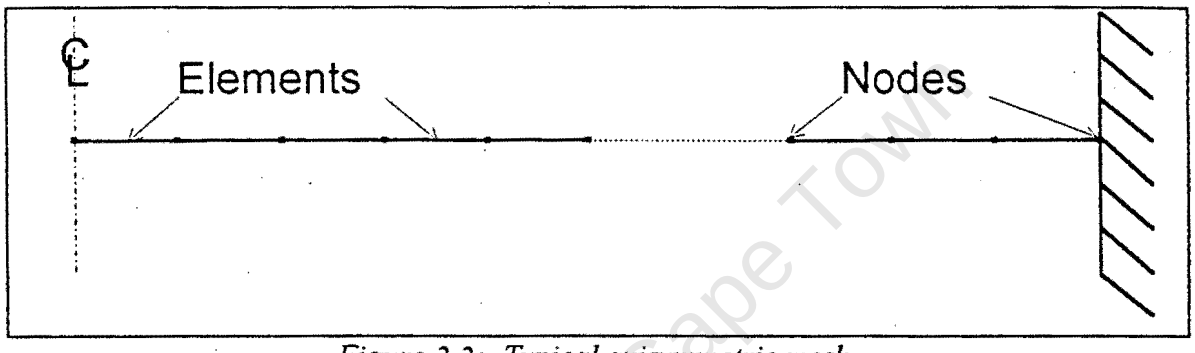

Figure 2.2: Typical axisymmetric mesh.

2.3 Material Modelling

ABAQUS offers several mechanical constitutive models to describe the behaviour of a wide variety of materials commonly encountered in stress analysis problems. For blast loaded thin steel plates a suitable constitutive model to describe the material's behaviour is the metal elasto-plasticity model that has a rate dependent option, a Mises yield surface criterion option and an isotropic hardening option.

The rate dependent model that is intended for relatively high strain rate applications, such as dynamic events, was used in the present analysis. Strain rate effects are included by

adjusting the static yield stress σ_0 at each Gauss point according to the Cowper-Symonds relation [21]

$$\dot{\bar{\varepsilon}}^{pl} = Q\left(\frac{\bar{\sigma}}{\sigma_0} - 1\right)^p, \qquad \text{for } \bar{\sigma} \geq \sigma_0 \qquad (2.4)$$

where $\dot{\bar{\varepsilon}}^{pl}$ is the equivalent plastic strain rate, $\bar{\sigma}$ is the yield stress at non-zero plastic strain rate, σ_0 is the static yield stress, and Q and p are material parameters. The commonly accepted values of the strain rate material parameters for steel are $Q = 40.4s^{-1}$ and $p = 5$; and are the values chosen in the present work. The model assumes that the shapes of the hardening curves at different strain rates are identical but this can be changed to include different hardening curves for specific strain rates [21].

The ABAQUS/Explicit ductile failure model which provides a simple failure criterion that is designed to allow the stable removal of elements from the mesh as a result of tearing of the structure was included in the model [19]. Elements will automatically be deleted from the mesh as they exceed the failure criteria. The failure model is based upon the value of the equivalent plastic strain. When the equivalent plastic strain at a material point reaches the plastic failure strain, $\bar{\varepsilon}_p^f$, the material point is assumed to have failed. If all the material points in the element fail, the element is removed from the mesh. The failure model is based on a damage Mises plasticity theory with isotropic hardening [19]. The material behaves as an elastic material until the initial yield stress, σ_0, is reached. Plastic strain then occurs following the Mises plasticity theory. If the strain continues to increase, damage will accumulate from zero once the plastic strain reaches the offset plastic strain, $\bar{\varepsilon}_0^{pl}$, to a value of one when the plastic strain reaches the plastic failure strain, $\bar{\varepsilon}_f^{pl}$, and the corresponding total strain $\bar{\varepsilon}_f$.

The damage is calculated from the equivalent plastic strain according to the following

relation [19]:

$$D = \frac{\bar{\varepsilon}^{pl} - \bar{\varepsilon}_0^{pl}}{\bar{\varepsilon}_f^{pl} - \bar{\varepsilon}_0^{pl}}, \tag{2.5}$$

where $\bar{\varepsilon}^{pl}$ is the current equivalent plastic strain experienced by the material. Figure 2.3 illustrates the stress/strain behaviour of the material model.

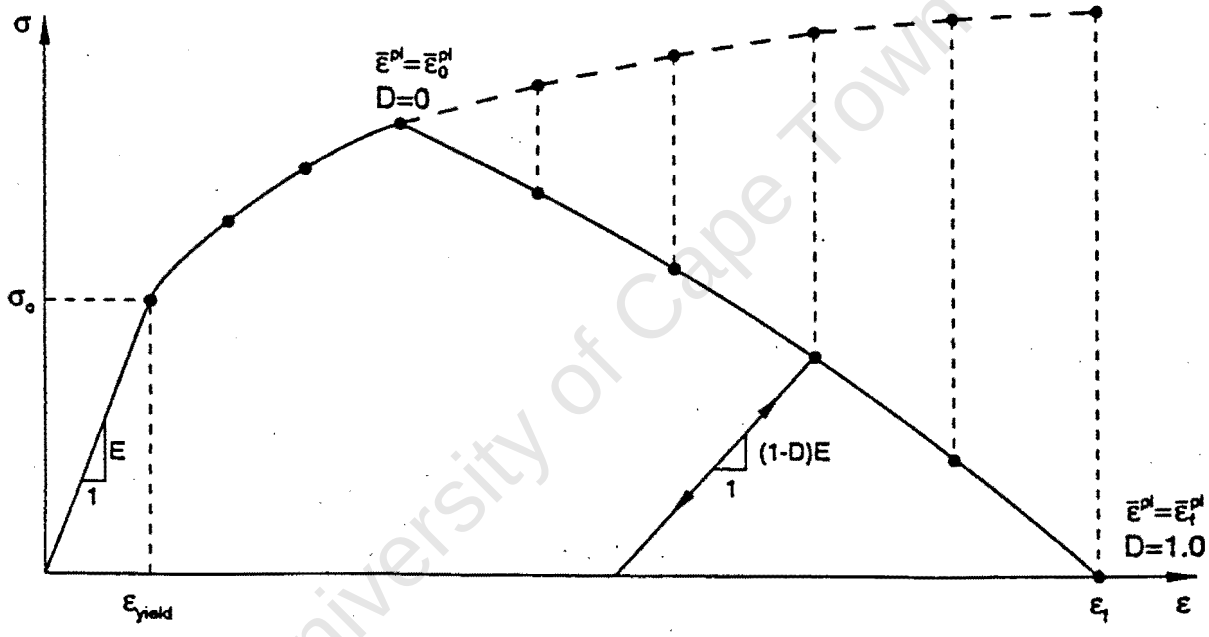

Figure 2.3: Stress-strain curve using the ductile failure model [19].

All the material properties and parameters used in the present model are assumed to be independent of temperature. This assumption is due to lack of quantification of temperature changes in experimental work.

The material properties used in most of the calculations are: elastic modulus, E=210GPa; density, ρ=7830Kgm^{-3}; Poisson's ratio, ν=0.33; static yield stress, σ_0=194MPa; plastic

failure strain, $\bar{\varepsilon}_f^{pl}$=0.30; offset plastic strain, $\bar{\varepsilon}_0^{pl}$=0.15; and the true stress versus true strain plot shown in Figure 2.4. The material properties are for the test specimens of Radford [9].

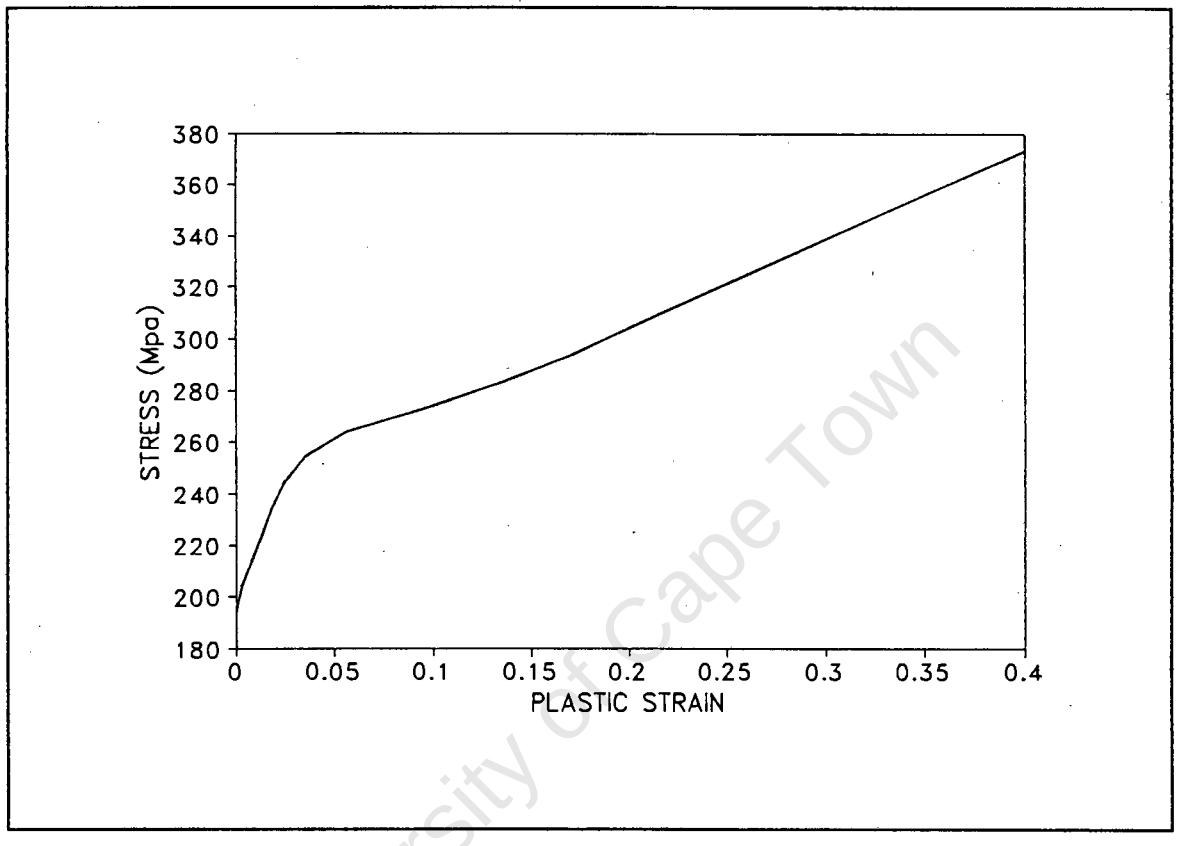

Figure 2.4: Material hardening curve at zero plastic strain rate.

2.4 Boundary Conditions Modelling

The effects of different boundary conditions on the response of centrally blast loaded thin circular plates are explored by looking at two cases.

The first case assumes complete edge fixity, which correspond to a fully built-in boundary

(see Figure 2.6a). The edges are constrained in all translational and rotational degrees of freedom by constraining the outer nodes of the boundary elements in all the active degrees of freedom. The active degrees of freedom are 1, 2 and 6 (u_r, u_z *and* θ) corresponding to the R and Z translational and the R-Z rotational degrees of an element node respectively (see Figure 2.5) [19].

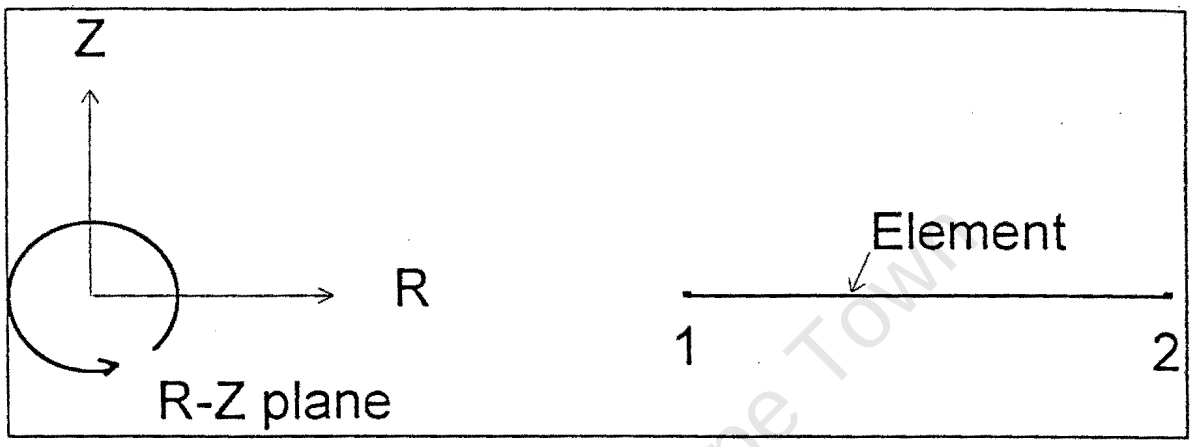

Figure 2.5: Sign convention and node numbering for SAXI axisymmetric shell elements.

The second case is an idealisation of a plate clamped by bolts. In this condition, radial slippage occurs (see Figure 2.6b). The plate is constrained in all the active degrees of freedom of nodes along the line of bolts and is unconstrained in all but one of the active degrees of freedom of nodes along the inner edge of the plate. The inner edge is free to translate in the radial direction and rotate in the R-Z plane. The idealisation is intended to only obtain a general understanding of the effects of clamping on the response of the plates. Detailed modelling of a boundary condition where plates are secured by clamping is beyond the scope of this study; the subject is currently receiving considerable research effort [9, 13]. However, the results from tests where the plate is secured by clamping and radial slippage does not occur [10] are expected to be bounded by the predictions of the two cases modelled in the present study. Figure 2.7 shows picture plots of the undeformed models with the boundary conditions plotted in. Plot (a) is for a fully built-in plate while plot (b) is for a clamped plate.

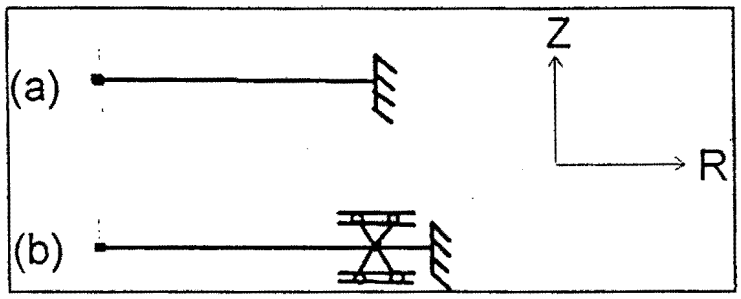

Figure 2.6: Edge boundary conditions used in the model.

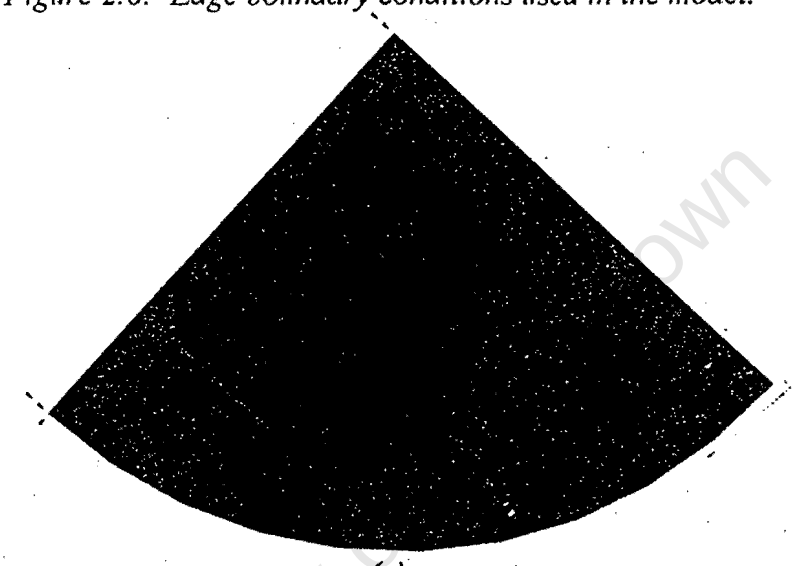

(a)

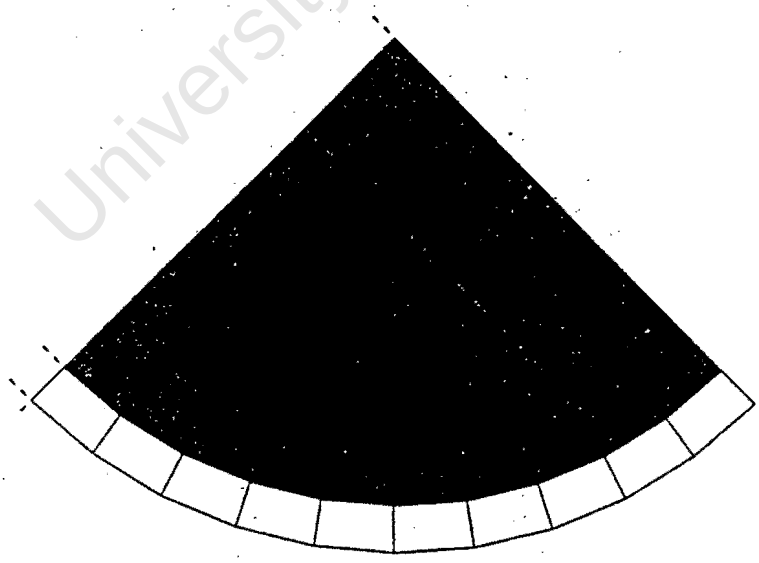

(b)

Figure 2.7: ABAQUS plots of the undeformed models.

2.5 Loading Conditions Modelling

Loads imposed as a result of an explosion are complex. Deriving an accurate spatial distribution function of pressure due to a central blast load over a plate is difficult. Assumptions have to be made to obtain a load distribution function to use in the analyses. In the present study the explosive pressures are due to detonation of explosive sheets. The centrally located sheets were spread evenly onto a polystyrene foam pad over differing circular areas of radius '*a*'. The load configuration is illustrated in Figure 2.8.

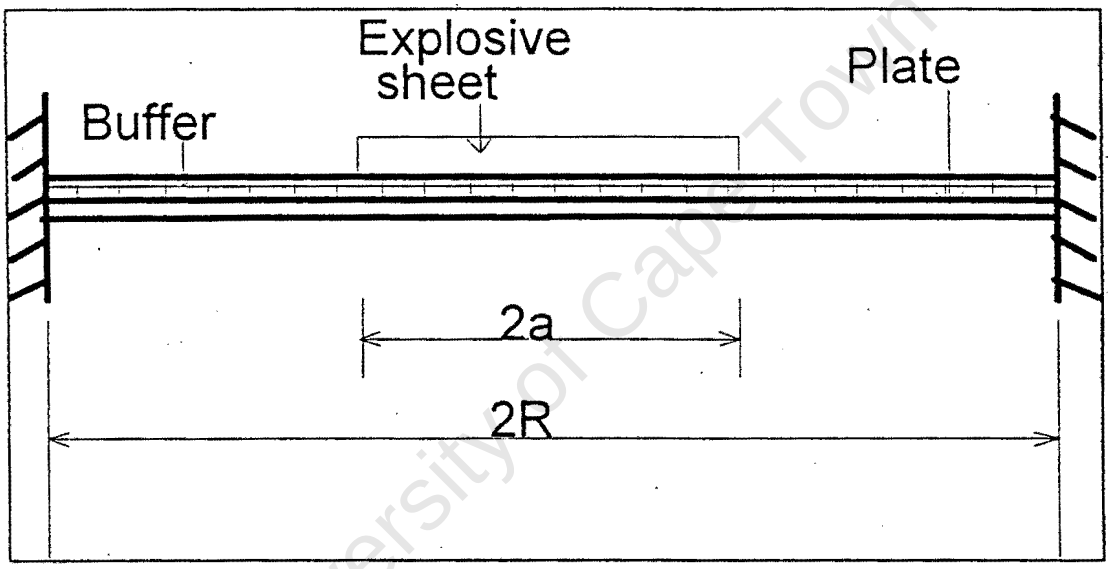

Figure 2.8: Load configuration.

For each loaded area the total impulse I was measured by a ballistic pendulum [10]. For loading over a given radius it is assumed the imparted pressure is uniform over the loaded area and decays exponentially to the plate boundary. The relation between measured impulse I and the imparted pressure is

$$I = \tau \int_0^R P(r) dA \qquad (2.6)$$

where τ is the duration of the loading and $P(r)$ is a pressure distribution function. The above relation is for a rectangular pressure pulse. (See Figure 1.2(c)).

If the imparted pressure is taken as

$$P_0 = \text{Constant} \qquad \text{for } r \leq a \qquad (2.7a.)$$

and

$$P(r) = P_0 e^{-k(r-a)} \qquad \text{for } a \leq r \leq R \qquad (2.7b)$$

where k is the exponential decay constant. Equation 2.6 can now be written as

$$I = \tau \int_0^a P_0 dA + \tau \int_a^R P_0 e^{-k(r-a)} dA \qquad (2.8a)$$

which becomes

$$I = \tau \int_0^a 2\pi r P_0 dr + \tau \int_a^R 2\pi r P_0 e^{-k(r-a)} dr \qquad (2.8b)$$

where $dA = 2\pi r dr$. After integration, the first term $I^{(1)}$ becomes

$$I^{(1)} = \left[\tau \pi r^2 P_0\right]_0^a$$

The second term $I^{(2)}$ is obtained by partial integration using the relation

$$\int UdV = UV - \int VdU$$

Now, considering the term

$2\pi\tau P_0\int_a^R re^{-k(r-a)}dr$ Let $U = 2\pi\tau rP_0$ *and* $dV = e^{-k(r-a)}dr$

Then $dU = 2\pi\tau P_0 dr$ *and* $V = -\frac{1}{k}e^{-k(r-a)}$

Then, after using the partial integration relation, $I^{(2)}$ becomes

$$I^{(2)} = \left[-\frac{2\pi\tau rP_0}{k}e^{-k(r-a)}\right]_a^R + 2\pi\tau P_0\int_a^R \frac{1}{k}e^{-k(r-a)}dr$$

Which, after evaluating and re-arranging becomes

$$I^{(2)} = 2\pi\tau P_0\left[\left(\frac{a}{k}+\frac{1}{k^2}\right)-\left(\frac{R}{k}+\frac{1}{k^2}\right)e^{-k(R-a)}\right]$$

The relation between measured impulse I and the imparted presssure is now obtained by summing $I^{(1)}$ and $I^{(2)}$. The result is

$$I = \pi\tau P_0\left[a^2 + 2\left\{\left(\frac{a}{k}+\frac{1}{k^2}\right)-\left(\frac{R}{k}+\frac{1}{k^2}\right)e^{k(a-R)}\right\}\right] \qquad (2.8c)$$

From Equation 2.8c if a=R, a case where the explosive sheet spreads uniformly over the whole plate, the result is

$$I = \pi\tau P_0 a^2 \qquad (2.9)$$

a relation which is widely used for a blast loading distributed uniformly over the entire area of a plate [8,12,13,17,18,2].

Given the impulse I, to obtain P_0 from Equation 2.7, the duration of the loading τ and

the decay constant k must be known. The duration of the loading is estimated from

$$\tau = \frac{a}{V_b} \tag{2.10}$$

where the speed of detonation of the explosives V_b is 6500-7500m/s [8,10,17,18,20] and a is the radius over which the explosive sheets are spread. The assumption that the duration of the loading τ is equal to the approximate explosive burn time has been adopted widely in explosively loaded plate analysis problems [8,12,13,17,18,2].

The experimental results of Radford [10] were used to develop a relationship for obtaining a decay constant for a given load configuration. At first, a relationship between the slope of the S (deflection versus impulse) linear plots (for impulses that causes permanent deformation without rupture), and $\frac{a}{R}$, the ratio of the load radius to plate radius, was obtained. The relationship was obtained from fitting a quadratic polynomial through the slopes of the S linear plots (obtained from fitting linear polynomials on the experimental data for mid-point deflections) for

$\frac{a}{R}$	0.183	0.250	0.330	0.400	1.000

Figure 2.9 shows the S linear plots used to develop the relation. The relation is

$$\frac{\delta}{I} = 3.21 - 2.29\left(\frac{a}{R}\right) + 0.519\left(\frac{a}{R}\right)^2 \tag{2.11}$$

where; δ is the mid-point deflection, I is the total impulse, a is the explosive sheet radius and R is the plate radius. The plot of the the relation is shown in Figure 2.10. The relation can be used to predict the mid-point deflection for $\frac{a}{R}$ between 0.400 and 1.00; a range where experimental data is not available.

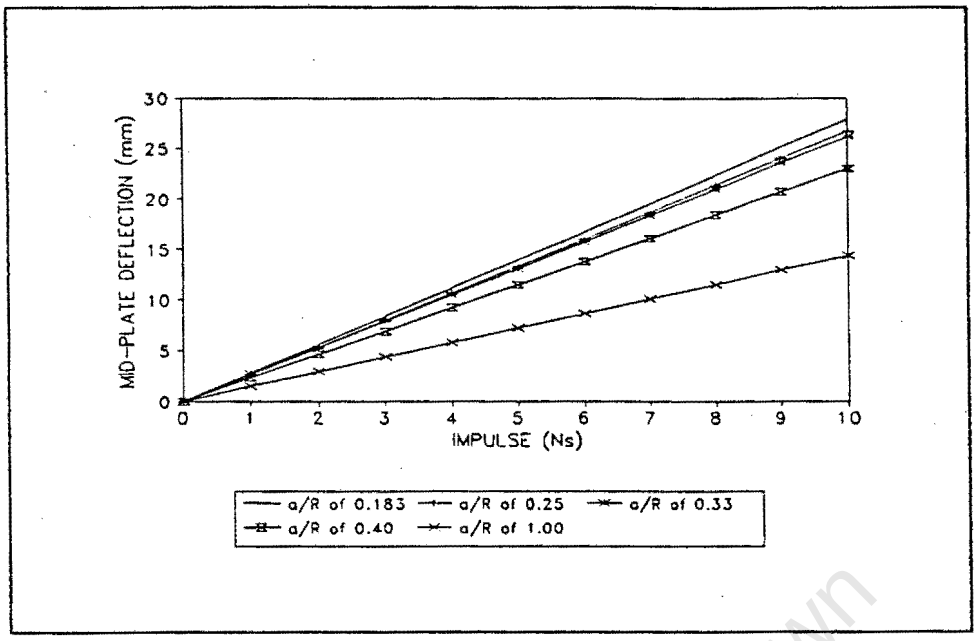

Figure 2.9: Deflection vs impulse. (The experimental data lie within the 90% confidence interval [23] bounding the linear curves).

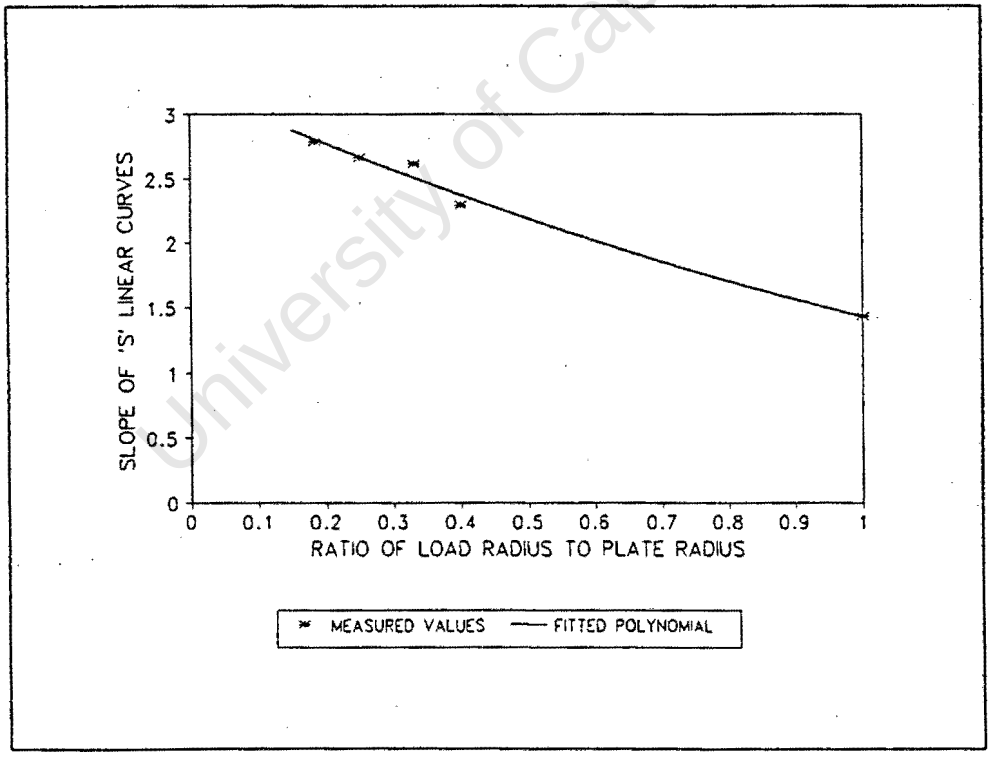

Figure 2.10: Variation of $\frac{\delta}{I}$ *with* $\frac{a}{R}$.

To then obtain a relationship between the decay constant k, and the ratio of the load radius to the plate radius $\frac{a}{R}$, a range of values of k were chosen for use in Equations 2.7 and 2.8. The corresponding pressure distributions were used in the model to obtain mid-point deflections for a range of $\frac{a}{R}$. The results from the model were compared to the experimental data for

$\frac{a}{R}$	0.183	0.250	0.330	0.400

and were compared to the predictions of Equation 2.11 for

$\frac{a}{R}$	0.450	0.500	0.600

which is a range where experimental data is not available.

A value of the decay constant giving the best correlation for a given loaded diameter was then chosen. A quadratic polynomial was fitted through the chosen decay constants to obtain a relationship between the decay constant k and the ratio of the loaded radius to the plate radius $\frac{a}{R}$. The fitted polynomial is

$$k = 130 - 261\left(\frac{a}{R}\right) + 948\left(\frac{a}{R}\right)^2 \qquad (2.12)$$

and was derived for the range

$$0.15 < \left(\frac{a}{R}\right) < 0.6$$

Figure 2.11 shows a plot of the relationship between k and $\frac{a}{R}$ and upper and lower values of k corresponding to the 90% confidence interval [23] and Appendix A shows the affects of varying the decay constant on the predictions of the final mid-point displacement.

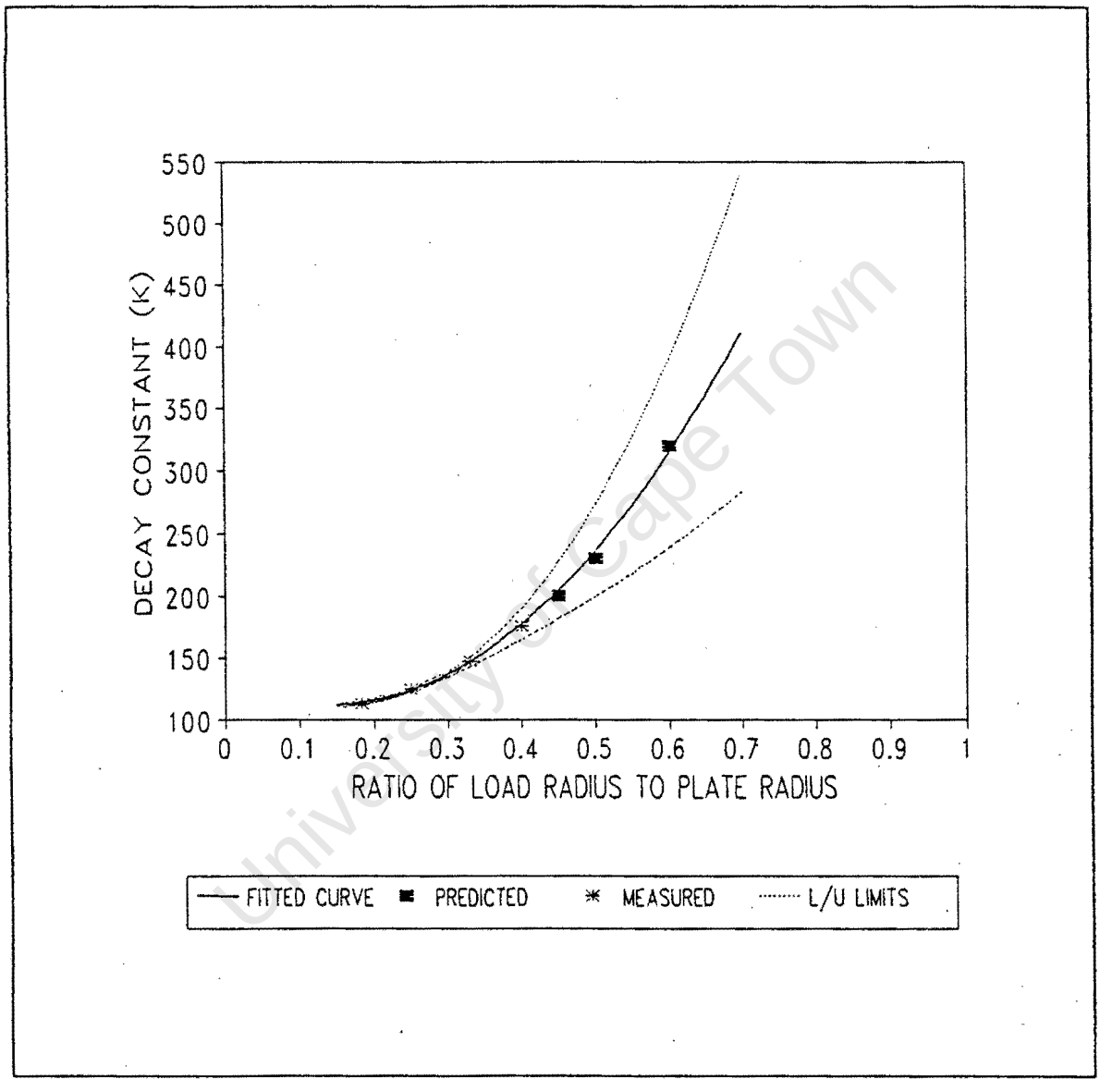

Figure 2.11: Variation of the decay constant k with the $\frac{a}{R}$.

Appendix B shows typical pressure distribution profiles used in the present study. The profiles are obtained from Equation 2.7 as detailed in this section.

Chapter 3

Results and Comparisons

In this chapter the ABAQUS finite element code predictions of the response of thin circular plates subjected to central blast loading are presented. The predictions are for permanent mid-plate deflection, permanent plate deformation shape, response time, residual strains, strain rate sensitivity influence factors and plate tearing. The predictions are compared with results (experimental and analytical) reported in [10] and with theoretical predictions reported in other works.

3.1 Permanent Mid-Plate Deflection

The permanent mid-plate deflection of a plate is the commonly used parameter for comparison of results. In this section predictions of the final mid-point deflections are given for a range of loaded diameters subjected to impulsive pressures that cause large deformations without rupture. The predictions are for a material that does not include a failure criterion and are for fully built-in (fixed) and clamped (where radial slippage occurs) plates. Results presented are for

$\frac{a}{R}$	0.183	0.250	0.330	0.400	0.500	1.000

Figure 3.1 shows typical plots of the variation of permanent mid-plate deflection with impulse for fixed and clamped plates.

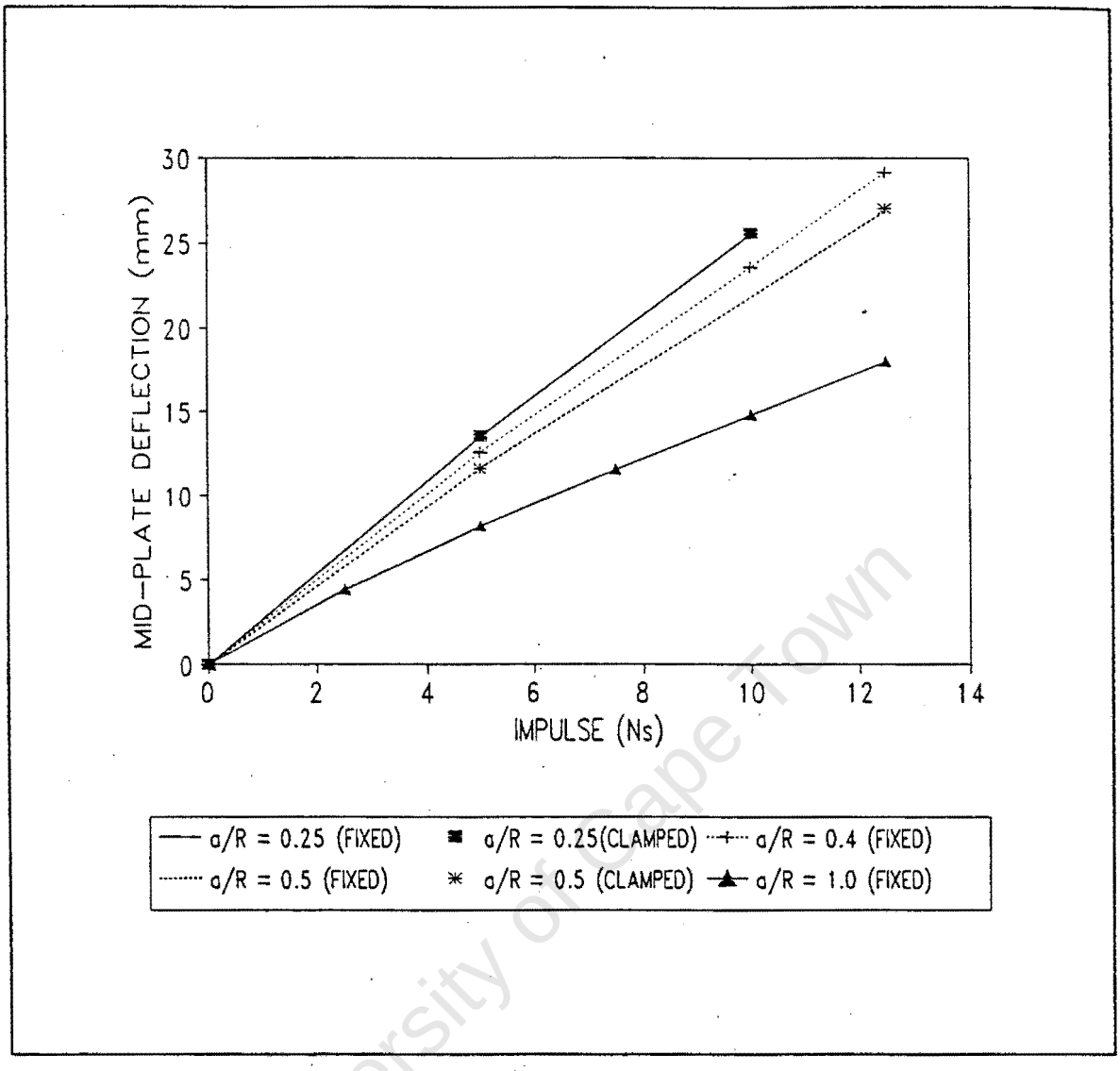

Figure 3.1: Predicted permanent mid-plate deflection as a function of impulse.

The deflections increase almost linearly with increasing impulse and, for a given impulse, the deflections decrease with increasing $\frac{a}{R}$. The difference in the predicted mid-plate deflection between plates secured by clamping and plates that are integral with their supports is insignificant. Results of an experimental investigation on effects of edge boundary conditions carried out by Thomas [9] for $\frac{a}{R} = 1.00$ also showed that the large inelastic deformation response of clamped plates and fully built-in plates is practically the same.

In Figure 3.2, the present permanent mid-plate deflection predictions are compared with analytical (for cubic shape functions) and experimental results reported in [10].

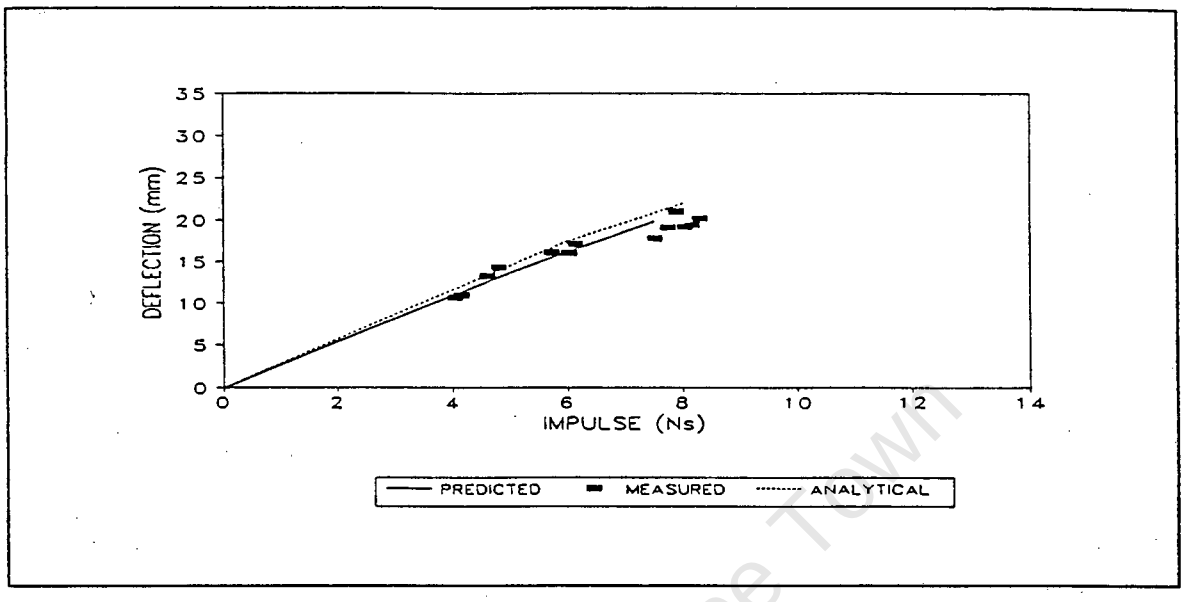

$$\frac{a}{R} = 0.183$$

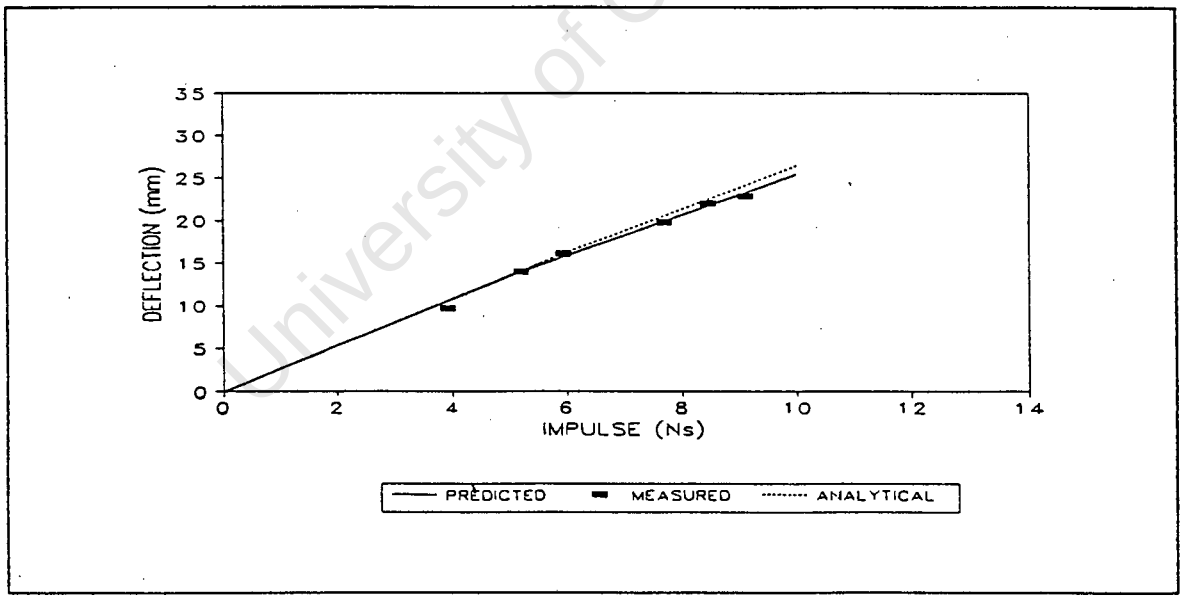

$$\frac{a}{R} = 0.250$$

Figure 3.2: Comparison between predicted and reported [10] variation of permanent mid-plate deflection with impulse.

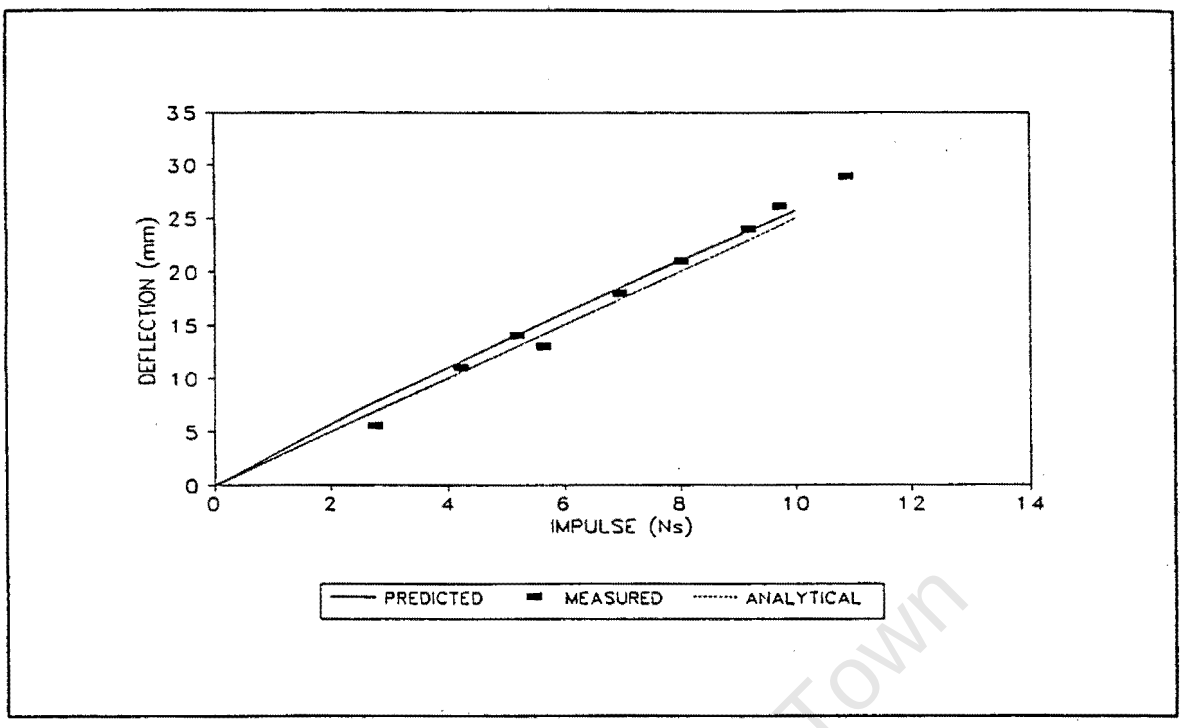

$$\frac{a}{R} = 0.330$$

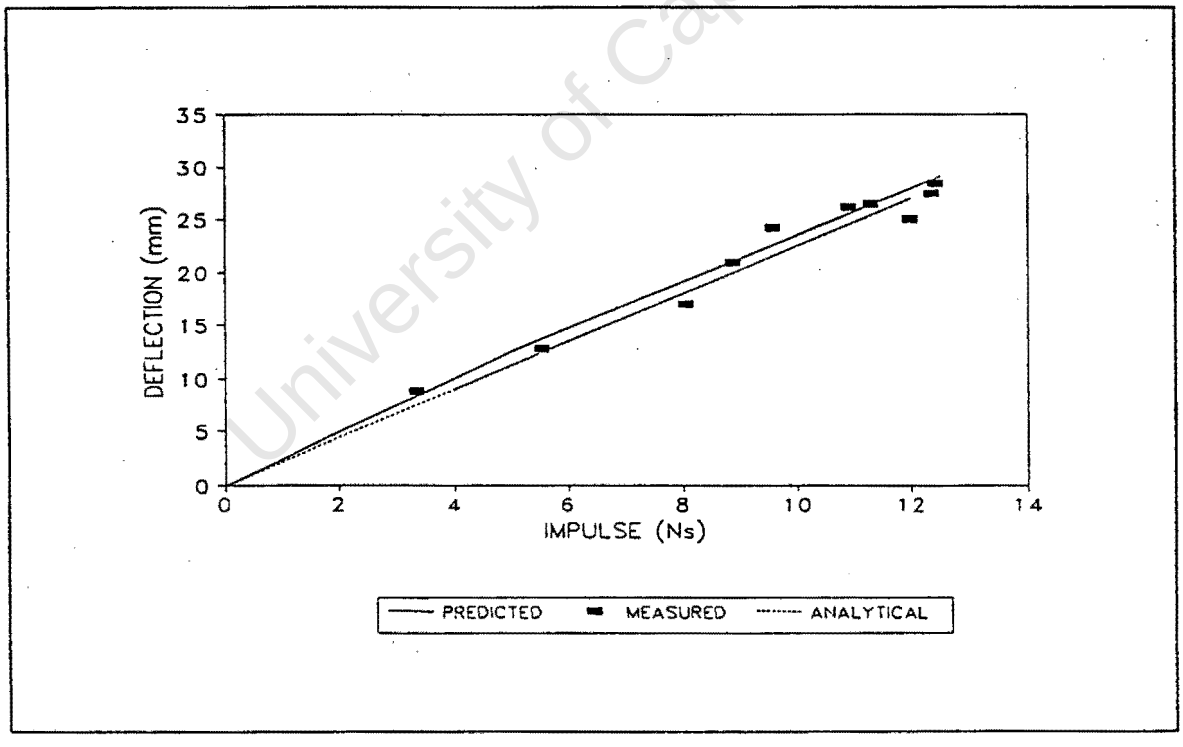

$$\frac{a}{R} = 0.400$$

Figure 3.2: continued.

The predicted deflections are for fully built-in plates while the reported values are for clamped plates; there is no difference in the predicted deflections between a clamped and a fixed boundary. The predictions show good correlation with the reported values.

Symonds and Wierzbicki [14] used a membrane mode solution for predicting the final mid-plate deflection for a centrally blast loaded plate fully clamped at the boundary. The predictions are obtained from solutions to relations tabulated below:

$\frac{a}{R}$	$\frac{1}{3}$	$\frac{1}{2}$	1
W_f	$0.4527\frac{I}{RH\sqrt{\rho\bar{\sigma}}}$	$0.4077\frac{I}{RH\sqrt{\rho\bar{\sigma}}}$	$0.2120\frac{I}{RH\sqrt{\rho\bar{\sigma}}}$

Table 3.1: Relations for predicting permanent mid-plate deflections for centrally blast loaded fully clamped circular plates.

where W_f is the final mid-point deflection, I is the total impulse, R is the plate radius, H is the plate thickness, ρ is the mass density and $\bar{\sigma}$ is the flow stress.

The effect of rate dependence is calculated by equating the predicted average strain rate (which is obtained from relations given in the table below)

$\frac{a}{R}$	$\frac{1}{3}$	$\frac{1}{2}$	1
$\dot{\bar{\varepsilon}}_{avg}$	$0.2445\frac{I^2}{R^5H^2\sqrt{\rho^3\bar{\sigma}}}$	$0.1183\frac{I^2}{R^5H^2\sqrt{\rho^3\bar{\sigma}}}$	$0.0537\frac{I^2}{R^5H^2\sqrt{\rho^3\bar{\sigma}}}$

Table 3.2: Relations for predicting average strain rates for centrally blast loaded fully clamped circular plates.

and the Cowper-Symonds relation [Equation 2.4] to give

$$\frac{I^2}{R^5.H^2.\sqrt{\bar{\sigma}.\rho^3}} = 40\left(\frac{\bar{\sigma}}{\sigma_o} - I\right)^5 \qquad (3.1)$$

from which the flow stress $\bar{\sigma}$ is calculated using an iterative procedure. The present predictions are compared to the membrane mode solutions in Figure 3.3.

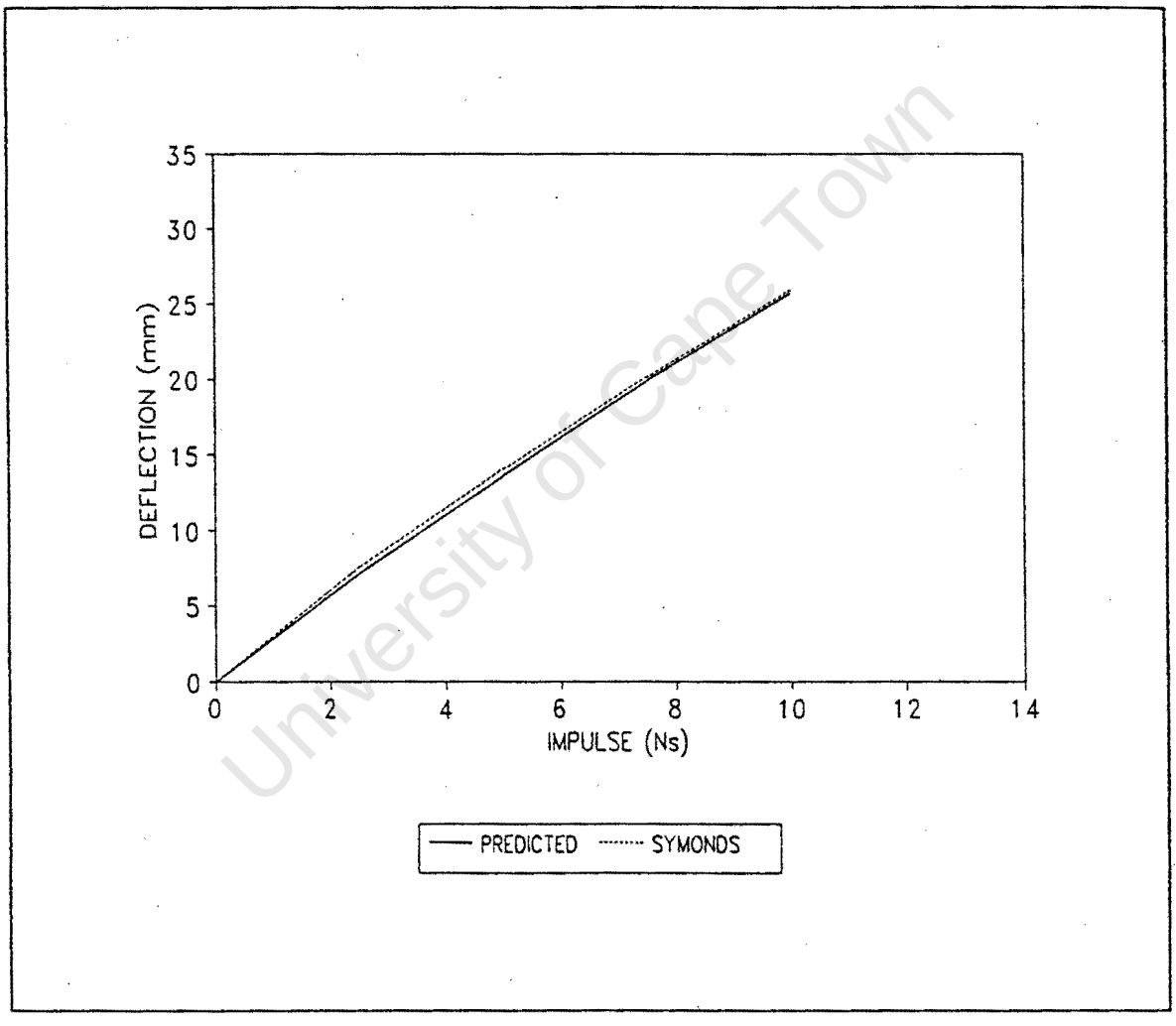

$$\frac{a}{R} = 0.33$$

Figure 3.3: Comparison between present and theoretical predictions [14] of the variation of permanent mid-plate deflection with impulse.

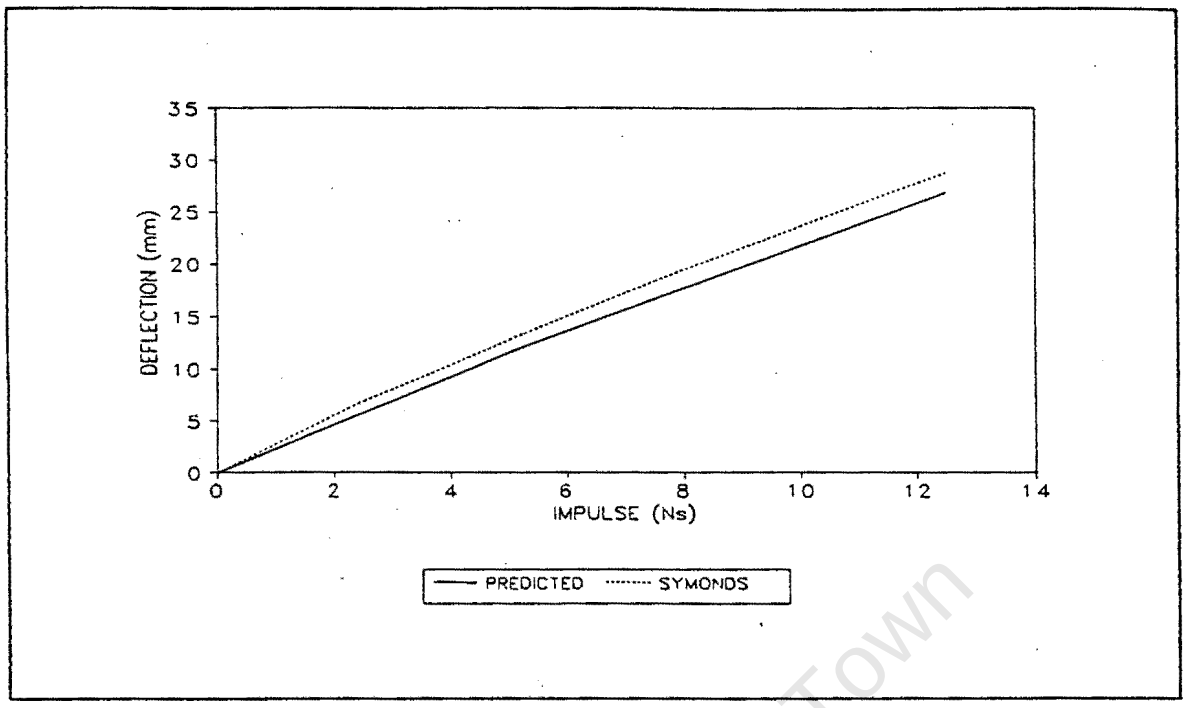

$$\frac{a}{R} = 0.50$$

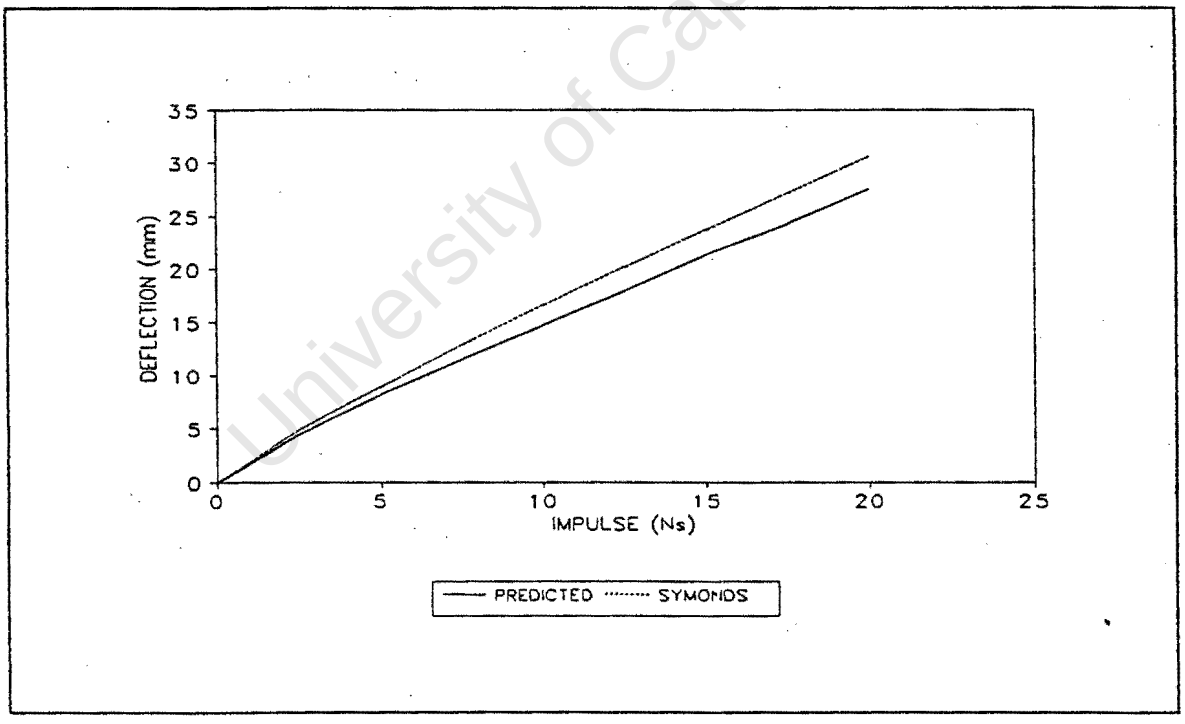

$$\frac{a}{R} = 1.0$$

Figure 3.3: continued.

Good correlation exists for $\frac{a}{R}$ = 0.33 while for $\frac{a}{R}$ = 0.5, the membrane mode solution gives slightly higher (one plate thickness) mid-point deflection predictions. For $\frac{a}{R}$ = 1.0, the difference in the results approaches two plate thicknesses for higher impulses. It is thought that the difference is due to assuming, in the membrane solution, a rigid-plastic material model (that ignores the influence of material strain hardening) and an average strain rate for the whole plate. These assumptions result in the analytical solutions underestimating the material stiffness.

Jones [12] proposed an approximate theoretical procedure for predicting the maximum permanent transverse displacement for a circular membrane loaded impulsively. The procedure predicts the displacement (W_f) for a rigid, perfectly plastic membrane of radius R, mass density, ρ and quasi static yield stress σ_0 subjected to a uniformly distributed impulsive velocity V_0 from the relation

$$W_f = \left(\frac{2.\rho.V_o^2.R^2}{3n\sigma_0} \right)^{\frac{1}{2}} \tag{3.2}$$

$$\text{where} \quad n = 1 + \left[\frac{V_o^2}{3QR} \left(\frac{\rho}{3\sigma'_o} \right)^{\frac{1}{2}} \right]^{\frac{1}{p}} \tag{3.3}$$

and Q and p are strain-rate material parameters.

The Jones [12] final mid-plate predictions are compared with the current predictions in Figure 3.4. Good correlation exists for the lower impulse range while for higher impulses, the difference approaches two plate thicknesses. The difference is again attributed to the use of a rigid-plastic material model and an average strain rate in the theoretical procedure.

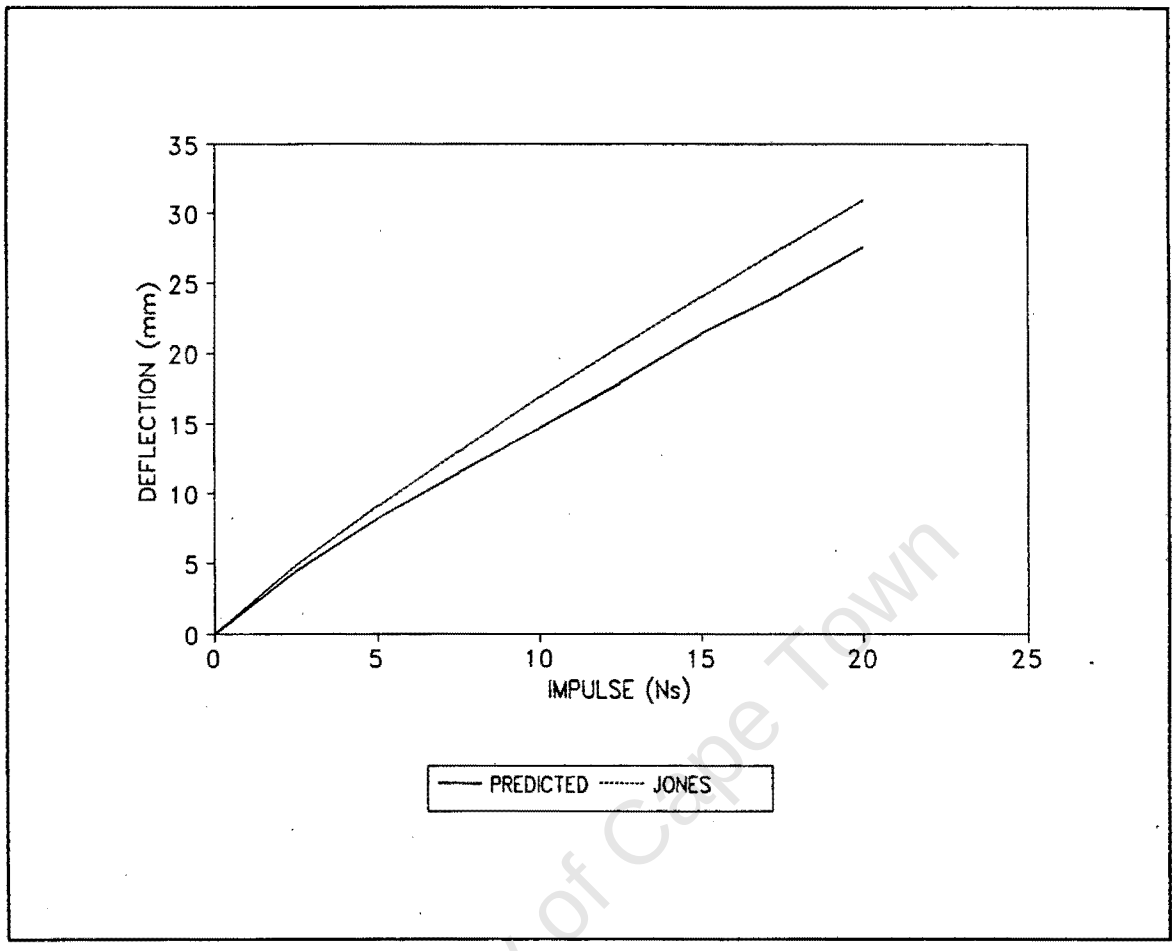

Figure 3.4: Comparison for $\frac{a}{R} = 1.0$ *between present and theoretical predictions [12] of the variation of permanent mid-plate deflection with impulse.*

3.2 Permanent Deformation Shape

The predicted permanent deformation shapes are presented in this section. The shapes are for selected loading configurations and for impulses that do not cause rupture of the plate. Figure 3.5 shows the predicted deformation shapes for $\frac{a}{R} = 0.33$ for impulsive loads of 2 and 8 Ns. For higher impulses it is observed that the plate bends inwards and outwards in

a sine wave form from the plate centre where the displacement is maximum to the fixed boundary. The local bends disappear at low impulses and at high load radius to plate radius ratios.

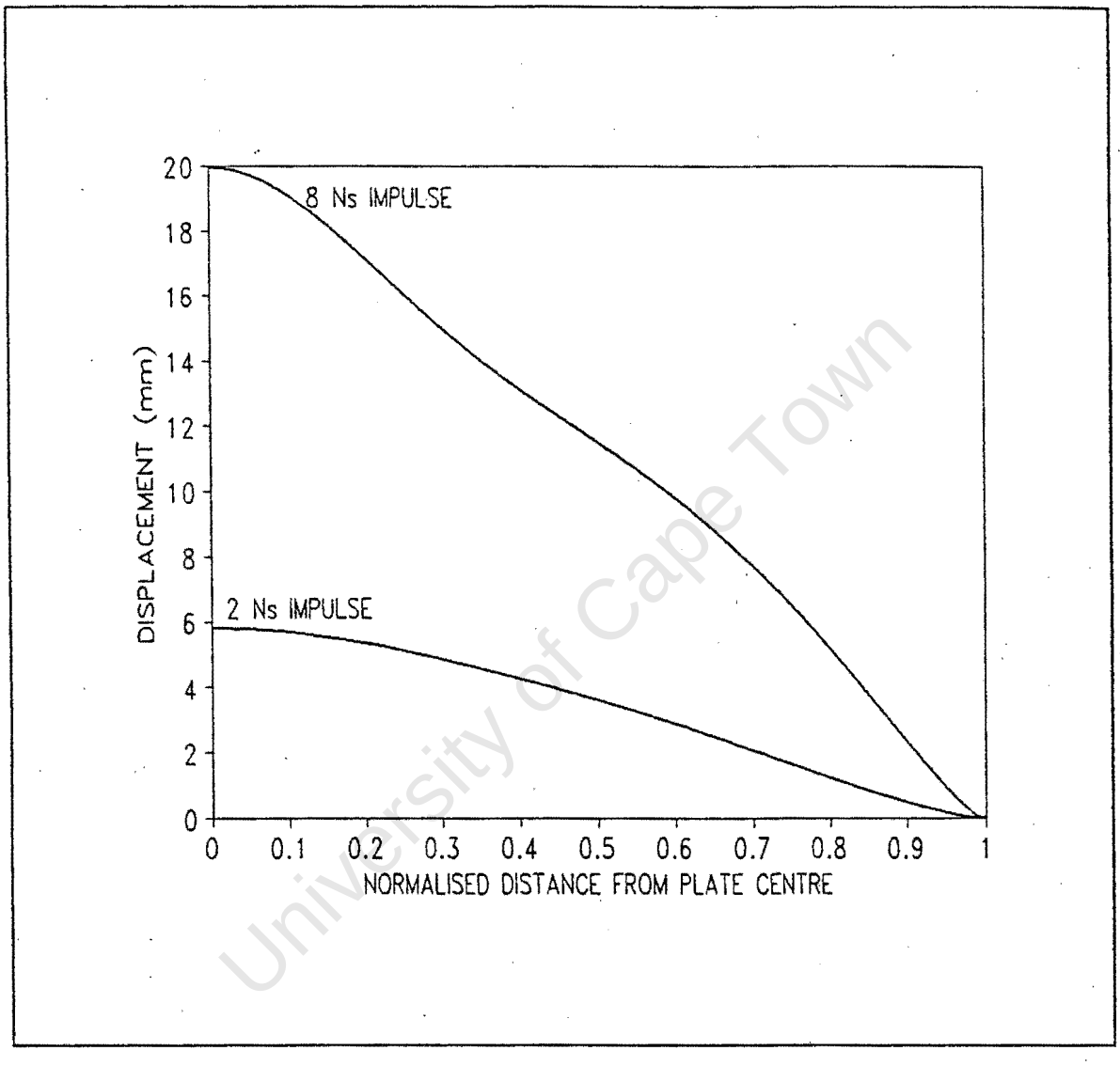

Figure 3.5: Predicted permanent deflection shapes for $\frac{a}{R} = 0.33$ *for 2 Ns and 8 Ns impulse.*

Figure 3.6 shows a comparison of the predicted shapes for $\frac{a}{R}$ =0.183, 0.25, 0.33 and 0.40 for an impulsive load of 8 Ns. The plates bend inwards and outwards from the plate centre to the fixed boundary. The diameter of a nipple at the centre of a plate increases with increasing load diameter.

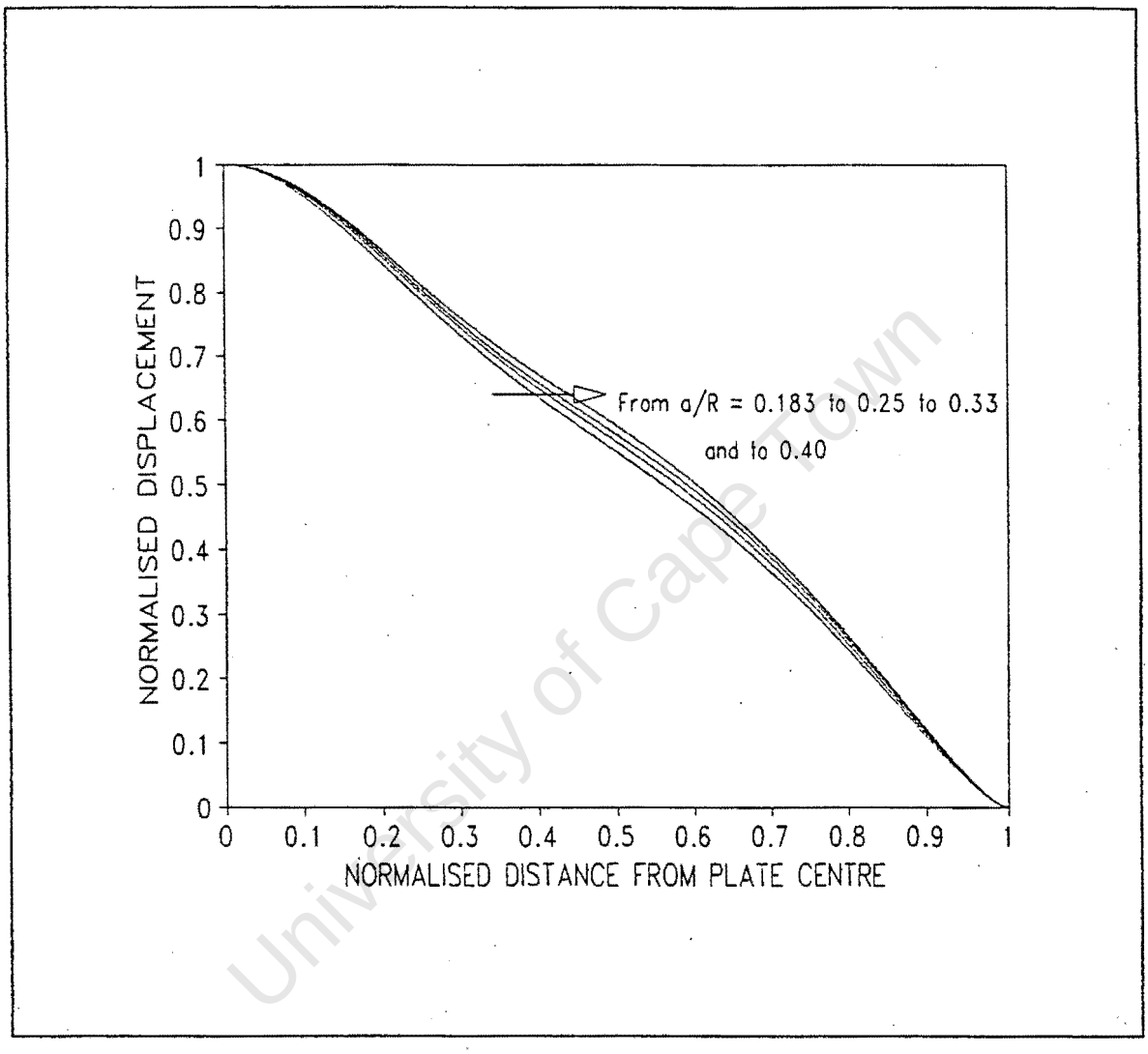

Figure 3.6: Predicted permanent deflection shapes for $\frac{a}{R}$ *= 0.183, 0.25, 0.33 and 0.40 for an impulsive load of 8 Ns.*

A typical ABAQUS plot of a deformed plate (fixed) for $\frac{a}{R}$ = 0.40 subjected to an impulse of 15 Ns is shown in Figure 3.7.

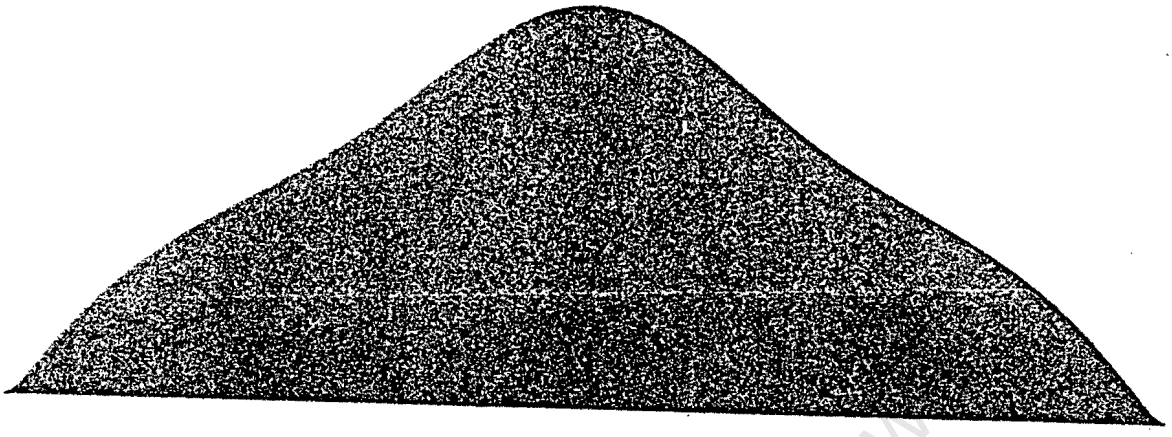

Figure 3.7: An ABAQUS plot of a deformed plate (fixed) for $\frac{a}{R}$ = 0.40 subjected to an impulse of 15 Ns.

The experimental and analytical results [10] for loading over circular areas of radius a, with $\frac{a}{R}$ = 0.183, 0.25, 0.33 and 0.4 are compared with the present predictions in Figure 3.8. For $\frac{a}{R}$ = 0.183 and 0.25, good correlation exists for maximum displacement but the difference between experimental and predicted deflections half way between the boundary and the plate centre is about 30%. The measured profiles bends inwards (within approximately the middle third of the plate radius) much more than the predicted profiles.

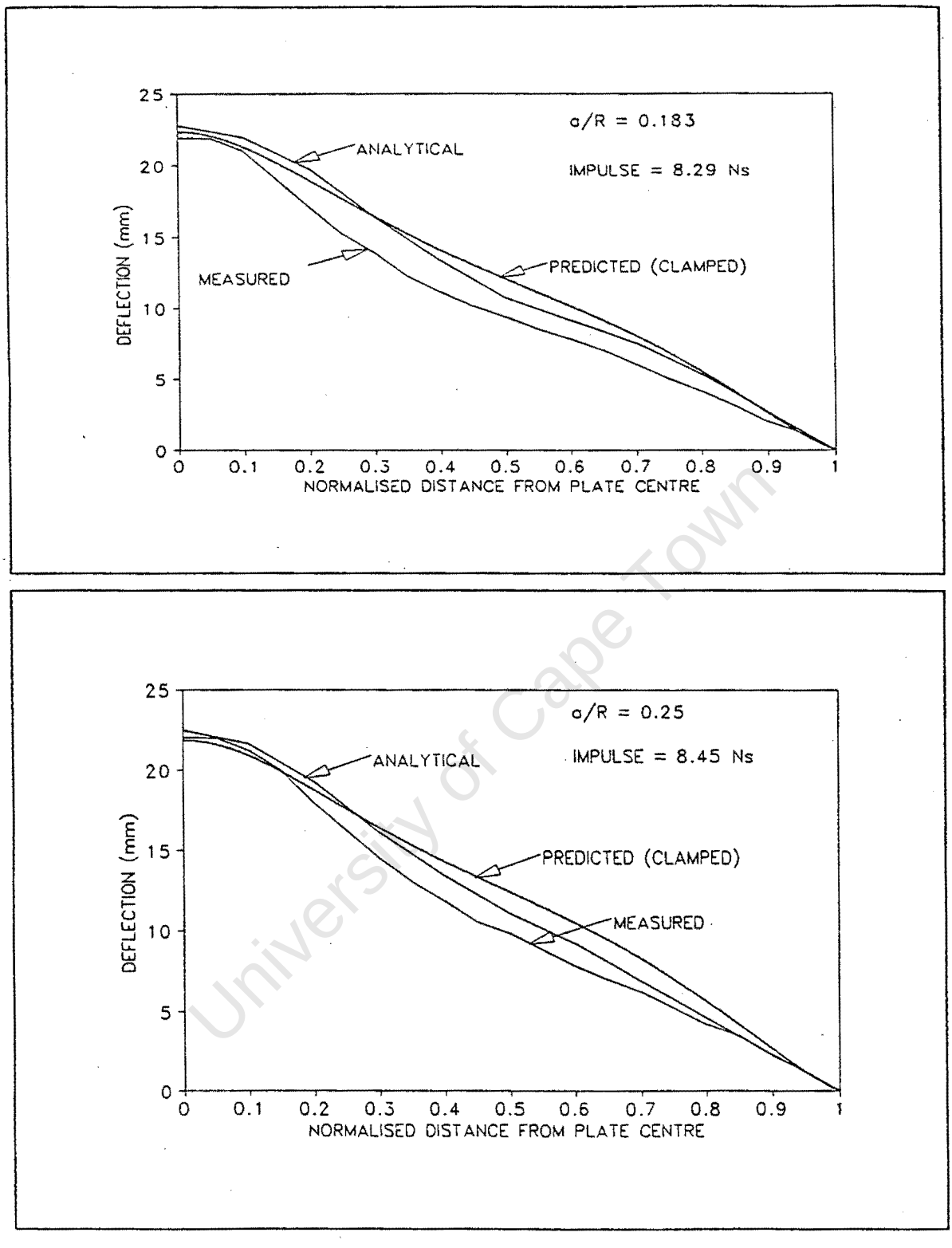

Figure 3.8: Comparison of predicted and reported [10] permanent deflection profiles for $\frac{a}{R}$ *= 0.183, 0.25, 0.33 and 0.40.*

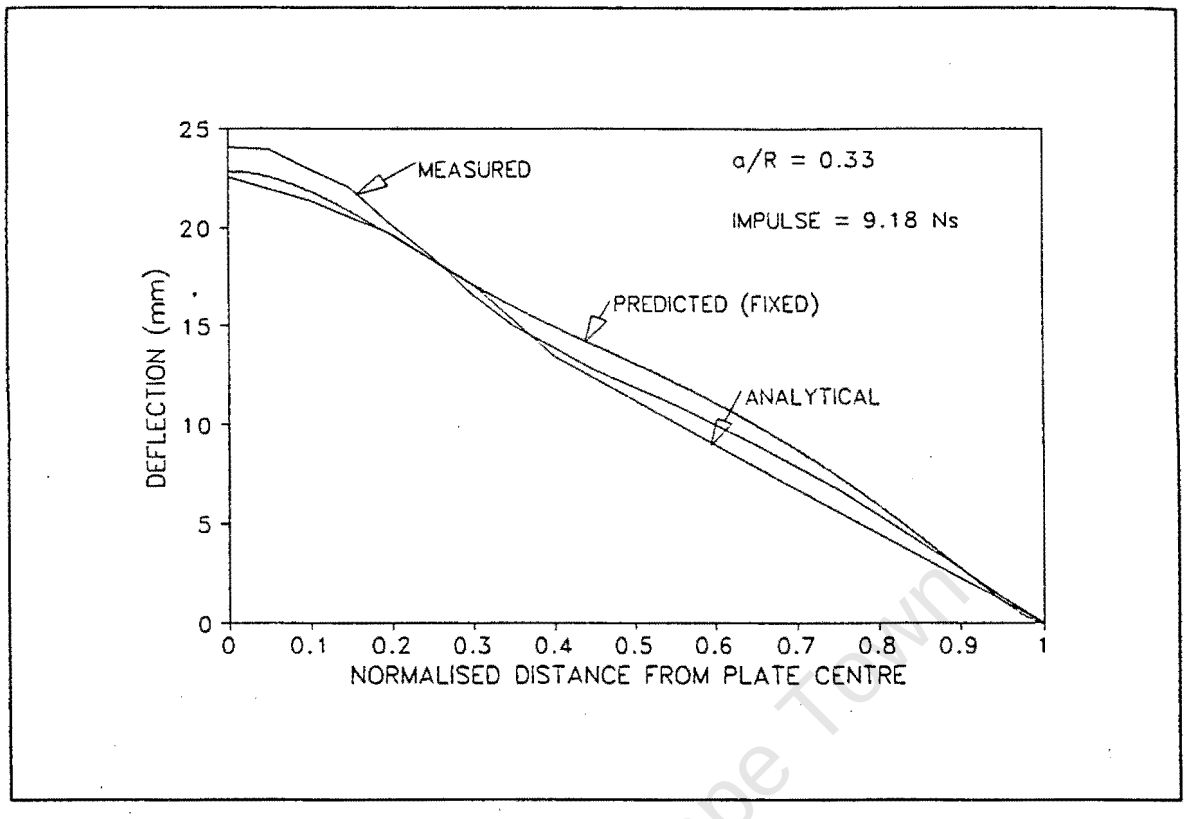

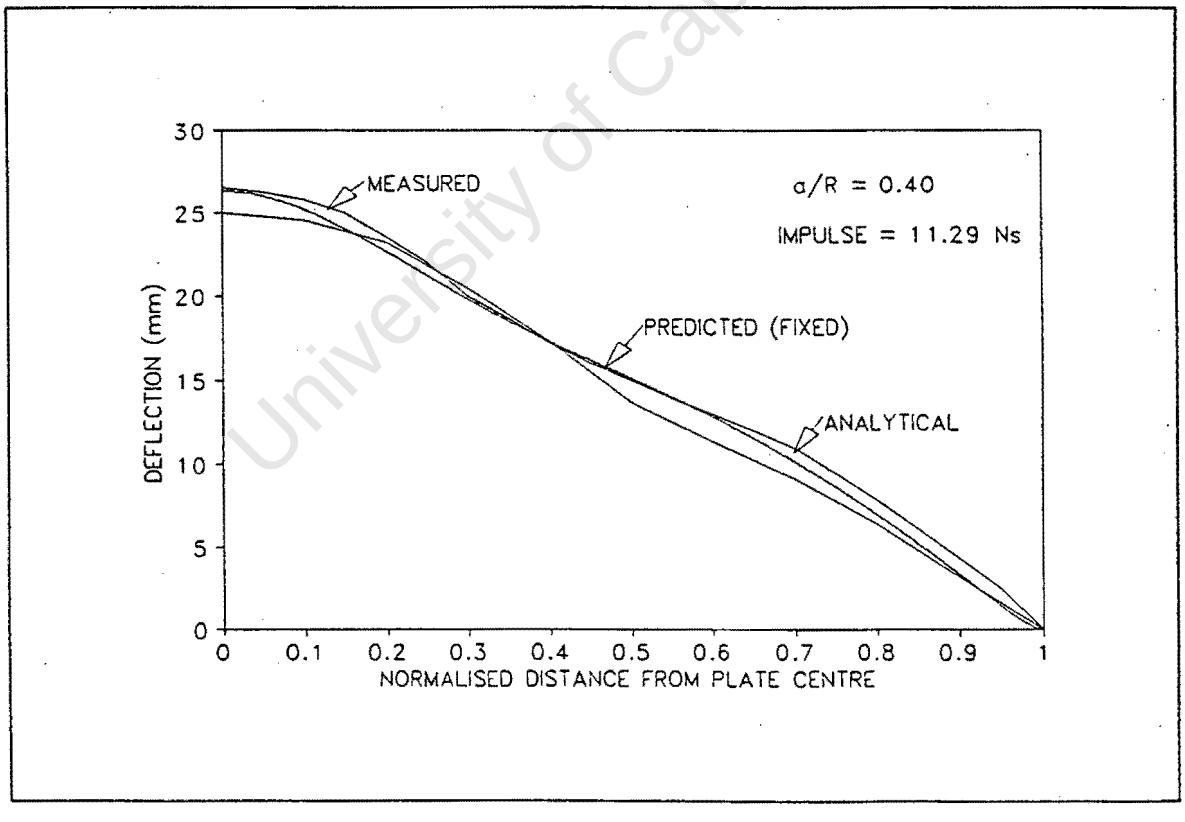

Figure 3.8: continued.

Experimental and predicted (clamped model) profiles rise in a linear manner from the boundary, whereas predicted (fully built-in model) profiles show zero slope and sharp curvature at the boundary. In the experimental work the plates were clamped and the measured shapes at the boundary compare well with the predictions of the clamped model. The results confirms the experimental work by Thomas [9] where it was shown that in the case of integral plates, the curve of the bend starts at the boundary, while in the case of clamped plates, the curve extends into the clamped region. The difference in the shapes is thought to be due to the load model used in the numerical analysis. The assumed pressure distribution profile might not idealise the real situation quite well for small load diameters. For $\frac{a}{R}$ = 0.33 and 0.4 the predicted final plate shapes show satisfactory correlation with the experimental shapes. The effect of the boundary condition on the final plate shape near the boundary can also be noticed for the two load configurations.

In Figure 3.9, the predicted final deformed shape for $\frac{a}{R}$ = 1.0 is compared with deformation shape functions used by Duffey [24] and used by Westine and Baker [25].

Duffey [24] used the relation

$$W(r) = Wo \operatorname{Cos} \frac{\pi r}{2R} \tag{3.4}$$

and Westine and Baker [25] used the relation

$$W(r) = \frac{Wo}{2}\left(1 + Cos\frac{\pi r}{R}\right) \tag{3.5}$$

where $W(r)$ is the deflection at radius r and Wo is the deflection at the plate centre.

The predicted final shape compares well with the shape used by Westine and Baker [25] from the plate centre to approximately 0.33 of the plate radius and is bounded by the two

theoretical predictions from 0.33 of the plate radius to the boundary. It was observed by Farrow [20] that an initial velocity model gives predictions which correlates better with experimental and Duffey's shapes than predictions from a pressure loading model.

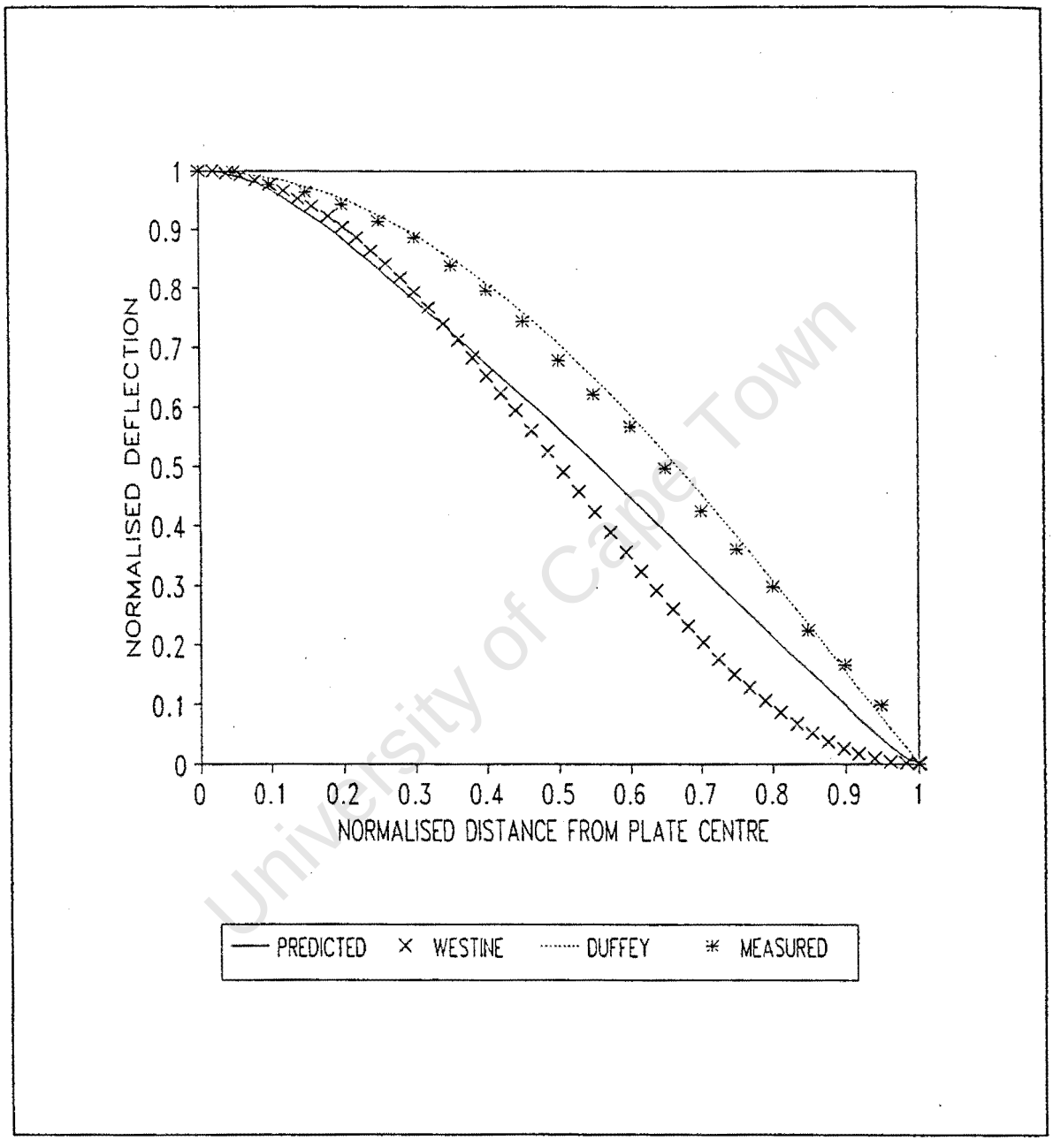

Figure 3.9: Comparison of predicted and other reported [24,25] permanent deflection profiles for $\frac{a}{R} = 1.0$.

3.3 Response Time

The response time T_r, for a centrally loaded plate, varies with the applied impulse and the ratio of loaded radius to plate radius, $\frac{a}{R}$. Typical time history plots for the displacement of the centre of the plate (as well as the variation of T_r with impulse) for $\frac{a}{R} = 0.33$ are shown in Figure 3.10.

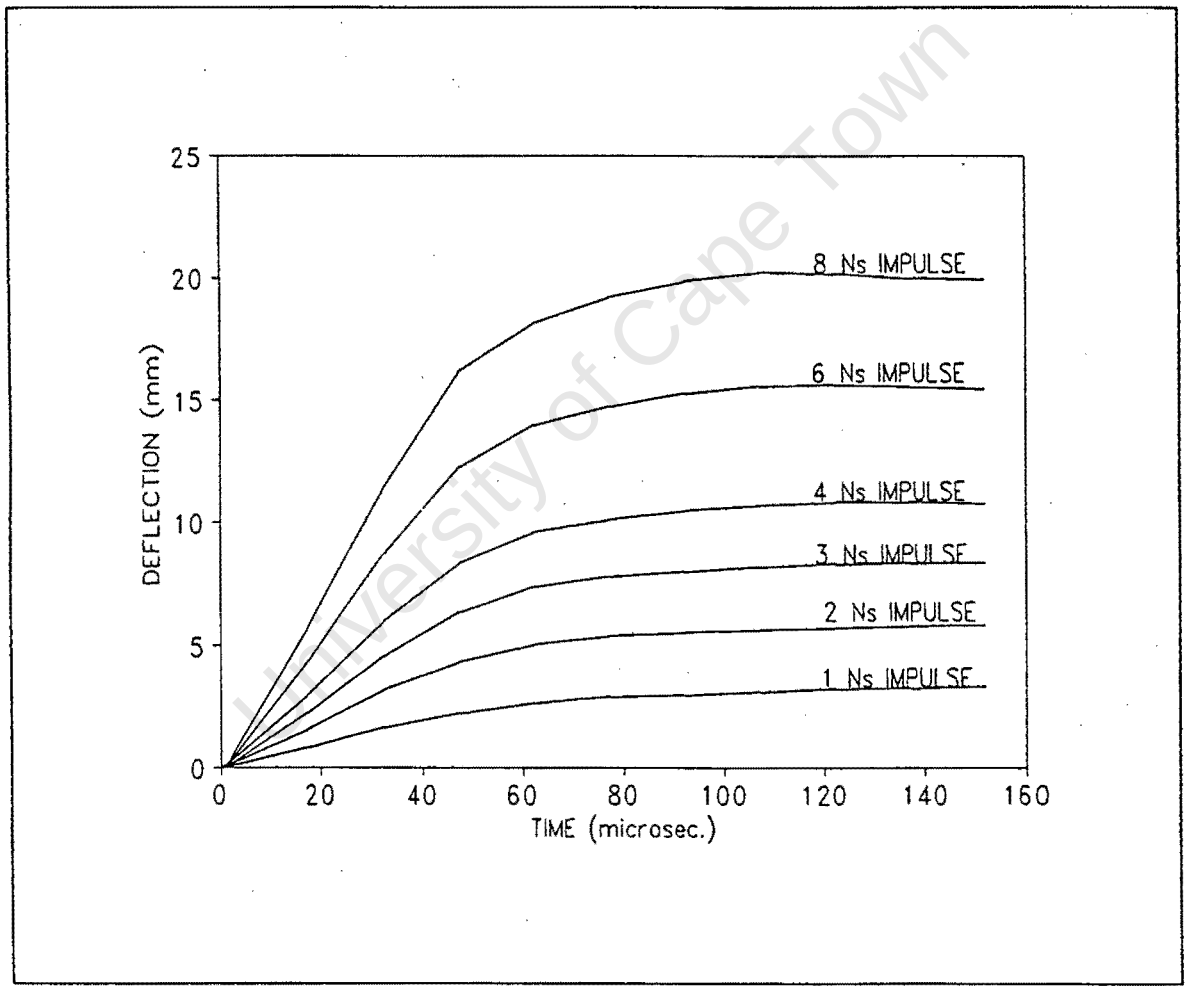

Figure 3.10: Predicted and reported [14] response time T_r for $\frac{a}{R} = 0.33$.

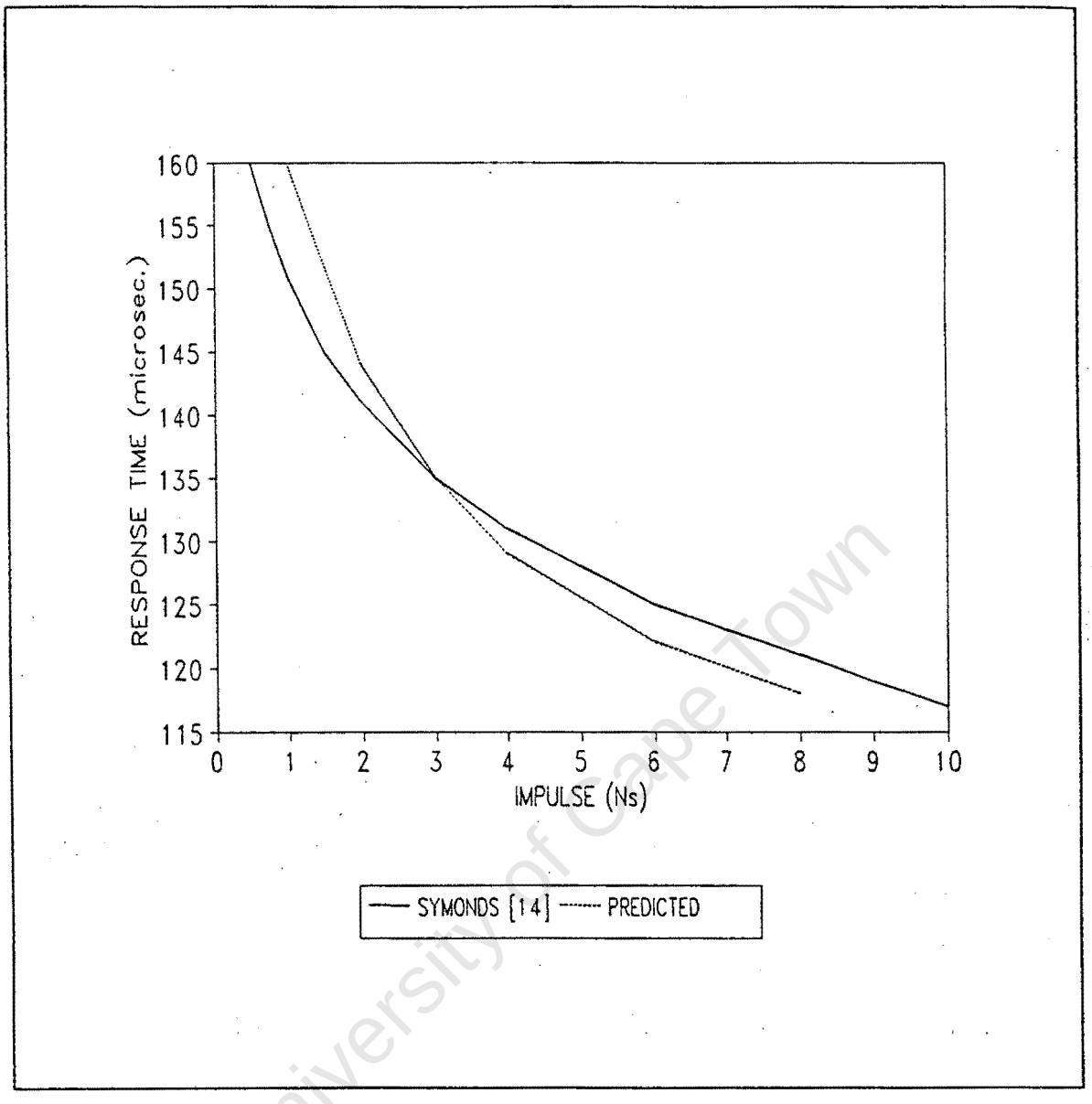

Figure 3.10: continued.

The predicted times to permanent displacement for an impulse of 1 Ns is approximately 160 μs. It is observed that the estimated response time first decreases fast with impulse to approximately 130 μs (corresponding to an impulse of 4 Ns) beyond which the response time exhibits a slow decrease. At an impulse of 8 Ns, a response time of approximately 120 μs is predicted. A comparison between the current predictions and the predictions of Symonds and Wierzbicki [14] is made and the predicted variation of the

response time with impulse compares well with the reported variation. Figure 3.11 shows time history plots for the displacement of the centre of the plate for $\frac{a}{R}$ = 0.183, 0.25, 0.33, 0.40 and 1.0. for an impulsive load of 8 Ns.

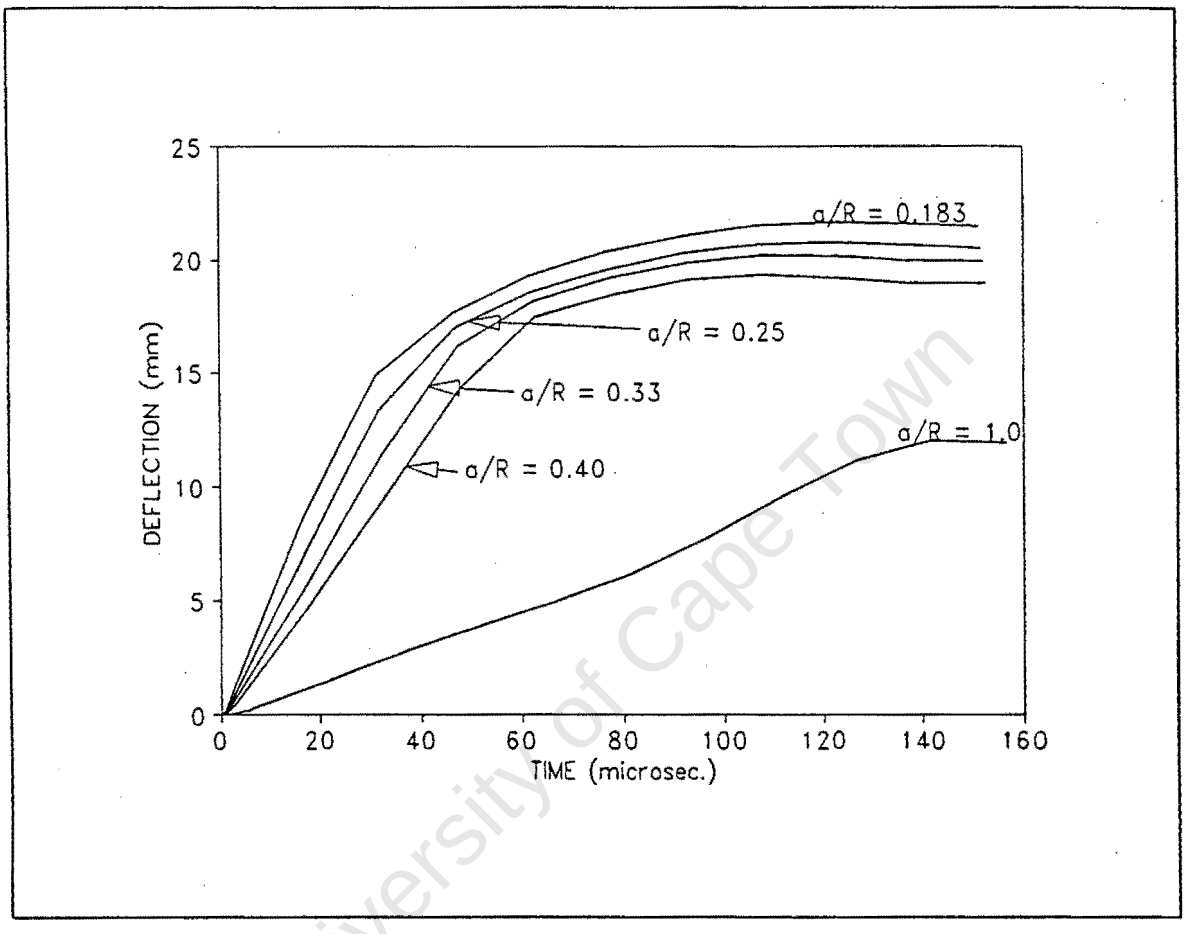

Figure 3.11: Predicted mid-plate deflection as a function of time for $\frac{a}{R}$ = 0.183, 0.25, 0.33, 0.40 and 1.0 subjected to 8 Ns impulse.

The predicted response time increases from approximately 115 μs for $\frac{a}{R}$ = 0.183 to approximately 140 μs for $\frac{a}{R}$ = 1.0. The response time of 140 μs for $\frac{a}{R}$ = 1.0 compares

well with the large permanent ductile deformation (Mode I) response time reported by Olson, Fagnan and Nurick [8].

The transient deformation profiles $S(T_r)$ of a plate for $\frac{a}{R}$ = 0.40 subjected to an impulse of 11.29 Ns are shown in Figure 3.12.

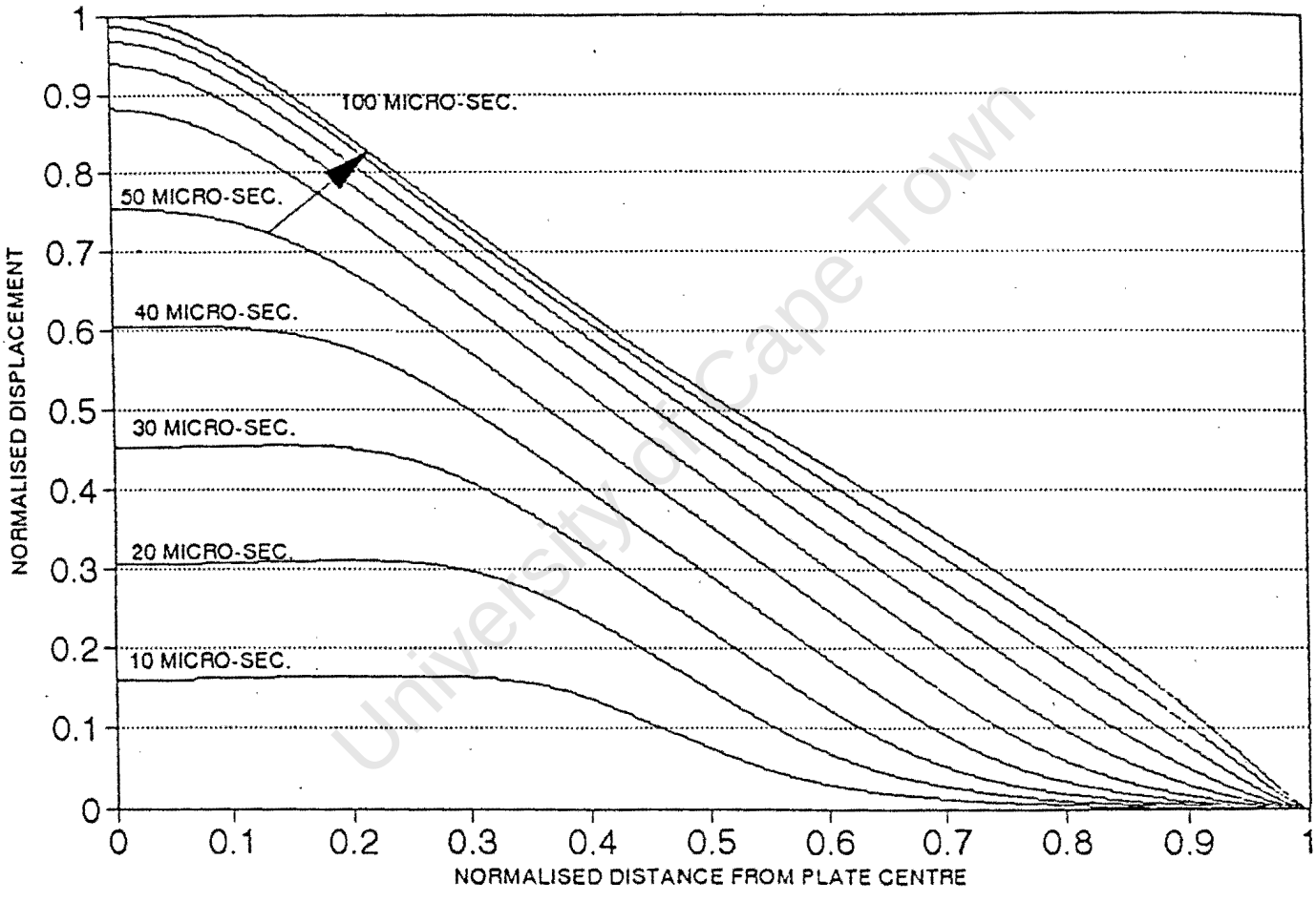

Figure 3.12: Plate predicted transient profiles for $\frac{a}{R}$ *= 0.40 subjected to 11.29 Ns impulse.*

It is seen that the central region of the plate responds faster and remains relatively flat early in the analysis. An estimate of the deflection rate (velocity) is shown in Figure 3.13. The profiles $V(T_r)$ are obtained from

$$V(T_r) = \frac{S(T_r)}{T_r} \tag{3.6}$$

As expected, the deflection rate decreases with increasing time.

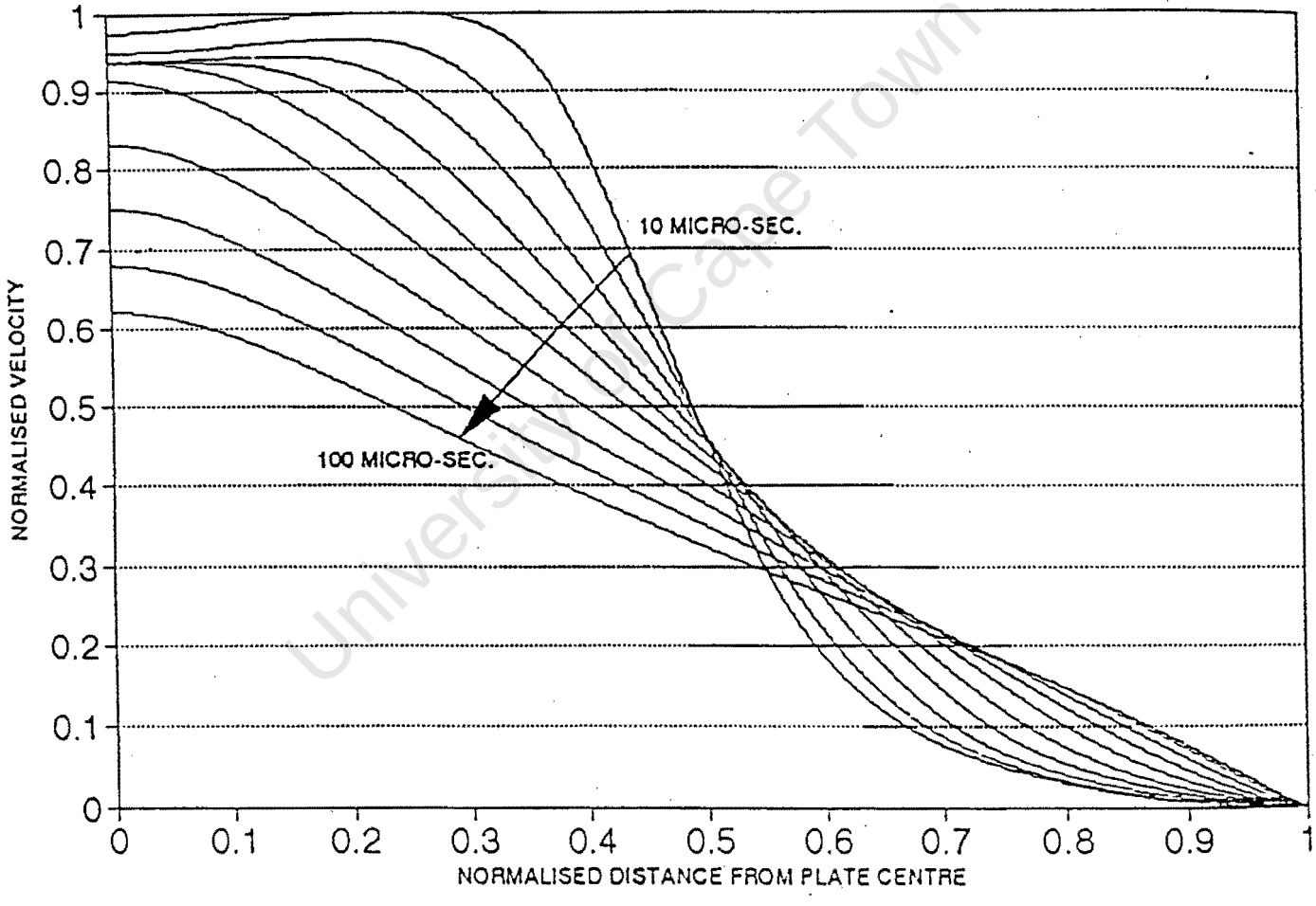

Figure 3.13: Plate predicted deflection rate profiles for $\frac{a}{R}$ *= 0.40 subjected to 11.29 Ns impulse.*

3.4 Strain Predictions

The equivalent plastic strains are calculated at five integration points through the plate thickness for each element. These strains are shown in Figure 3.14 for the integration point at the centre of the plate-section. The strains are due to an impulse of 10 Ns and are normalised to obtain a better comparison of the distribution profiles for different load configurations.

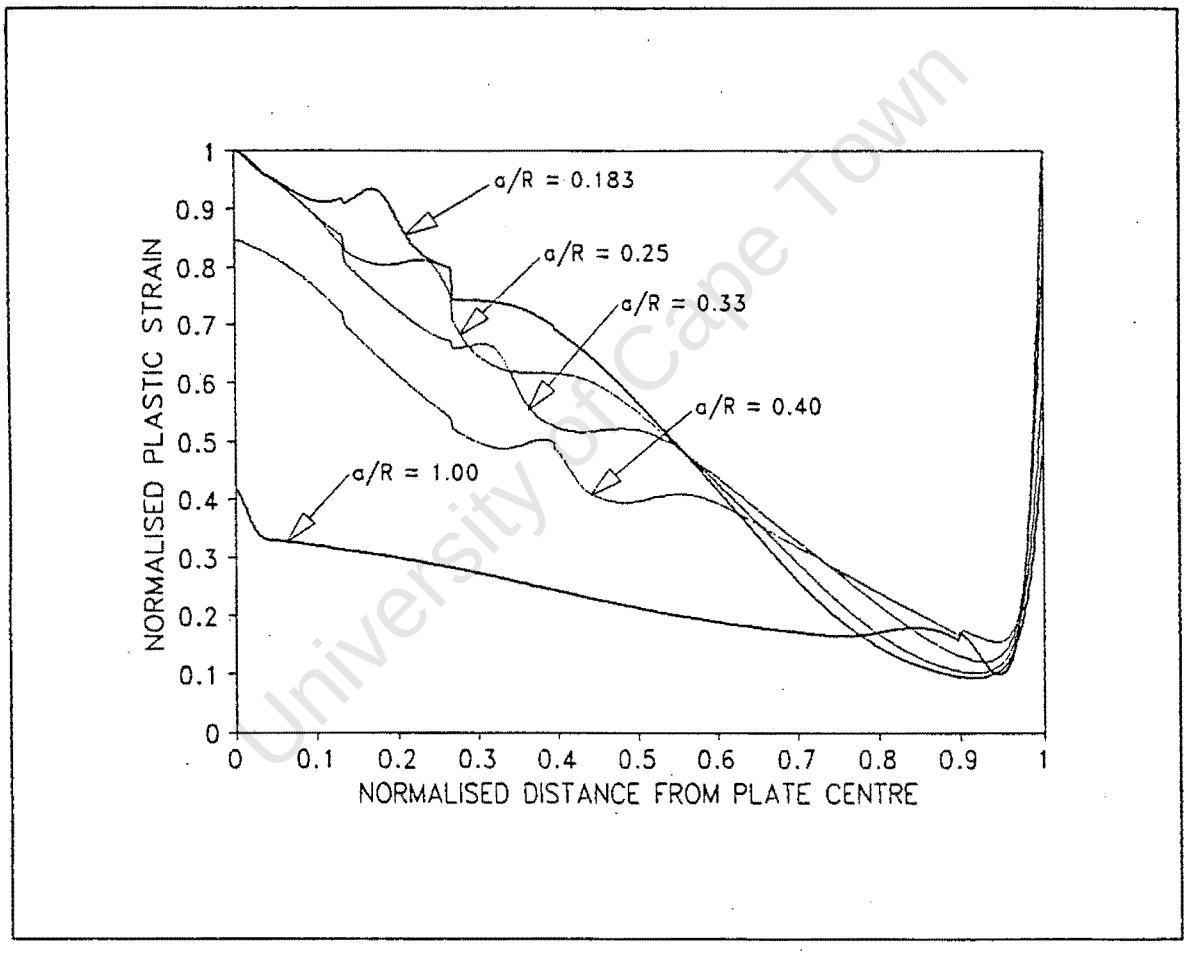

Figure 3.14: Plate predicted equivalent plastic strain distribution profiles for $\frac{a}{R}$ = *0.183, 0.25, 0.33, 0.40 and 1.0.*

For $\frac{a}{R}$ = 0.183, 0.25 and 0.33 the maximum predicted equivalent plastic strain occurs at the plate centre while for $\frac{a}{R}$ = 0.4 and 1.0 the maximum is at the boundary. It can be seen from the plots that several locations of local maximum strain exist along the profiles. In particular, for $\frac{a}{R}$ = 0.183, 0.25, 0.33 and 0.40, local maximum strains are predicted at the plate centre, near the load boundary and at the plate boundary. If a maximum equivalent plastic strain measure is used to indicate failure, failure would occur at locations of local maximum equivalent plastic strain (which is consistent with experimental evidence [8,9,10,13]); plate rupture has been shown to occur near the load boundary. The plots of Figure 3.14 are for a time (200 μs) when the plate has fully responded to the impulse and are for an analysis which does not include a material failure criterion. As will be shown later in a section on tearing predictions, rupture occurs earlier than the response times corresponding to the plotted plastic strains and it is likely that the load boundary (one location of local maximum equivalent strain) reaches the failure strain first, hence rupture occurs there before strain distributions shown in Figure 3.21 are reached.

The effect of the plate boundary conditions on the distribution of equivalent plastic strains is shown in Figure 3.15 for $\frac{a}{R}$ = 0.33 and an impulse of 9.18 Ns. It is evident from these plots that the equivalent plastic strain distribution profiles for a fully-built in boundary and a clamped boundary are identical. Hence the predicted large ductile deformation (Mode I) response of thin circular plates to central blast loading is identical for the two edge conditions modelled in the present study.

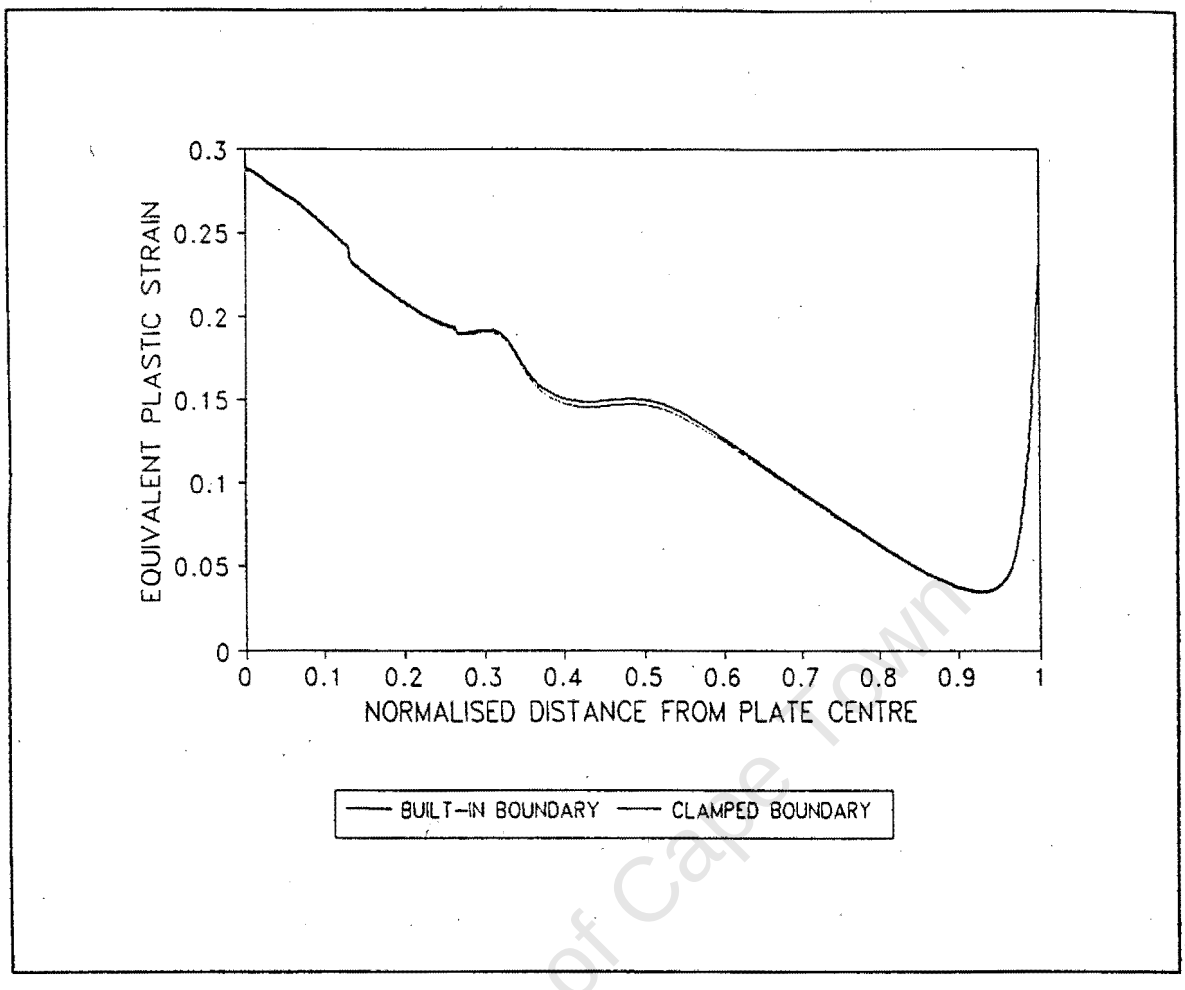

Figure 3.15: Comparison of predicted equivalent plastic strain distribution profiles between two edge conditions for $\frac{a}{R} = 0.33$.

3.5 Strain Rate Dependence

The plastic behaviour of mild steel is highly sensitive to strain rate. The plastic flow stress in blast loaded structures can treble the static flow stress [12, 14, 20]. A comparison of the predicted deflection-time history plots with and without strain rate effects included in the model is shown in Figure 3.16. An over-estimation of the permanent deflection of 100% can occur if strain rate effects are not included.

Symonds and Wierzbieki [14] also predicted mean strain rates for the response of circular plates in order to estimate the strain rate dependence of materials.

In this section the strain rate sensitivity influence factors are estimated from the predicted equivalent plastic strain distributions. An estimate of the mean strain rate (which varies from point to point across the plate and with time) is calculated at each node by dividing the equivalent plastic strain by the response time. These nodal mean strain rates are weighted according to the circumference of their radial co-ordinate and are averaged to give the average mean strain rate of the plate. The mean strain rate of the plate is substituted into the Cowper-Symonds relation [Equation 2.4] to obtain the strain rate sensitivity influence factor '*n*'. The variation of the estimated strain rate sensitivity influence factor '*n*' with impulse is shown in Figure 3.17.

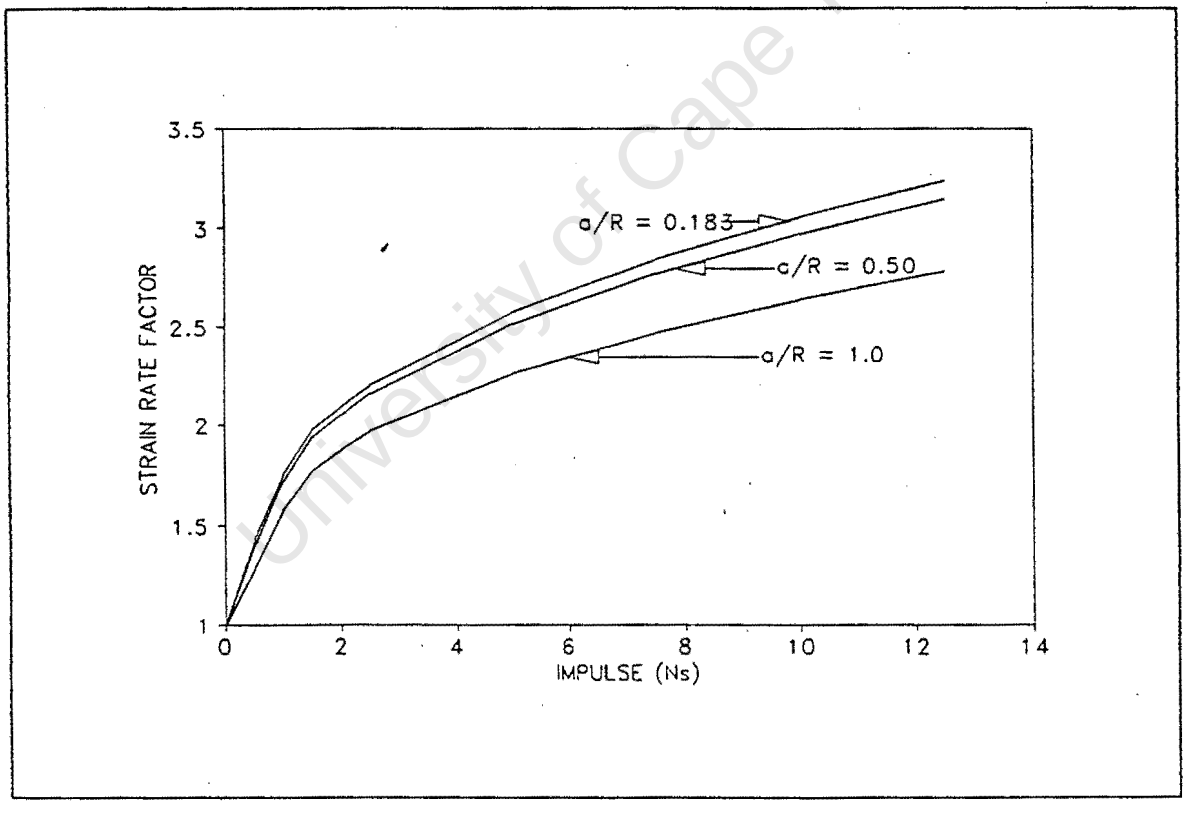

Figure 3.17: Variation of the estimated strain rate sensitivity influence factor 'n' with impulse.

The strain rate factor, at the same impulsive loading, increases with decreasing ratio of load radius to plate radius. Figures 3.18 and 3.19 show a comparison of the current predicted strain rate sensitivity influence factors to Symonds and Wierzbieki's [14] and Jone's [12] factors.

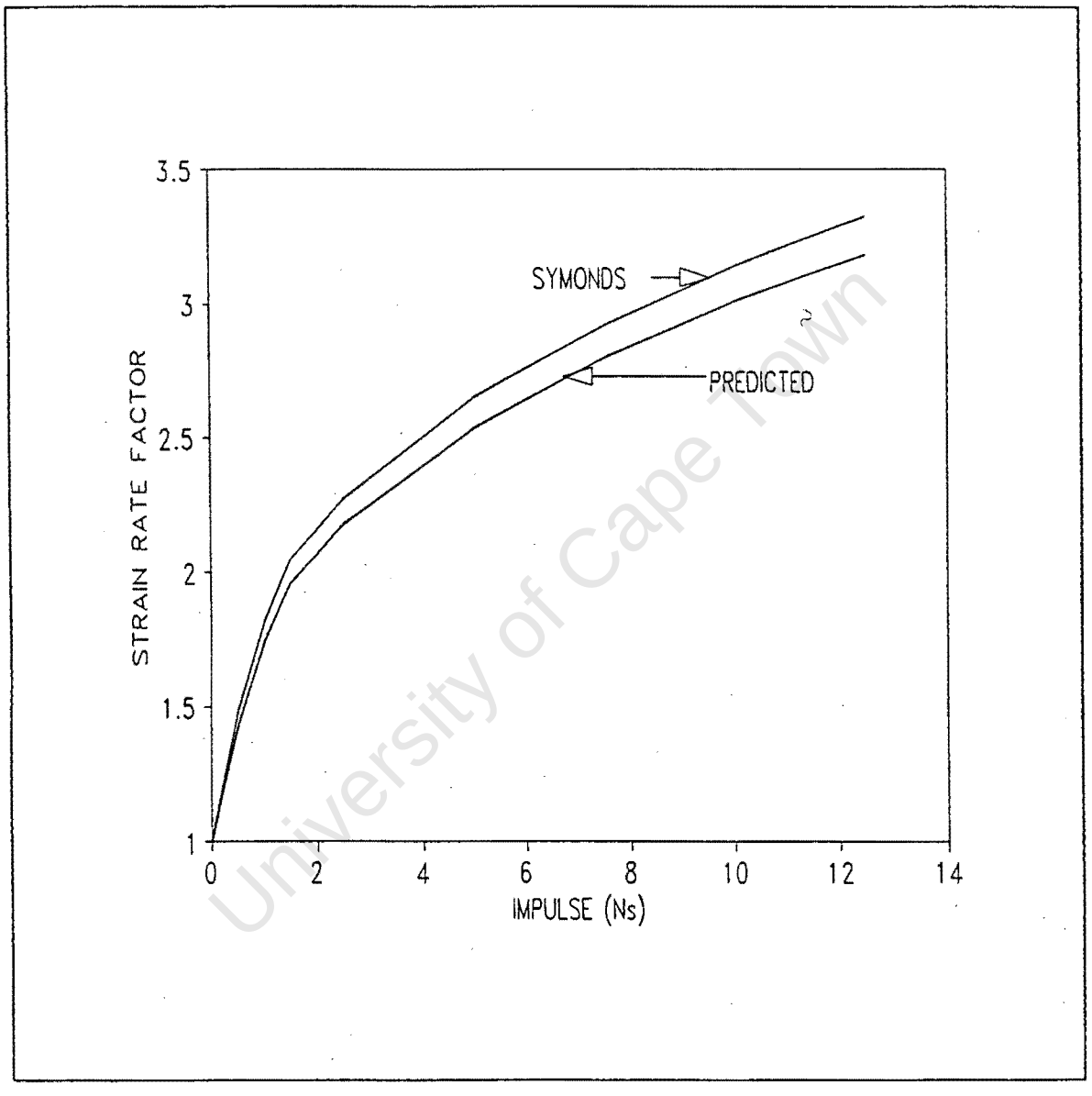

Figure 3.18: Comparison of estimated strain rate sensitivity influence factors 'n' with reported values [14] for $\frac{a}{R} = 0.50$.

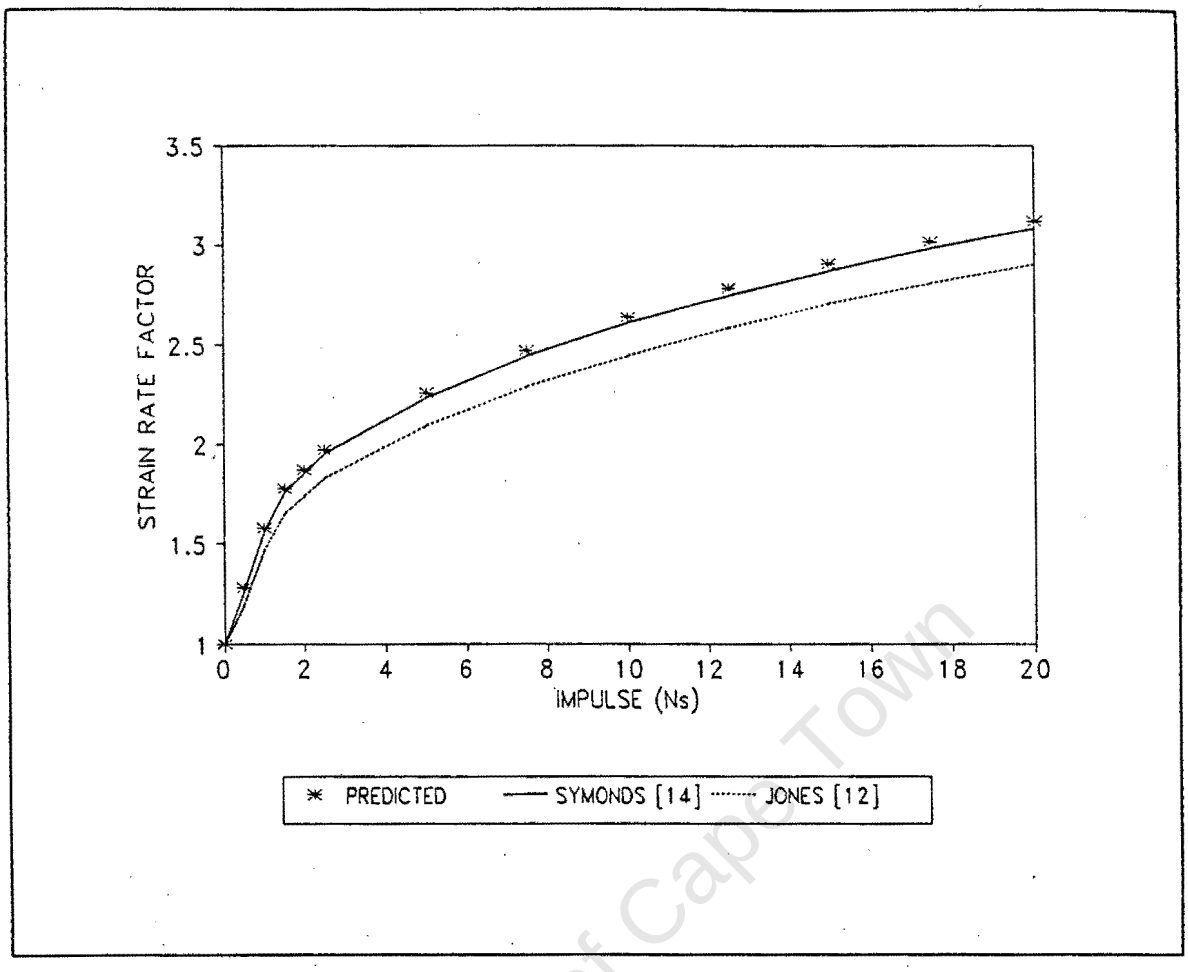

Figure 3.19: Comparison of estimated strain rate sensitivity influence factors 'n' with reported values [12, 14] for $\frac{a}{R} = 1.00$.

It is evident from the plots that good correlation exists between the current numerical predictions of an average strain rate for the plate and the analytical predictions. The strain rate sensitivity influence factor increases with increasing impulse.

In the current analysis the strain rate varies from point to point across the plate and with time. The effect of using an average mean strain rate (an average over the response time and over the volume of the plate) on the plate response is obtained from the current model as follows: The quasi-static stress versus plastic strain [Figure 2.4] is modified by

multiplying the static flow stress with a strain rate sensitivity influence factor '*n*' (See Figure 3.20): the factor '*n*' is obtained by using the predicted average mean strain rate. The modified stress versus plastic strain curve is then used in the finite element model with the strain rate dependence option removed.

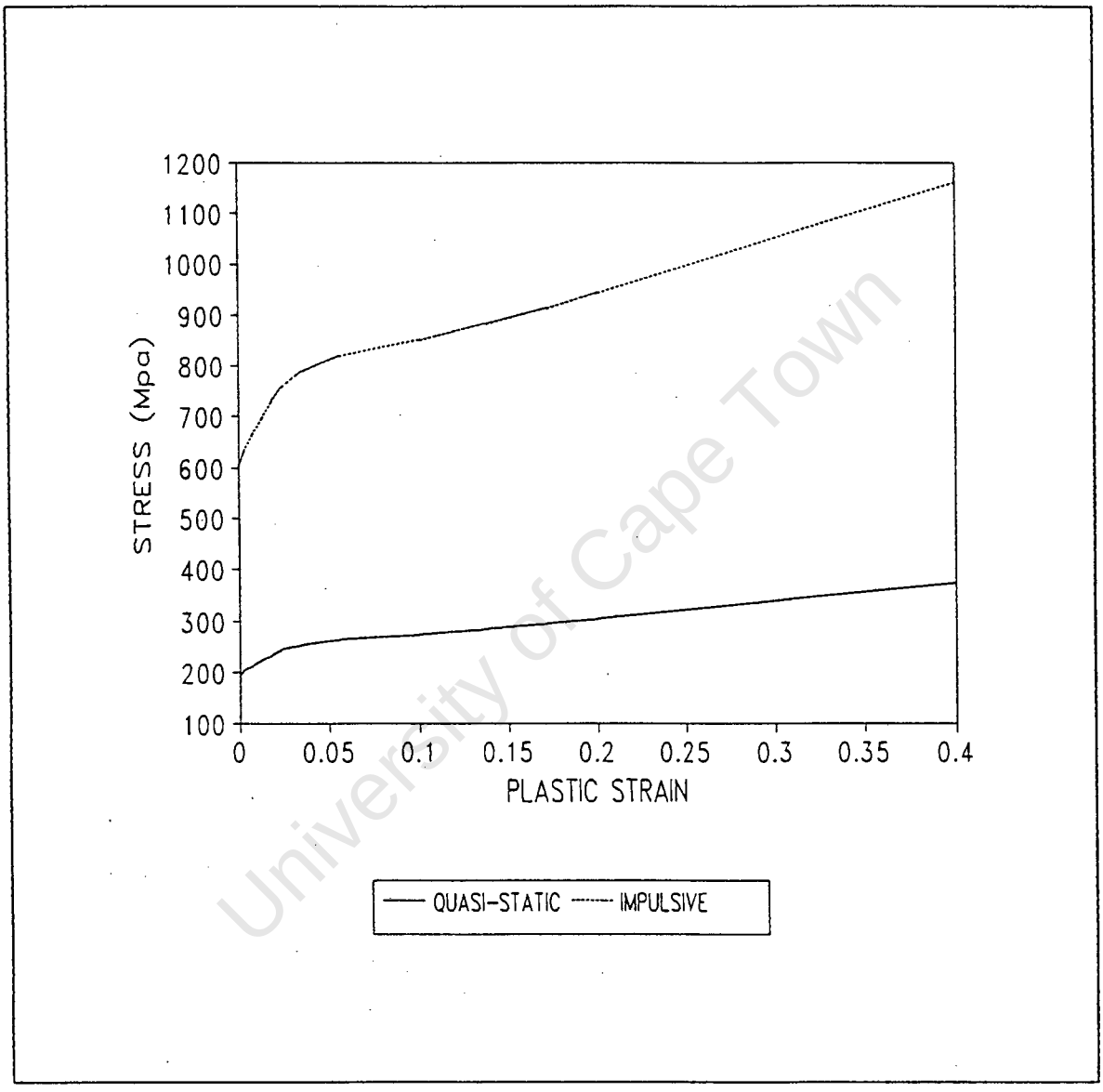

Figure 3.20: Stress versus plastic strain plots at zero strain rate (quasi-static) and at an average mean strain rate for $\frac{a}{R} = 0.40$ *for 10 Ns impulse.*

Figure 3.21 shows the effect, on the response of a plate, of using an average mean strain rate. The maximum permanent displacement is slightly higher when an average mean strain rate is used.

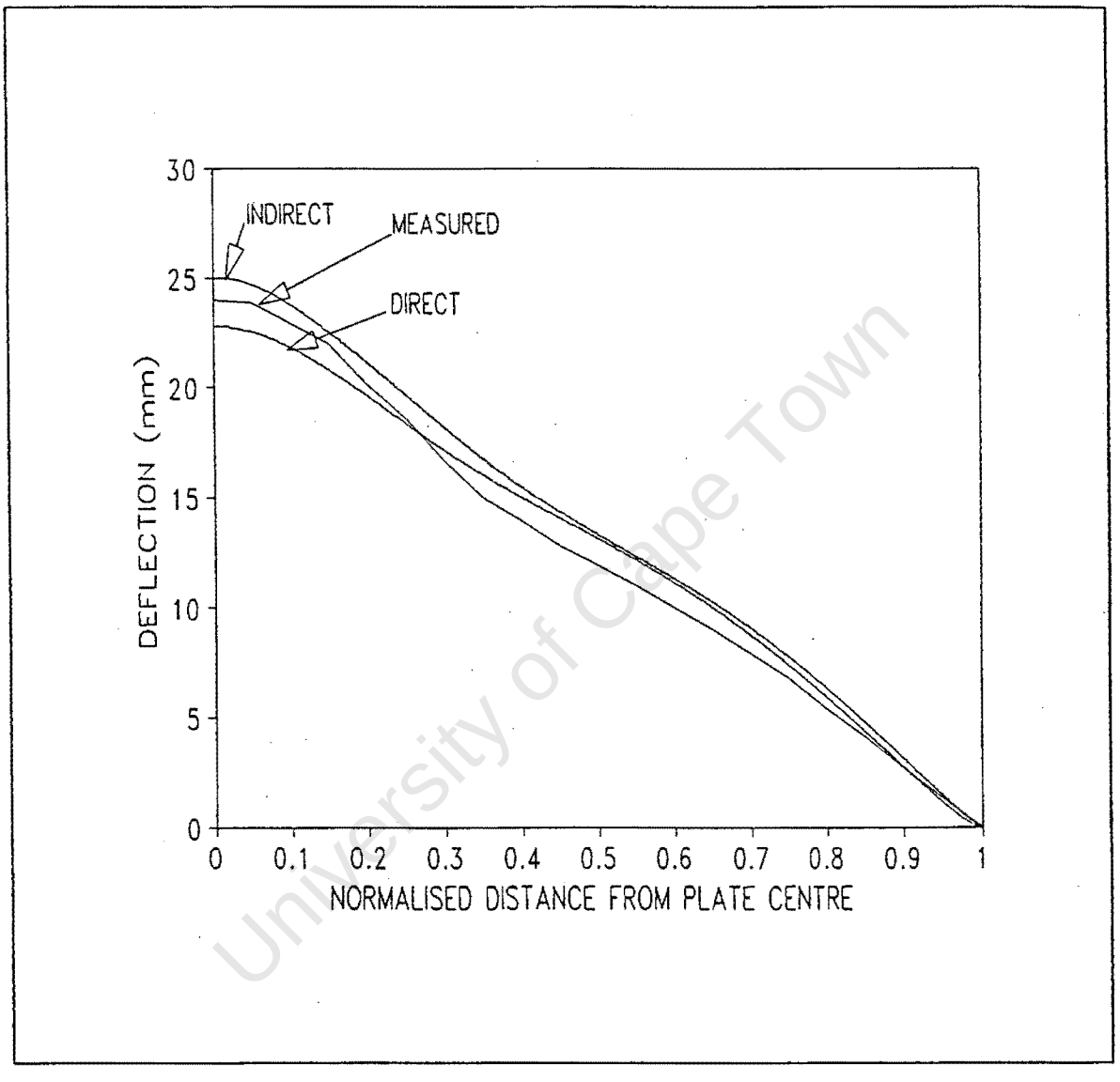

Figure 3.21: Affects of using strain rate parameters directly or indirectly (using the estimated average mean strain rate for the plate) in the analysis for $\frac{a}{R} = 0.33$ *for 9.18 Ns impulse.*

3.6 Plate Tearing

The ABAQUS/Explicit failure option (mentioned in Section 2.3) was included in the model to investigate tearing of the plates. The failure option was only used for impulsive loads expected to cause rupture of the plate. For predicting other failure modes the failure option was not used since, during the time of writing, the ABAQUS/Explicit scheme became unstable when the failure option was used with the strain rate dependence option in an analysis.

In this section results are for a failure model which incorperates the strain rate effects before an analysis by adjusting the quasi-static stress versus plastic strain material behaviour using the estimated average mean strain rates mentioned in the previous section (See Figure 3.19). The predicted diameters of the torn plate are shown in Table 3.3 with the measured values [10]. The predicted cap diameters from the analysis compare reasonably well with the experiments.

$\frac{a}{R}$	Impulse (Ns)	Predicted ratio of cap diameter to plate diameter	Measured ratio of cap diameter to plate diameter	Approximate time to failure (μs)
0.183	9.41	0.163	0.13	15
0.25	11.67	0.228	0.215	15
0.33	13	0.308	0.272	15
0.40	15	0.378	0.368	15
1.00	30	0.957	------	15

Table 3.3: Comparison between predicted and measured cap-diameters for cicular plates under a central blast load.

The predicted time to failure, for the range of impulses investigated, was between 10 and 20 μs. This time to failure compares well with the predictions of Olson et al [8]. Typical transient deflection profiles of a plate subjected to an impulse which causes rupture are shown in Figure 3.22. The profile before failure is at a time of 10 μs. At 20 and 30 μs, the plate had ruptured and the torn plate travelled freely. The present model predicted reasonably well the location and approximate time to failure. However, the model failed to predict the threshold impulse for the tearing of the plates. Failure occured even at very low impulses. This was probably due to the choice of the plastic failure and the offset plastic strains. In the present analysis, these values were taken from the measured [10] uniaxial quasi-static stress versus plastic strain behaviour of the plate material. The strain rate and the state of stress (simple or complex) dependency of these parameters was not taken into account.

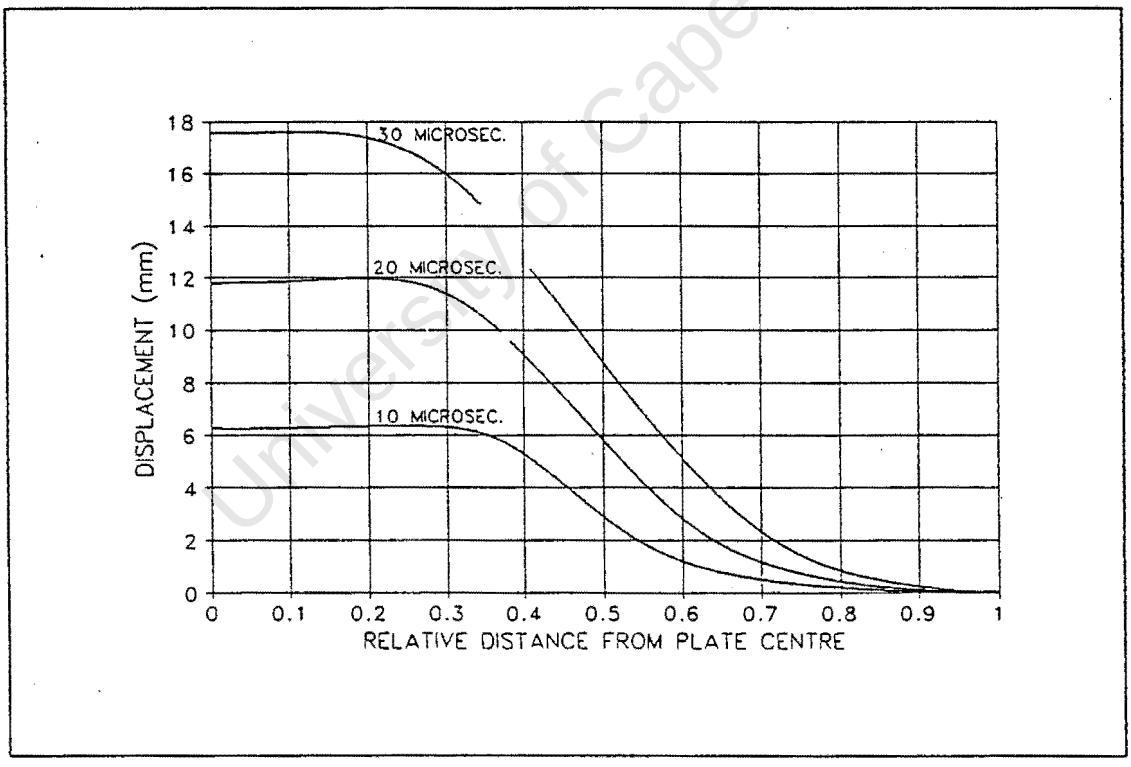

Figure 3.22: Predicted transient profiles from a failure model for $\frac{a}{R} = 0.40$ *subjected to an impulse of 15 Ns.*

An ABAQUS picture plot of the ruptured plate at a time of 40 microseconds after the explosion is shown in Figure 3.23

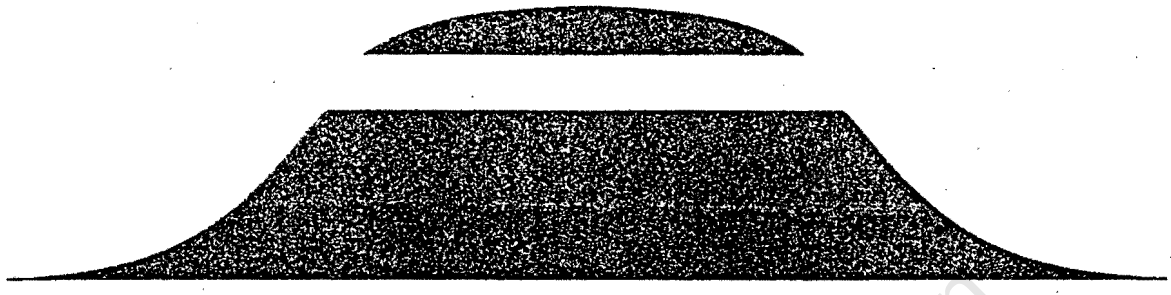

Figure 3.23: An ABAQUS picture plot of the ruptured plate at a time of 40 microseconds after the explosion.

Chapter 4

Discussion and Conclusions

This thesis presents an investigation into the response of thin circular metal plates to central blast loading. The investigation was carried out using the numerical analysis of the general purpose ABAQUS finite element code. In this chapter, comments are made on the numerical model used as well as on the predicted plate responses.

ABAQUS offers an element library and two analysis schemes for use in a wide variety of problems. In the present study, the SAXI axisymmetric shell element was chosen over two or three dimensional elements which could give comparable results. The geometry, physical properties and the loads of the circular plate subjected to central blast loading are axisymmetric making it efficient to use axisymmetric shell elements in the model. The cost of analysis associated with the SAXI axisymmetric element is reduced due to fewer elements being needed to model the plate, and meshes are easy to design. However, original and deformed picture plots from solutions using two or three dimensional elements give a better visual representation of the real situation. The explicit scheme holds certain advantages and disadvantages. The disadvantages relate to mesh design and stability of an analysis. The scheme is conditionally stable and to obtain numerical stability of the solution a more refined mesh is required for the same level of convergence of results as the implicit scheme. However, the cost of analysis associated with the explicit scheme is less due to fewer equations being formulated and solved (use of lumped mass matrices). Also, the explicit scheme provides a failure model for predicting tearing and rupture of plates which is not available in the implicit scheme.

The metal elasto-plasticity material model selected in the current study is suitable for blast loaded thin steel plates. The use of material parameters obtained from uniaxial quasi-static

tensile tests was found to give reasonable predictions of the large ductile deformation response of the plates. The parameters did not give good predictions for the tearing response of the plates. The failure model depends on choices of the equivalent plastic strain at ultimate failure and the equivalent plastic strain at start of the necking for the plate material; the dependence of these parameters to strain rate and state of stresses at rupture is an area that requires research.

One area of uncertainty in blast loaded structures is in the derivation and idealisation of net pressures from blast waves. In the present study, where the pressures are due to detonation of explosive sheets centrally spread over radius '*a*' of a circular plate of radius '*R*', it was assumed the imparted pressure is uniform over the loaded area and decays exponentially to the plate boundary. The decay constants, which varied with the loaded radius, were obtained empirically by fitting predicted mid-plate deflections to experimental values. Since the load durations for the impacts in the current study are fairly short and the pressures fairly high, idealising the pressure pulses as impulsive velocity loadings is an alternative method which requires investigation. However, predictions of plate responses from the pressure loading model compared favourably with results from experimental and analytical studies.

Permanent mid-plate predictions compare quite well with experimental values but analytical solutions of Symonds and Wierzibieki and of Jones give slightly higher predictions. It is known, however, that these analytical predictions use a rigid-plastic analysis (strain hardening of the material is ignored) and use a mean strain rate for the whole plate in incorporating strain rate effects in the solutions. The current mid-plate deflection predictions using a mean strain rate showed that the deflections are indeed slightly higher.

The predicted plate deformation shapes compare well with shapes from experimental work for larger ($\frac{a}{R} > 0.33$) load radii while for smaller radii the correlation is poor. It is

thought that this is due to the loading simplification and idealisation made in the model. The pressure distribution assumed in the model might be valid for larger radii and invalid for smaller load radii where the explosive burn time is very small (less than 1 μs). The impact is likely to be felt over a smaller area than assumed (decaying exponentially to the boundary from the loaded radius) in the current model. A different pressure distribution function might improve the results.

The ABAQUS/Explicit failure model used in predicting tearing could not handle an analysis with a strain rate dependence option. The failure model was in fact still being corrected for errors at the time of writing this thesis. However, an attempt was made to use the failure model to predict the tearing response of the plates. Strain rate effects were introduced indirectly in the model by adjusting the quasi-static material stress versus plastic strain curve (using predicted strain rate sensitivity influence factors). The torn plate diameters from the analysis compared quite well with experimental values. The predictions of time to failure also compared reasonably well with other reported numerical results. However, the model failed to predict the threshold impulse for the tearing of the plates (failure still occurred at very low impulses). It is thought that this is due to either the choice of the failure material parameters or the errors in the ABAQUS/Explicit failure model.

It was observed in this study that the mid-plate deflection as well as the deformed shape of a plate subjected to a central blast load is the same for a plate secured by clamping and for a fully built-in plate. This agrees with observations from experimental work where it was noted that large ductile deformation (Mode I) failure of plates is the same for clamped and fully built-in plates.

The presented numerical investigation results combined with the available experimental data provide valuable information for the understanding of the response of thin circular plates subjected to central blast loading and for the development of analytical procedures.

Chapter 5

Recommendations

In the present study, the large ductile deformation and rupture response of thin circular plates under central blast loads has been investigated. In the course of this investigation, a simplified and idealised loading model has been developed. It is recommended that further investigation be carried out in the modelling of the explosive pressure spreading beyond the load area particularly for small load to plate diameter ratios. One method that could be used is to develop and use initial velocity profiles instead of pressure profiles in the finite element model. The technique of using the experimental data to develop the load profiles can still be adopted in developing the initial velocity profiles.

Research on tearing and rupture of impulsively loaded plates should be continued. Of importance in this work would be the development of a material model which include a failure criterion. This can be achieved by developing a user-defined material model for use in place of the general ABAQUS material model (a capability which ABAQUS has).

The development of analytical analysis procedures using knowledge gained from experimental and numerical work is also an area that requires research and attention.

References

[1] R.B. Schubak, *Nonlinear Rigid-Plastic Analysis of Stiffened Plates Under Blast Loads*, Ph.D. Thesis, UBC, Vancouver, B.C., 1991.

[2] W.G. Shen and N. Jones, "Dynamic Response and Failure of Fully Clamped Circular Plates Under Impulsive Loading", *Int. J. Impact Engng.*, Vol. 13, No. 2, pp.259-279, 1993.

[3] The Steel Construction Institute, *The Effects of Simplification of the Explosion Pressure-Time History*, British Gas Research and Technology, 1992.

[4] G.N. Nurick and J.B. Martin, "Deformation of Thin Plates Subjected to Impulsive Loading: A Review, Part II", *Int. J. Impact Engng.*, Vol. 8, No. 2, pp. 171-186, 1989.

[5] S.B. Menkes and H.J. Opat, "Tearing and Shear Failures in Explosively Loaded Clamped Beams", *Experimental Mechanics*, Vol. 13, No. 11, pp. 480-486, 1973.

[6] R.G. Teeling-Smith and G.N. Nurick, "The Deformation and Tearing of Thin Circular Plates Subjected to Impulsive Loads", *Int. J. Impact Engng.*, Vol. 11, No. 1, pp. 77-91, 1991.

[7] G.N. Nurick and G.C. Shave, "The Deformation and Tearing of Thin Square Plates Subjected to Impulsive Loads: An Experimental Study", *Int. J. Impact Engng.*, Vol. 18, No. 1, pp. 99-116,1996.

[8] M.D. Olson, J.R. Fagnan and G.N. Nurick, "Analysis of the Deformation and Tearing of Blast Loaded Circular Plates", *to be published.*

[9] B.M. Thomas, *The Effects of Boundary Conditions on the Failure of Thin Plates Subjected to Impulsive Loading*, M.Sc. Thesis, University of Cape Town, 1995.

[10] A.M. Radford, *Thin Circular Metal Plates and Subjected to Localised Impulsive Loads*, M.Sc. Thesis, University of Cape Town, 1995.

[11] G.N. Nurick and J.B. Martin, "Deformation of Thin Plates Subjected to Impulsive Loading: A Review, Part I", *Int. Impact Engng.*, Vol. 8, No. 2, pp. 159-170, 1989.

[12] N. Jones, *Structural Impact*, Cambridge University Press, Cambridge, 1989.

[13] Q.M. Li and N. Jones, "Blast Loading of Fully Clamped Circilar Plates with Transverse Shear Effects", *Int. J. Solid Structures*, 1994.

[14] P.S. Symonds and T. Wierzbicki, "Membrane Mode Solutions for Impulsive Loaded Circular Plates", *J. Appl. Mech.* Vol. 46, pp. 58-64, 1979.

[15] A.L. Florence, "Clamped Circular Rigid-Plastic Plates Under Central Blast Loading", *Int. J. Solids Structures*, Vol. 2, pp. 319-335, 1966.

[16] D. Lui and W.J. Stronge, *Shear and bending response of a rigid-plastic plate to partially distributed blast-type loading*, Euromech, 2nd European Solid Mechanics Conference, Genoa, September 12-16, 1994.

[17] M.D. Olson, G.N. Nurick and J.R. Fagtnan, "Deformation and Rupture of Blast Loaded Square Plates: Predictions and Experiments", *Int. J. Impact Engng.*, Vol. 13, No. 2, pp. 279-191, 1993.

[18] G.N. Nurick, M.D. Olson, J.R. Fagnan and A. Levin, "Deformation and Tearing of Blast-Loaded Stiffened Square Plates", *Int. J. Impact Engng.*, Vol. 16, No. 2, pp. 273-291, 1995.

[19] Hibbet, Karlsson and Sorenson, INC., *ABAQUS/Explicit User's Manual*, Version 5.4, 1994.

[20] G.H. Farrow, G.N. Nurick and G.P. Mitchell, *Modelling of Impulsively Loaded Circular Plates Using the ABAQUS Finite Element Code*, Proceedings of the 13th Symposium on Finite Element Methods in South Africa, University of Stellenbosch, South Africa, 17-20 January, 1995.

[21] Hibbet, Karlsson and Sorenson, *ABAQUS Theory Manual*, Version 5.4, 1994.

[22] T.R.J. Hughes, R.L. Taylor and W. Kanoknukulchai, "A Simple and Efficient Element for Plate Bending," *Int. J. Num. Metds. Engng.*, Vol. 11, No.10, pp. 1529-1543, 1977.

[23] G.N. Nurick, "An Empirical Solution for Predicting Maximum Central Deflections of Impulsively Loaded Plates," *Inst. Phys. Conf. Ser.*, No. 102, Oxford, 1989.

[24] T.A. Duffey , *The large deflection dynamic response of clamped circular plates subjected to explosive loading*, Sandia Laboratories Research Report, SC-RR-67-532, 1967.

[25] P.S. Westine and W.E. Baker, *Energy solutions for predicting deformation in blast loaded structures*, Proceedings of the 19th Explosive Safety Seminar, Hollywood Beach, U.S.A., pp.849-879, 1974.

[26] N. Perrone and P. Bhadra, "A simplified method to account for plastic rate sensitivity with large deformations," *J. App. Mech.*, Vol. 46, pp. 811-816, 1979.

Appendix A

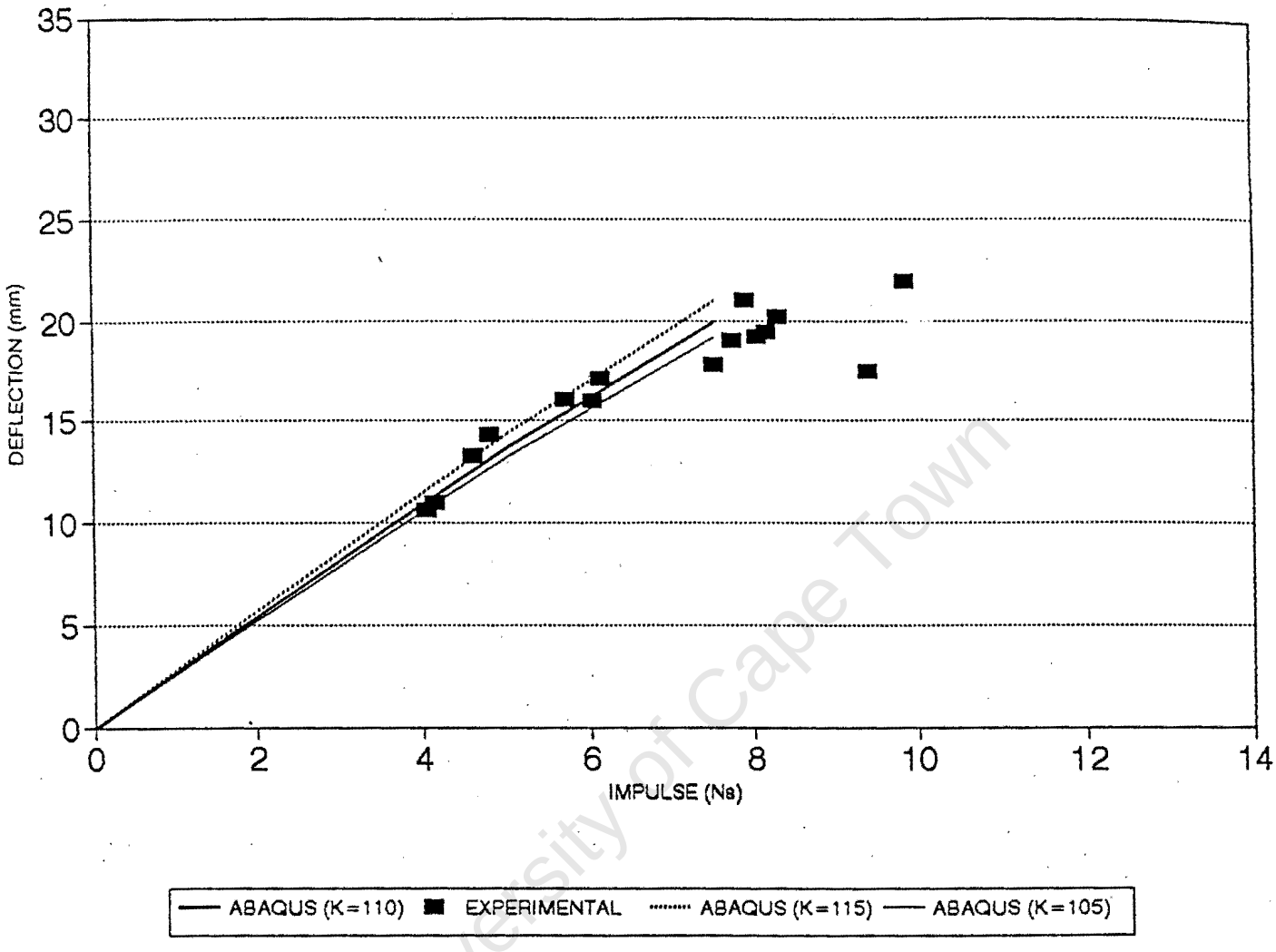

Appendix A.1: Affects of Changing the Decay Constant k on the Mid-point Permanent Deflection for $\frac{a}{R} = 0.183$.

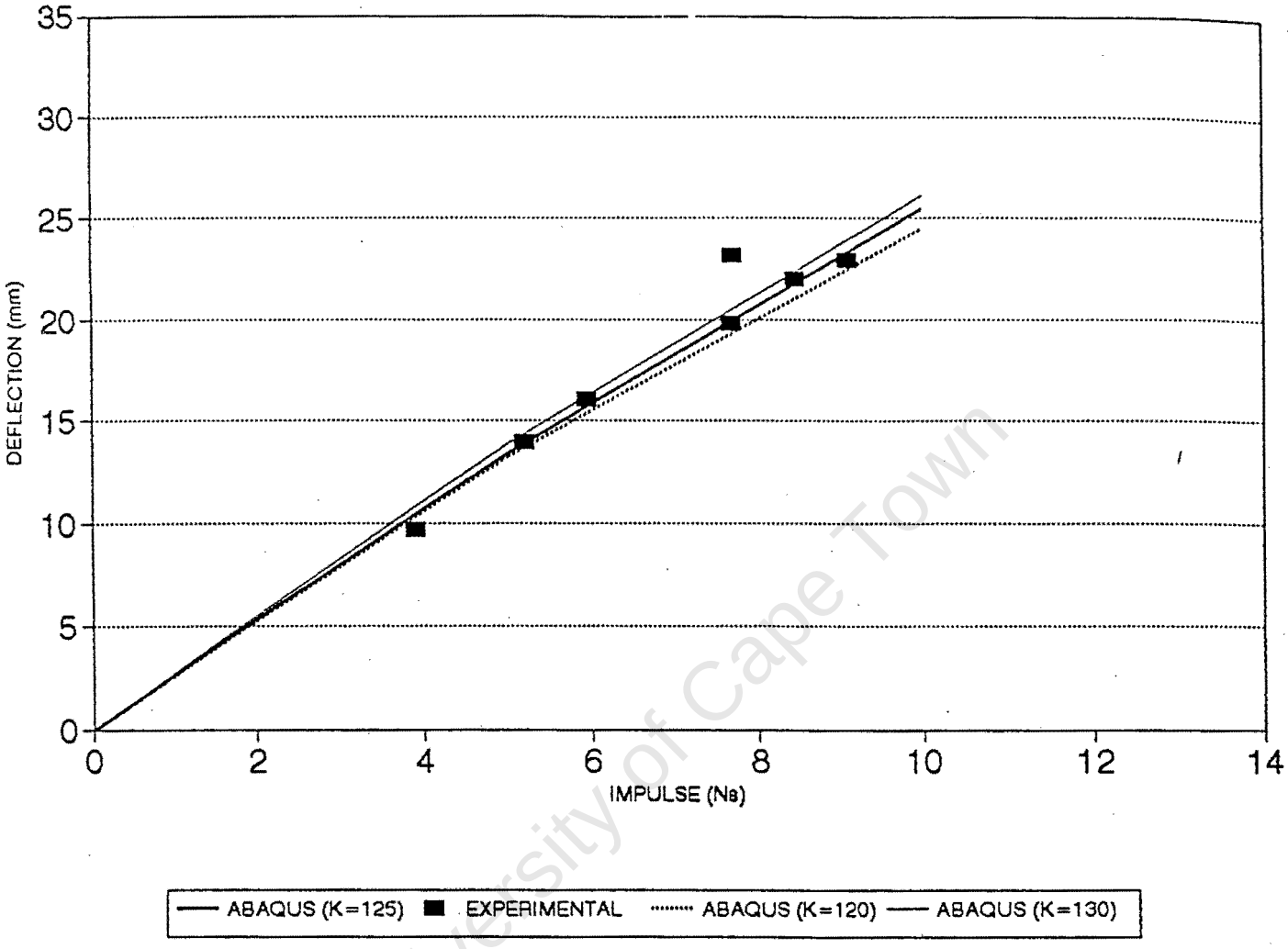

Appendix A.2: Affects of Changing the Decay Constant k on the Mid-point Permanent Deflection for $\frac{a}{R} = 0.25$.

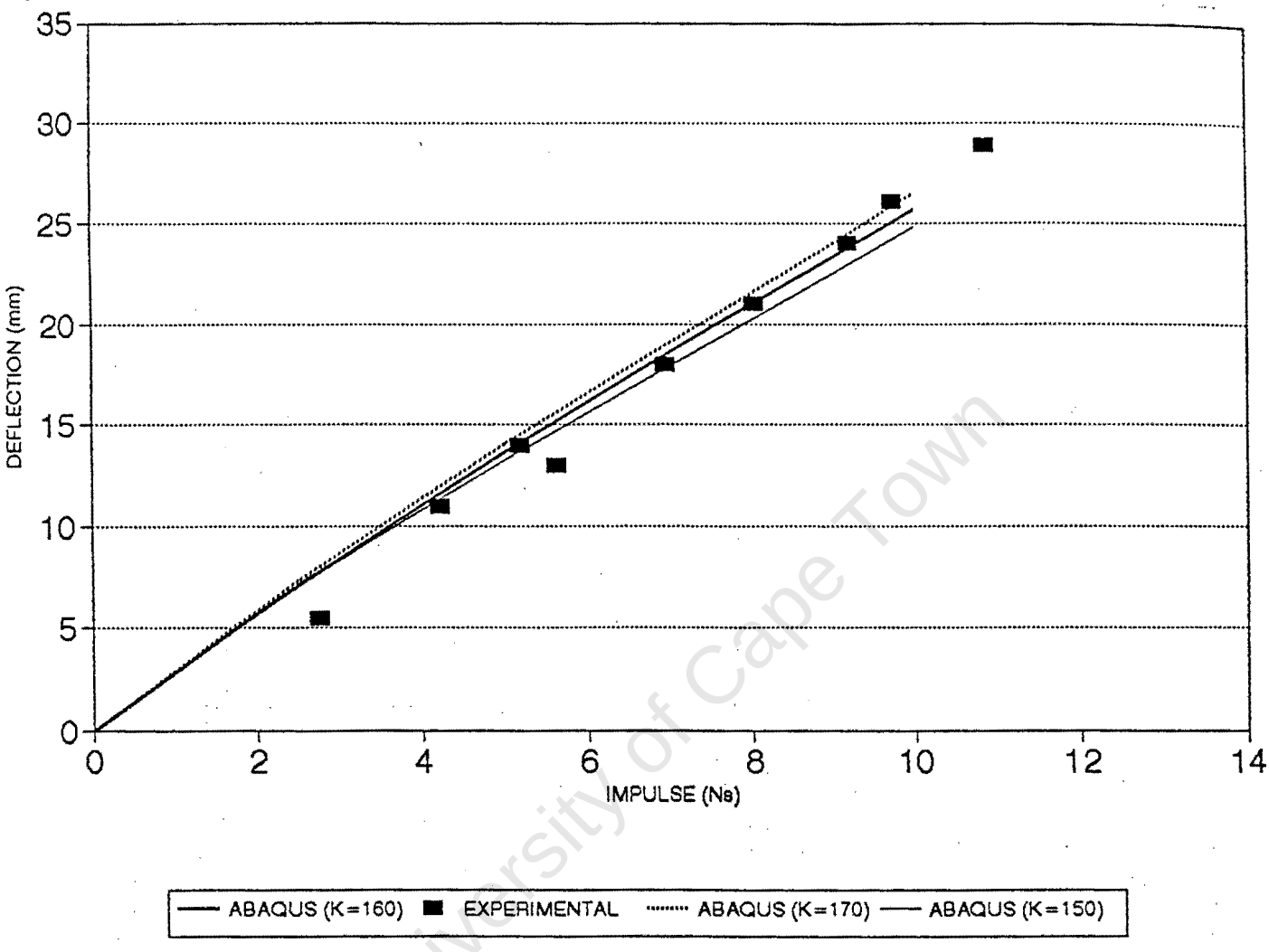

Appendix A.3: Affects of Changing the Decay Constant k on the Mid-point Permanent Deflection for $\frac{a}{R} = 0.33$.

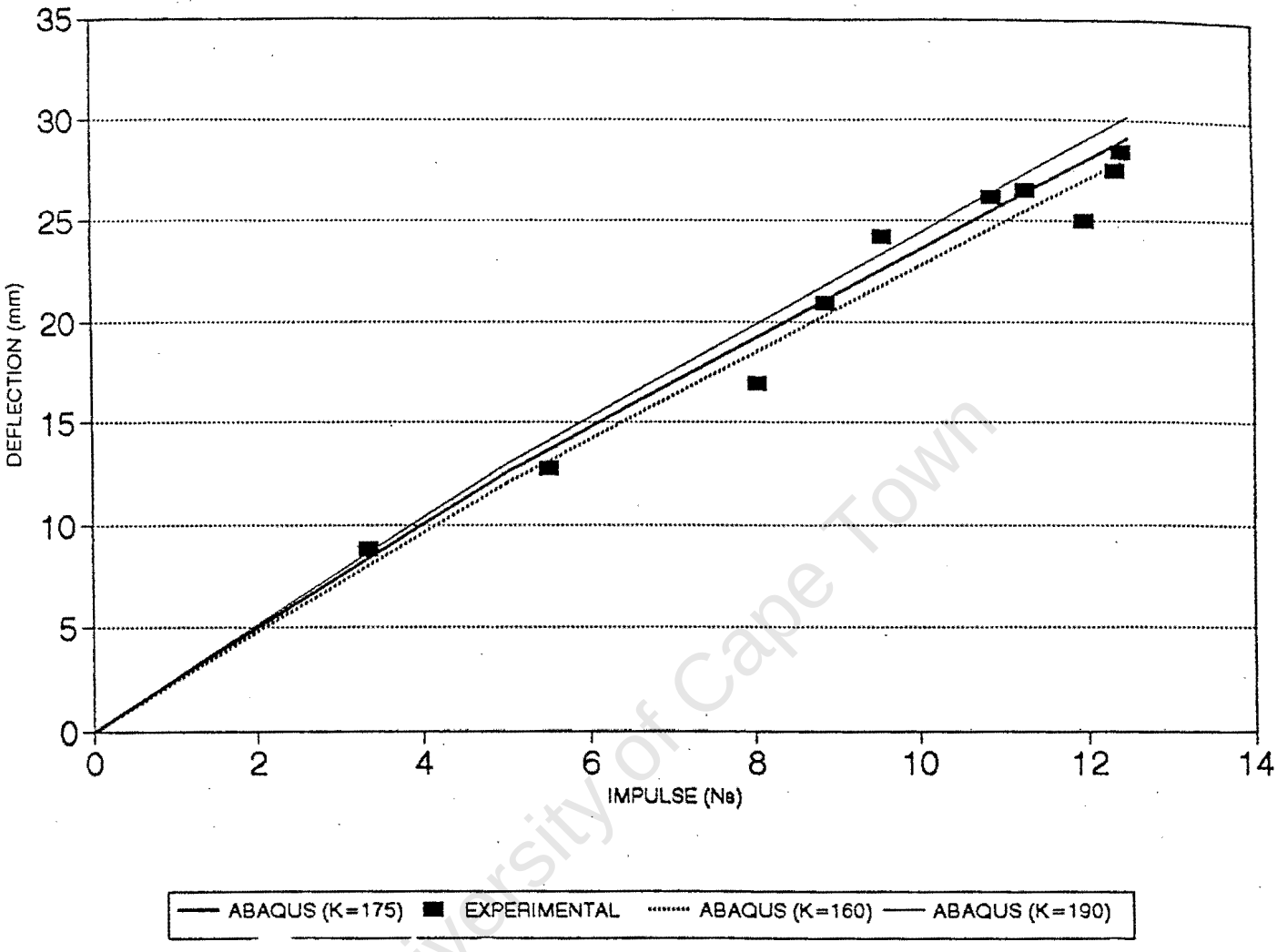

Appendix A.4: Affects of Changing the Decay Constant k on the Mid-point Permanent Deflection for $\frac{a}{R} = 0.40$.

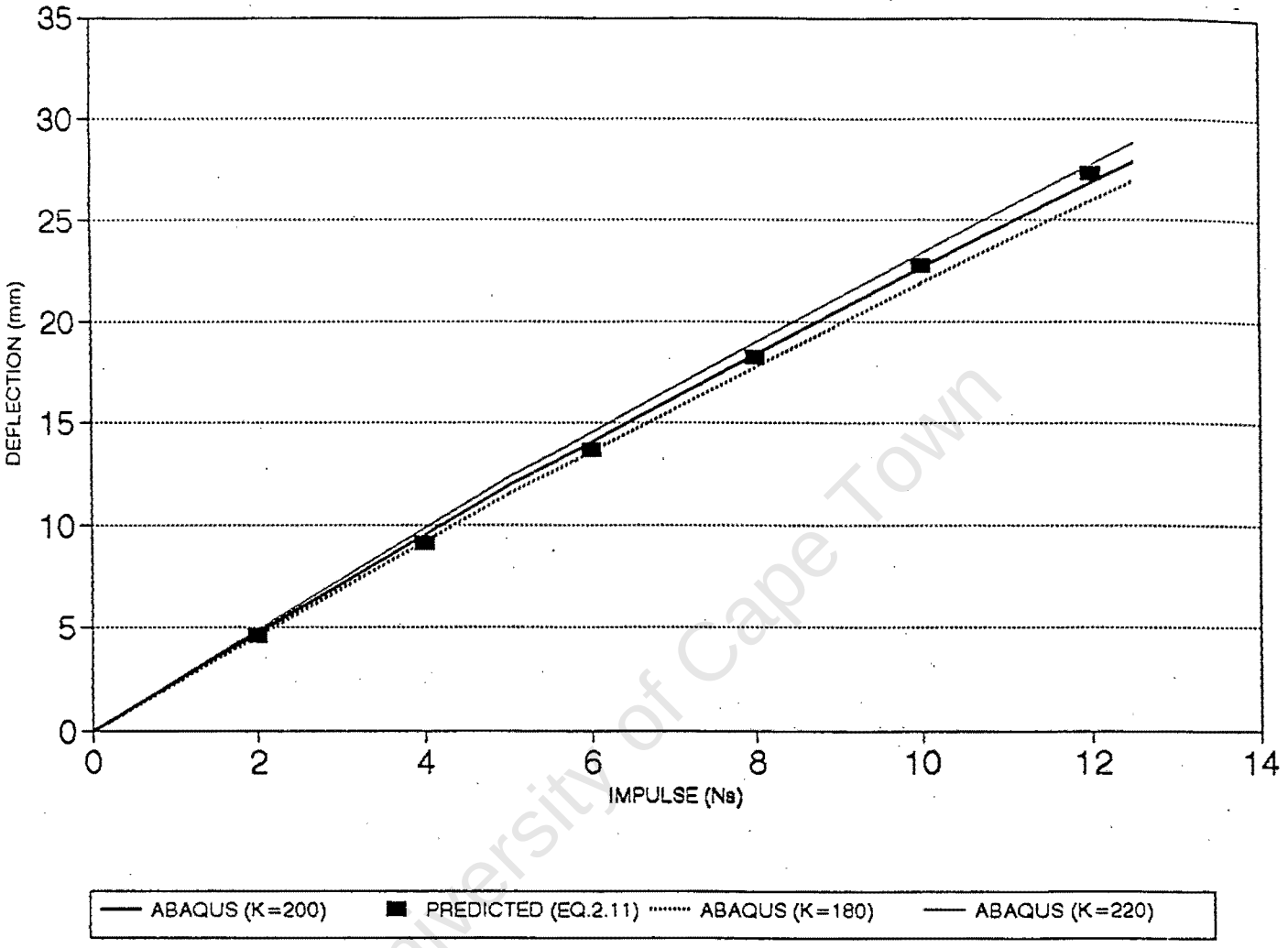

Appendix A.5: Affects of Changing the Decay Constant k on the Mid-point Permanent Deflection for $\frac{a}{R} = 0.45$.

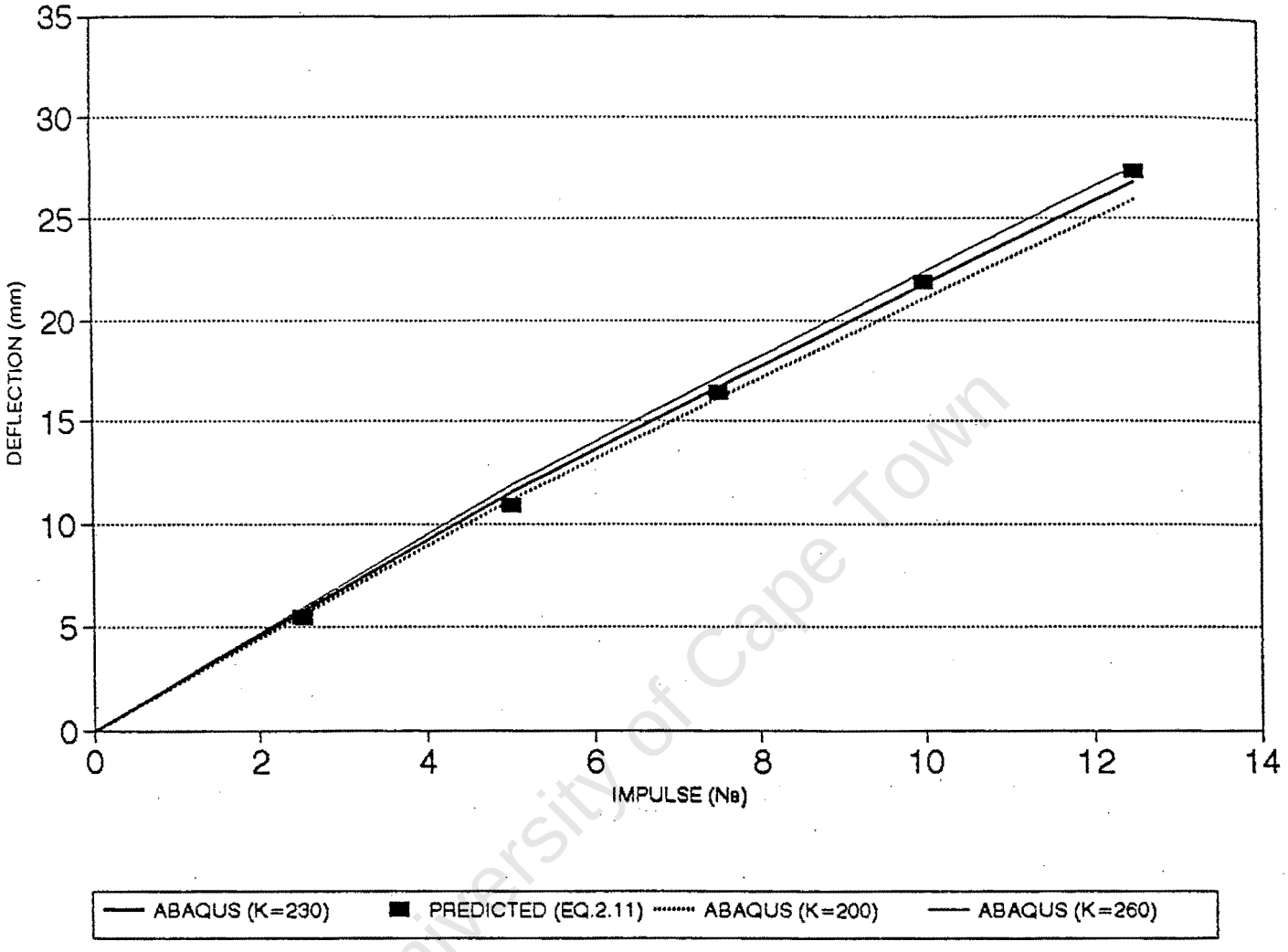

Appendix A.6: Affects of Changing the Decay Constant k on the Mid-point Permanent Deflection for $\frac{a}{R} = 0.50$.

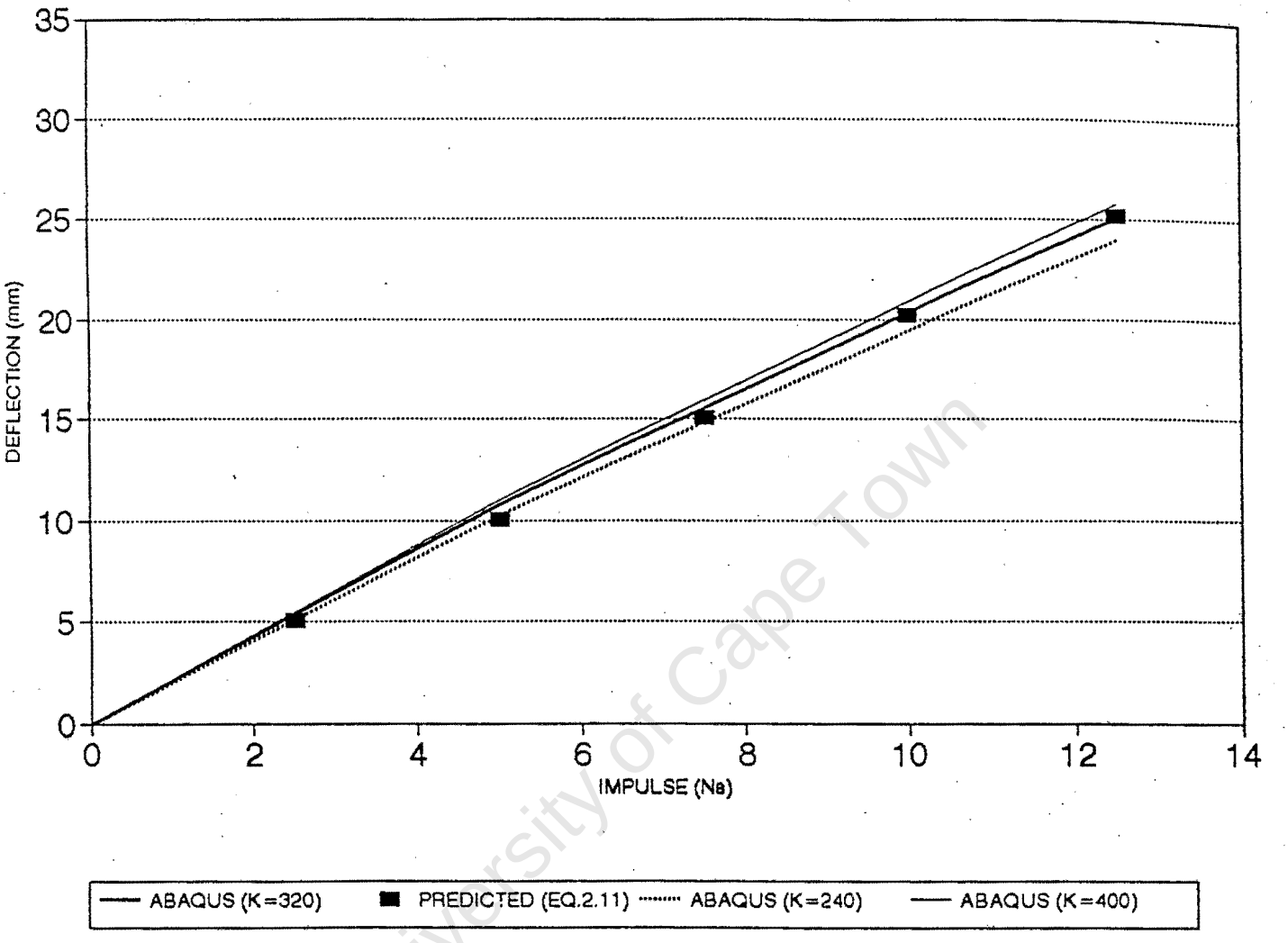

Appendix A.7: Affects of Changing the Decay Constant k on the Mid-point Permanent Deflection for $\frac{a}{R} = 0.60$.

Appendix B

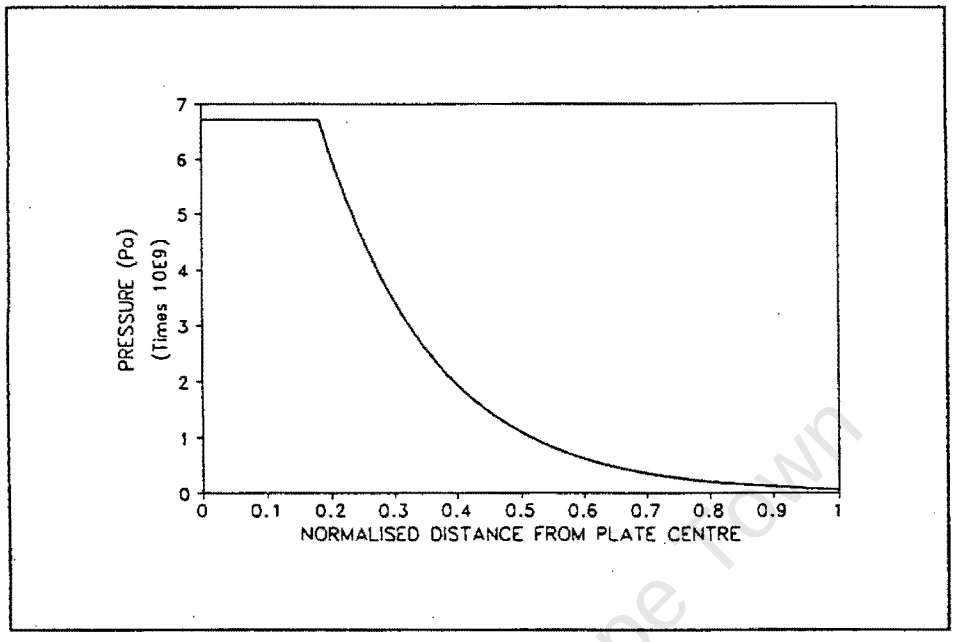

Appendix B.1: A typical pressure distribution profile for $\frac{a}{R} = 0.183$ *for 10 Ns impulse.*

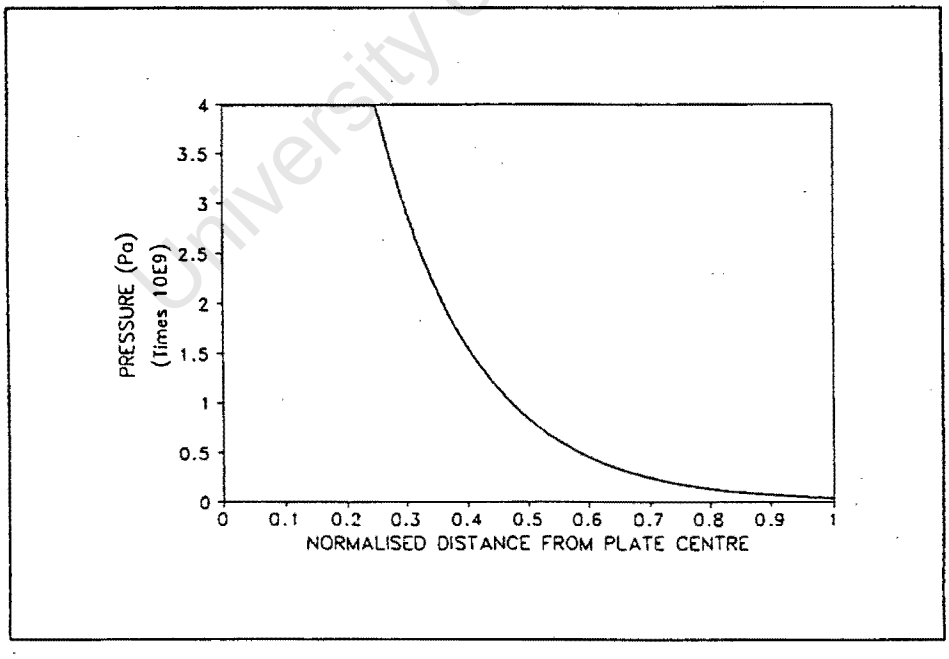

Appendix B.2: A typical pressure distribution profile for $\frac{a}{R} = 0.25$ *for 10 Ns impulse.*

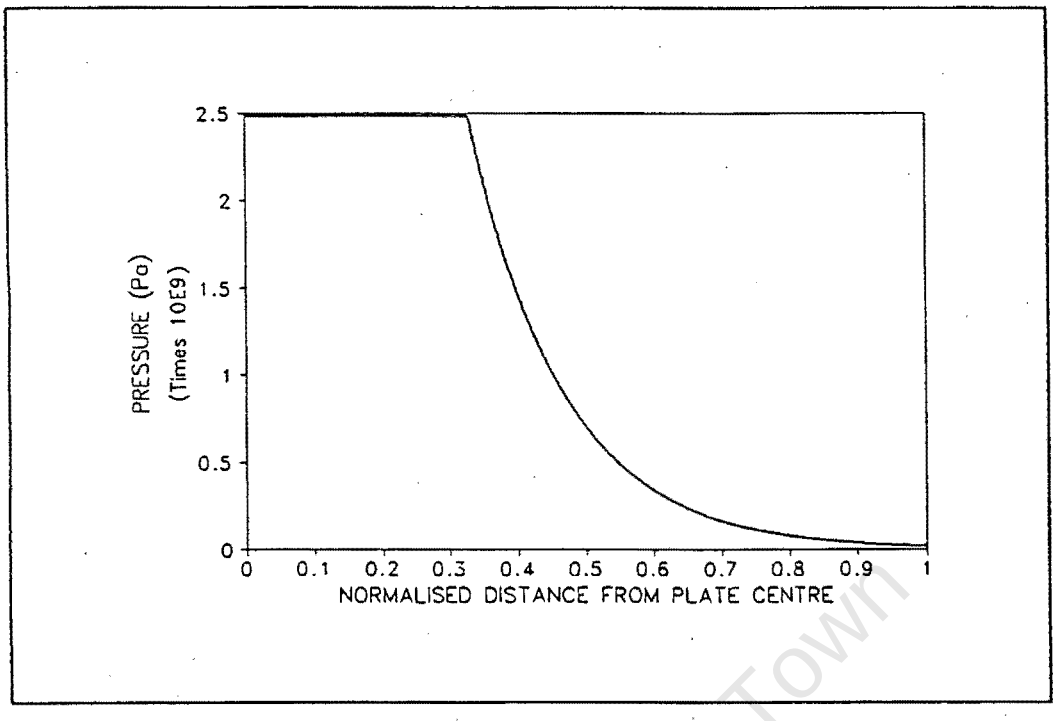

Appendix B.3: A typical pressure distribution profile for $\frac{a}{R}$ *= 0.33 for 10 Ns impulse.*

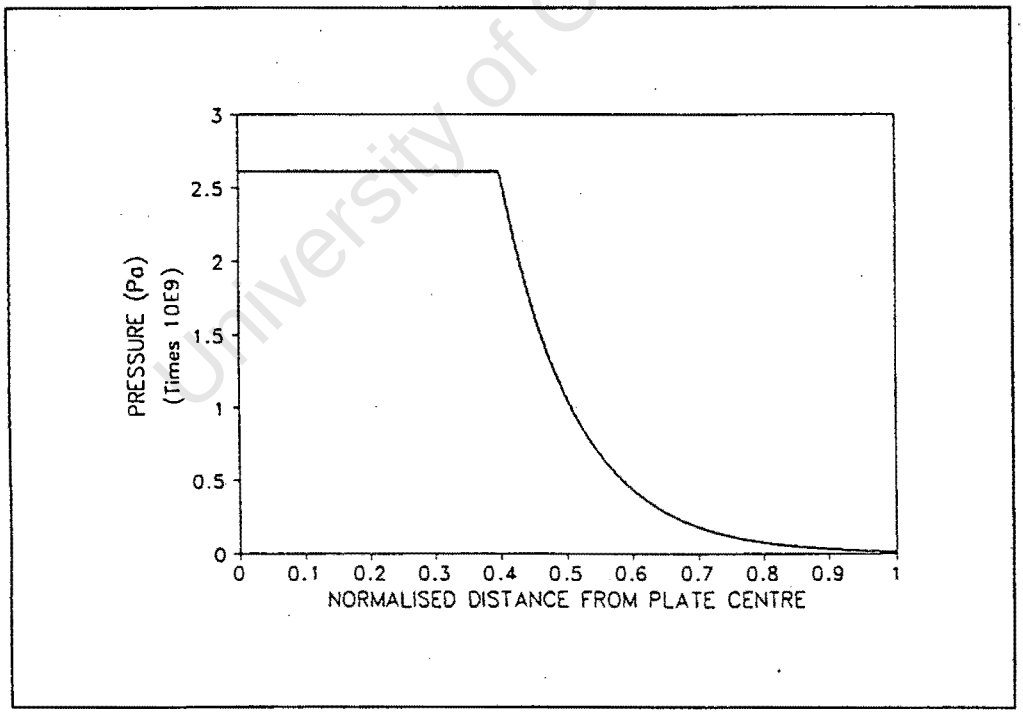

Appendix B.4: A typical pressure distribution profile for $\frac{a}{R}$ *= 0.40 for 15 Ns impulse.*

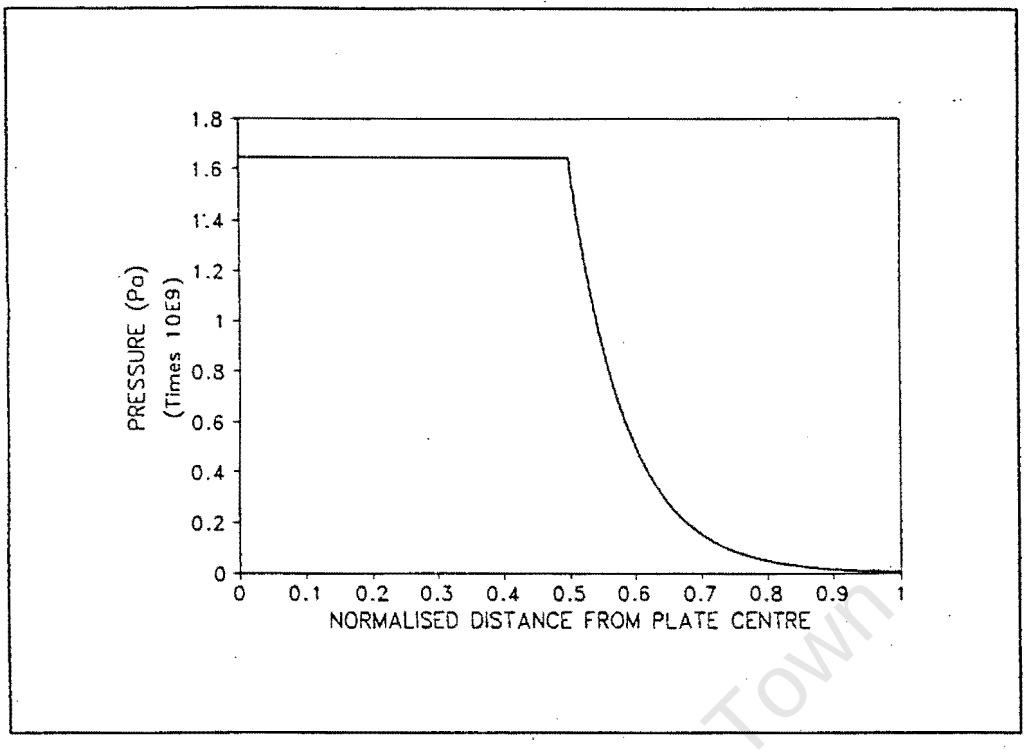

Appendix B.5: A typical pressure distribution profile for $\frac{a}{R}$ *= 0.50 for 15 Ns impulse.*

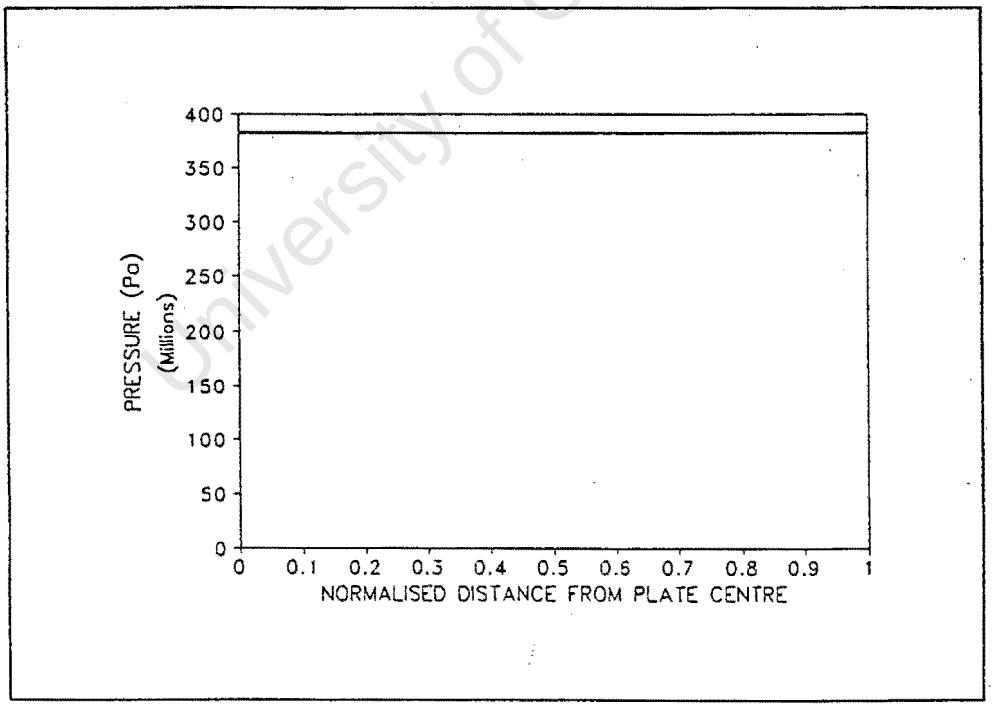

Appendix B.6: A typical pressure distribution profile for $\frac{a}{R}$ *= 1.00 for 20 Ns impulse.*